TOJSAT
the online journal of science and technology

The Online Journal of Science and Technology

ISSN: 2146-7390

APRIL 2012

Volume 2 - Issue 2

Published in TURKEY

Contact Address:

Prof. Dr. Aytekin İŞMAN- TOJSAT, Editor in Chief Sakarya-Turkey

Message from the Editor-in-Chief

Hello from TOJSAT

TOJSAT welcomes you.

I am very pleased to publish sixth issue in 2012. As an editor of The Online Journal of Science and Technology (TOJSAT), this issue is the success of the reviewers, editorial board and the researchers. In this respect, I would like to thank to all reviewers, researchers and the editorial road.

Sixth issue covers different research scopes, approaches which subjects about science and technology by valuable researchers. I and The Online Journal of Science and Technology (TOJSAT) editorial team will be pleased to share various researches with this issue as it is the miracle of our journal. All authors can submit their manuscripts to tojsateditor@gmail.com for the next issues.

Call for Papers

The Online Journal of Science and Technology (TOJSAT) invites article contributions. Submitted articles should be about all aspects of science and technology and may address assessment, attitudes, beliefs, curriculum, equity, research, translating research into practice, learning theory, alternative conceptions, socio-cultural issues, special populations, and integration of subjects. The articles should also discuss the perspectives of students, teachers, school administrators and communities.

The articles should be original, unpublished, and not in consideration for publication elsewhere at the time of submission to The Online Journal of Science and Technology (TOJSAT). For any suggestions and comments on TOJSAT, please do not hesitate to send mail.

April, 01, 2012

Prof. Dr. Aytekin İŞMAN

Editor-In-Chief

Message from the Editor

Dear Readers,

Welcome to the second issue of the Journal of Science and Technology which is used to fill in the gap between science and technology. Globally, this century is called as information era and therefore scientific and technological developments will be most important aspects of the papers.

The journal, which covers all scientific and technological subjects, is published 4 times a year. Selected paper presentations of the online science and technology conference will be published in the journal. The selected topics of this issue of the journal cover from Demonstration of an Electrospray Injection System and Effect of H2 Reduction on Carbon Nanotube Synthesis.

The main goal of this journal is to be indexed by science citation or social science citation indexes.

April, 01, 2012

Prof. Dr. M. Şahin DÜNDAR

Editor, TOJSAT

Table of Contents

An Emprical Investigation of Customer Satisfaction

Fatma Noyan and Gülhayat Gölbaşı Şimşek

Department of Statistics, Yildiz Technical University, Davutpaşa Campus, Esenler, 34210, Istanbul, Turkey
noyanf@gmail.com, gulhayatgolbasi@gmail.com

Abstract: This research has proposed a conceptual framework to investigate the effects of customers' perceived service quality and perceived product quality on customer satisfaction. To test the conceptual framework, structural equation modeling has been used to analyze the data collected from 1530 customers shopping from 102 stores belonging to four Turkish supermarket chains in Istanbul. The results of the study indicate that perceived service quality and perceived product quality are significantly related to customer satisfaction. Customer Satisfaction Index was also obtained and investigated according to supermarket chains.

Key words: Dimensionality, Customer satisfaction index, Service quality, Product quality

Introduction

Customer satisfaction is a key issue for organizations in today's competitive market place. To improve product and service quality, and maintain customer loyalty within a highly competitive marketplace, it became a central concern for companies and organizations. A key motivation for the growing emphasis on customer satisfaction is that high customer satisfaction lead to a stronger competitive position resulting in higher market share and profit (Fornell, 1992). Customer satisfaction is also generally assumed to be a significant determinant of repeat sales, positive word-of-mouth, and customer loyalty. Satisfied customers return and buy more, and they tell other people about their experiences (Fornell, et al., 1996). Thus, dynamic structure and intense competition in retail markets especially in supermarkets increase the need for supermarket retailers to use strategies focused on customer satisfaction (Okumuş & Temizerler,2006). The supermarket sector is characterized by increased competition, an enhanced opportunity to analyze markets, and greater shopper expectations. These aspects suggest that customer satisfaction management is especially critical and supermarket mangers recognize that customer satisfaction plays a key role in a successful business strategy.

Customer satisfaction is well known and established concept in several disciplines and different types of satisfaction have been identified. In line with Oliver (1989) we perceive satisfaction as a post-consumption evaluation or "A pleasurable level of consumption related fulfillment" (Blomer,2002). In this study we define the customer satisfaction is an affective reaction (Menon & Dubé,2000) in which the customers' needs, desires and expectations during the course of service and product quality experience have been met or exceeded (Lovelock,2001). Supermarkets offer a variety of products and services simultaneously so that, for the customer, there is more to visiting a store than the mere acquisition of consumption products. Differences in the "shopping experience" between retail outlets (e.g., store ambience, disposition of associates, store services) are often as important to the customer as differences in the physical characteristics of the products offered (e.g., quality) (Gómez, McLaughlin, Wittink, 2004).

The antecedents of customer satisfaction have been widely studied in the case of service companies. Results of most of the published studies identify positive influences of the perception of service quality on customer satisfaction. However, there is only a very limited number of studies examining the relationship both of the service and product quality on customer satisfaction in the supermarkets. In this study, a conceptual framework is proposed that analyses the effects of perceived service quality and perceived product quality on customer satisfaction in the supermarkets. To test the framework, structural equation modeling techniques are applied to a representative sample of four major supermarket chains in Istanbul. This paper is organized as follows: in the next section, we discuss and develop the conceptual model. We then describe the data, and we elaborate the statistical model. We conclude with the presentation of results and a discussion of possible extensions for future research.

Methods

CONCEPTUAL MODEL OF CUSTOMER SATISFACTION

The conceptual framework of this study builds upon the works from several disciplines such as retailing, consumer behaviour, marketing, and psychology. The conceptual models found in the literature mainly dealt with the image in consumer/shopping behaviour, store selection, store image and different levels of evaluations embedded in satisfaction structure (Noyan & Gölbaşı Şimşek,2011). We test the conceptual model introduced below on data collected by four large supermarket chains form their own shoppers. The proposed model has three latent variables, Perceived Service Quality (PSQ) and Perceived Product Quality (PPQ) are exogenous constructs, and Customer Satisfaction (CS) is endogenous construct based on the various areas in which the survey questions were asked. The aim of this paper is to improve empirical knowledge about the impact of supermarket satisfaction. Two distinct dimensions of perceived quality are identified: quality of service and quality of product. Our prime interest is in assessing some disregarded antecedents of customer satisfaction in terms of perceived service quality and perceived product quality.

DATA AND MEASURES

Data were collected from a sample of costumers of four supermarkets belonging to same Turkish store chain in Istanbul. 1530 correctly –filled-out questioners were collected across at least 15 customers per store for each of about 102 stores. The sample was found to be representative for the costumers of the local supermarket chain in terms of gender, age, number of household members ad net house hold income. The design of the questionnaire was based on multiple-item measured scales that have been validated and found to be reliable in previous research. All determinants were measured on ten-point Likert scales ranging from completely disagree to completely agree. The measurement items of the different constructs and their origin are shown in Table 1. Table 1 provides the results of the measurement model after the unreliable items were eliminated.

Reliability and Validity of Measures

At the first step, Exploratory Factor Analyses (EFA) were carried out using Maximum Likelihood (ML) extraction method with Promax rotation. ML factor analysis proceeds on the assumption that the data have a multivariate normal distribution, which in turn implies that each individual variable is normally distributed. Violation of this assumption may lead to distorted factor analytic results. West and Curran (1995) suggested that the ML can produce useful results as long as the skewness of each observed variable is less than 2.0 and kurtosis is less than 7.0. It can be seen from Table 1 that all the items of PSQ, PPQ, and CS meet these criteria.

Table 1. DESCRIPTIVE STATISTICS FOR THE ITEMS OF LATENT VARIABLES (N=1530)

	Items	Mean	Std. Deviation	Skewness	Kurtosis
	Service Quality Perceptions (Cronin et al., 2000)				
Q1	Staff have knowledge about products and campaigns.	7.78	1.849	-1.015	.915
Q2	Staff have enough experience to help customers.	7.77	1.833	-.952	.782
Q3	Staff are affable.	7.80	1.831	-.991	.932
Q4	Staff are polite and respectful.	7.81	1.813	-.946	.770
Q5	Staff are easy to reach.	7.82	1.748	-.920	.761
Q6	Easy to communicate with staff.	7.75	1.805	-1.001	1.058
Q7	Staff give understandable responses to questions.	7.75	1.842	-.934	.738
Q8	Staff are reliable.	7.79	1.759	-.887	.697
Q9	There is a sales person who is ready to help at any moment.	7.50	1.994	-1.010	.904
Q10	Staff strive to understand my needs.	7.65	1.831	-.887	.718
Q11	Cashiers are careful.	7.76	1.829	-.997	1.063
	Product Quality Perceptions (Sirohi et al., 1998)				
Q12	The products of vegetable-fruit department are very high in quality.	7.43	1.959	-.934	.754
Q13	The products of meat-fish department are very high in quality .	7.46	1.855	-.837	.612
Q14	Hot/frozen ready-made foods are very high in quality.	7.50	1.782	-.739	.385
Q15	The products of bakery department are very high in quality.	7.48	1.851	-.743	.269
Q16	Packaged-frozen products are very high in quality.	7.51	1.785	-.703	.307
Q17	Not packaged dried foods (dried beans, pasta, grain,…) are very high in quality.	7.60	1.808	-.899	.842
Q18	Milky products are very high in quality.	7.62	1.766	-.727	.244
Q19	There are no out-of-date products on shelves.	7.36	1.895	-.758	.346
Q20	In general, products of this supermarket are very high in quality.	7.85	1.784	-.950	.776
Q21	The products of vegetable-fruit department are very high in quality.	7.58	1.752	-.772	.618
	Customer Satisfaction (Brumly,2002)				
Q22	I think, shopping with this supermarket is a good decision.	7.16	1.766	-.391	-.176
Q23	This supermarket takes customer satisfaction as a goal.	7.20	1.716	-.414	-.180
Q24	I am satisfied with preferring this supermarket.	7.20	1.753	-.401	-.324
Q25	I am satisfied with shopping this supermarket.	7.28	1.748	-.406	-.333
Q26	In general, I am satisfied with this supermarket.	7.23	1.757	-.444	-.163
Q27	I am satisfied with pricing to product quality by this supermarket.	7.13	1.856	-.477	-.105
Q28	I am really satisfied with this supermarket.	7.22	1.820	-.501	-.002

Factor analysts have developed a wide range of techniques that may be used to decide the number of factors to extract. Empirical investigations have shown that these techniques not always point to same number of factors and experts have recommend that analysts (a) consider the information provided by several techniques, and (b) make a final decision on the number of factors against the background of the theoretical meaningfulness and interpretability of the factors obtained (Preacher & MacCallum, 2003).

The following techniques and criteria were used to decide the number of factors to retain. These empirical criteria include the popular eigenvalues-greater-than-one (eigenvalues>1) criterion (KG; Guttman, 1954; Kaiser, 1960) and the scree test (Catell,1978), as well as the less commonly applied techniques of parallel analysis (PA; Horn,1965) and the minimum average partial test (MAP; Velicer,1976). From the result of simulation studies of Zwick&Velicer (1982,1986) and Glorfeld (1995), KG rule tends to underestimate and PA overestimate the number of factors. It is better to extract too many rather than too few factors. Underextraction leads to distortion of the extracted factors. In contrast, overextraction generally does not distort the character of the major factors (Wood, Tataryn & Gorsuch, 1996). Fortunately, there is increasing consensus among statisticians that two less well-known procedures, PA and MAP test, are superior to other procedures and typically yield optimal solutions to number of factor problem (Wood et al., 1996; Zwick & Velicer, 1982, 1986). These procedures are statistically based, rather than being mechanical rules of thumb. In PA, the focus is on the number of factors that account for more variance than the components derived from random data. The MAP test uses a principal components analysis followed by an examination of a series of matrices of partial correlations. Specifically, on the first step the first principal component is partialed out of the correlations between the variables of interest, and the average squared coefficient in the off diagonals of the resulting partial correlation matrix is computed. On the second step, the first two principal components are partialed out of the original correlation matrix and the average squared partial correlation is again computed. These computations are conducted for (number of items-1) steps, where p is the number of variables. The number of components is chosen to be the step number in the analyses that resulted in the average squared partial correlation. O'connor (2000) wrote codes for SAS and SPSS for the PA and MAP procedures. After examination all of the above procedures, scree plot in Figure 1, KG rule and PA analysis with its results given in Table 2, and the MAP test showed three factors solution.

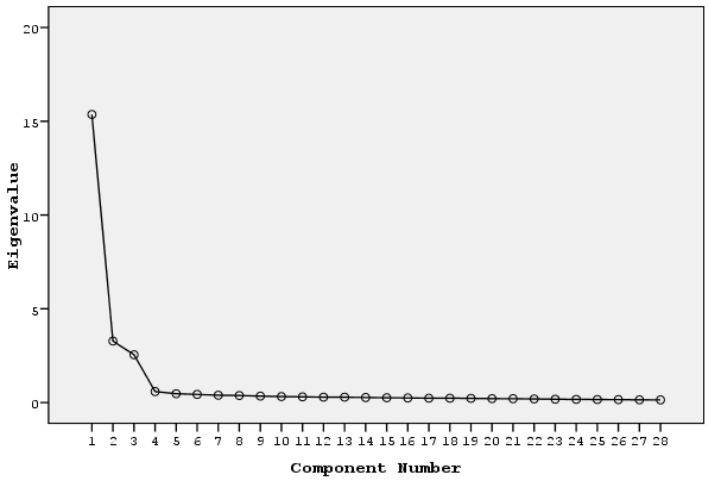

Figure 1. SCREE PLOT

Table 2. RAW DATA EIGENVALUES, MEAN & 95 % RANDOM DATA EIGENVALUES

Root	Raw Data	Means	95%
1	**15.362805**	**1.25872**	**1.28798**
2	**3.276793**	**1.22092**	**1.24454**
3	**2.547975**	**1.19358**	**1.2114**
4	0.585774	1.17214	1.18694
5	0.471483	1.15014	1.16676
6	0.434512	1.13256	1.14657
7	0.388863	1.11386	1.13045
8	0.377663	1.09594	1.11087
9	0.342143	1.07905	1.09317
10	0.318059	1.06347	1.07933
11	0.30225	1.04796	1.06116
12	0.288822	1.03206	1.04577
13	0.285798	1.01695	1.02958

14	0.26725	1.00077	1.01468
15	0.255466	0.98555	0.99751
16	0.243713	0.97171	0.98197
17	0.231403	0.95881	0.97387
18	0.230225	0.94329	0.95594
19	0.22358	0.92805	0.94083
20	0.210547	0.91341	0.92491
21	0.204868	0.89917	0.91362
22	0.194927	0.88424	0.8966
23	0.178643	0.86899	0.88017
24	0.171382	0.85126	0.86496
25	0.160737	0.83492	0.84892
26	0.156878	0.81655	0.83146
27	0.146141	0.79659	0.8155
28	0.1413	0.76935	0.79237

Going forward to three factors solution, Kaiser-Meyer-Olkin (KMO) Measure of Sampling Adequacy was .977 indicating higher sampling adequacy. The first factor accounted for 54.867 %, the second factor accounted for 11.703% and third factor accounted for 9.100% of the total variance. These three factors accounted for 75.670% of the total variance. The communality values of observed variables ranged from .595 to .835. Pattern loadings are shown in Table 3, which are noticeable higher on underlying factor indicating construct validity from the exploratory points of view.

Table 3. PATTERN LOADINGS

items	Factors		
	PSQ	PPQ	CQ
Q1	**.874**	.028	-.046
Q2	**.889**	.016	-.021
Q3	**.901**	-.031	.019
Q4	**.898**	-.030	.018
Q5	**.903**	-.023	.014
Q6	**.905**	-.022	.005
Q7	**.909**	-.007	.009
Q8	**.854**	.001	.033
Q9	**.797**	.044	-.011
Q10	**.831**	.044	-.021
Q11	**.755**	.055	.037
Q12	-.046	**.877**	-.021
Q13	-.021	**.892**	-.023
Q14	.025	**.906**	-.053
Q15	.031	**.885**	-.024
Q16	.013	**.886**	-.013
Q17	.020	**.824**	.010
Q18	.005	**.818**	.039
Q19	-.058	**.813**	.019
Q20	.116	**.610**	.132
Q21	.056	**.788**	.056
Q22	.003	.051	**.864**
Q23	.012	.064	**.843**
Q24	.009	.019	**.892**
Q25	-.009	.007	**.914**
Q26	-.018	.019	**.889**
Q27	.028	-.072	**.901**
Q28	.004	-.027	**.911**

The second goal of the study in order to reach acceptable measurement model, was to confirm that each measure taps facets of the three latent constructs (convergent validity) and that the constructs are distinct from each other (discriminant validity). Confirmatory Factor Analysis (CFA) was used for establishing the validity of the constructs.

Unidimensionality is a necessary condition for reliability and construct validation (Mak & Sockel, 2001, p.271). The unidimensionality of the constructs was analyzed by specifying a measurement model for each construct. According to Jöreskog and Sörbom (1993), a goodness of fit index (GFI) of 0.90 or above suggests that each of the construct is unidimensional.

Convergent validity is examined by using the Bentler-Bonett normed fit index (NFI) (Bentler & Bonett,1990). As seen from the Table 4, all of the construct have GFI and NFI values above 0.90 indicating that all of the construct are unidimensional and, convergent validity was achieved for all the construct. Acceptable model fits are indicated by goodness of fit indices, and RMSEA (Root Mean Square Error of Approximation) values below 0.08 and, SRMR (Standardized Root Mean Square Residual) below 0.05 represent an acceptable model fit (Browne & Cudeck, 1992)

Table 4. GOODNESS OF FIT INDICES FOR UNIDIMENSIONAL CONSTRUCTS

Latent Constructs	GFI	NFI	RMSEA	SRMR
PSQ	0.94	0.97	0.085	0.019
PPQ	0.91	0.96	0.11	0.029
CS	0.98	0.99	0.064	0.011

In assessing discriminant validity the factor correlation matrix given in Table 5 was examined, and showed that three factors did not overlap substantially. To test discriminant validity, CFA was performed on selected pair of scales, allowing correlation between two construct. The analysis was rerun with the correlation the two constructs fixed at 1. A chi-square difference tests were conducted for these unrestricted and rectricted models. The results suggest that for three pairs of constructs, the two-factor solutions were better than the single factor solutions ($p<0.01$).

Table 5. INTERCORRELATIONS OF THE LATENT CONSTRUCTS

	PSQ	PPQ	CS
PSQ	1		
PPQ	0.61	1	
CS	0.57	0.62	1

The factor loadings and construct reliabilities for the measurement model are presented in Table 6. The individual item loadings (lambdas) on the constructs were all highly significant ($p<0.001$, t value >10) with values ranging from 0.733 to 0.901. All the individual scales exceeded the recommended minimum standards proposed by Bagozzi and Yi (1988) in terms of construct reliability (composite reliability greater than 0.70). Şimşek & Noyan's (2012) generalized theta coefficient $-\theta_G-$ for composite reliability of the total scale was 0.9614, which indicates high reliability of total scores.

Table 6. STANDARDIZED CFA COEFFICIENTS AND CONSTRUCT RELIABILITY

Constructs	**Items**	**Loadings**	**t**	**Item Reliability (R^2)**	**Constructs Reliability**
PSQ	Q1	0.850	*	0.723	0.968
	Q2	0.876	46.401	0.768	
	Q3	0.885	47.252	0.783	
	Q4	0.882	46.959	0.778	
	Q5	0.890	47.788	0.792	
	Q6	0.885	47.295	0.783	
	Q7	0.900	48.882	0.810	
	Q8	0.860	44.788	0.739	
	Q9	0.792	38.933	0.628	
	Q10	0.825	41.662	0.681	
	Q11	0.784	38.247	0.614	
PPQ	Q12	0.815	*	0.665	0.956
	Q13	0.851	40.543	0.724	
	Q14	0.880	42.735	0.774	
	Q15	0.881	42.821	0.776	
	Q16	0.878	42.603	0.771	
	Q17	0.818	38.184	0.668	
	Q18	0.823	38.581	0.678	
	Q19	0.753	33.951	0.567	
	Q20	0.733	32.707	0.537	
	Q21	0.837	39.569	0.701	
CS	Q22	0.879.	*	0.773	0.959

	Q23	0.870	48.589	0.757	
	Q24	0.897	51.869	0.804	
	Q25	0.901	52.513	0.813	
	Q26	0.871	48.698	0.759	
	Q27	0.845	45.779	0.714	
	Q28	0.875	49.154	0.765	

*Fixed parameter for scaling purpose

Structural Model

The reliability and validity analysis results indicate that the scales for the constructs appear to have satisfactory measurement qualities. After measurement model was built, a structural model with latent variables considered adding proposed structural paths between latent constructs. The proposed model was analyzed via ML estimation using covariance matrix of observed variables as input. Table 7 reports goodness of fit indices, parameter estimates and their t- values for the structural model. The overall $\left(\chi^2_{(347)} = 1935.72, p<0.01\right)$, which is expected given the large sample size (Bagozzi & Yi, 1988). All other goodness of fit indices are within the acceptable ranges (GFI=0.91, AGFI=0.90, SRMR=0.031, CFI=0.96, NFI=0.96, NNFI=0.96, RMSEA=0.058 and, CN=325.81). All of the fit indices indicate that the proposed model exhibits good fit to the data.

Table 7. SUMMARY OF THE RESULTS FROM PROPOSED MODEL

Path	Estimate	Standard Error of Estimate	Standardized Estimate	t-value
PSQ → CS	0.307	0.027	0.311	11.563*
PPQ → CS	0.415	0.027	0.427	15.290*
Squared Multiple Correlation (SMC) = 0.44				

$\chi^2_{(347)} = 1935.72, p<0.01$

Goodness of Fit Index (GFI) = 0.91
Adjusted Goodness of Fit Index (AGFI) = 0.90
Standardized Root Mean Square Residual (SRMR)= 0.031
Comparative Fit Index (CFI) = 0.96
Normed Fit Index (NFI) = 0.96
Non-Normed Fit Index (NNFI) = 0.96
Root Mean Square Error of Approximation (RMSEA) = 0.058
Critical N (CN) = 325.81

*$p<0.01$

In accordance with the parameter estimates shown in Table 7, Perceived service quality and Perceived product quality have direct positive and significant effects on Customer satisfaction. From standardized estimates, the effect of Perceived service quality was lower than the effect of Perceived product quality, their effects on Customer satisfaction were comparable in terms of magnitude. From the SMC value in Table 8, 44% variance of Customer satisfaction was explained by Perceived service quality and Perceived product quality, which indicates a fairly high level of explanatory power.

Discussion and Conclusions

The main purpose of this study was carried out modeling Customer Satisfaction using Perceived Service Quality and Perceived Product Quality as exogenous latent constructs. A well fitting structural and accompanying measurement models were developed. It was concluded that Perceived Service Quality and Perceived Product Quality affect Customer Satisfaction positively, and their effects on Customer Satisfaction were comparable in terms of effect sizes. Therefore, policy makers in Turkish retailing sector should be consider Service Quality as well as Product Quality to provide satisfied customers.

We also obtained Customer Satisfaction Index (CSI) using the Structural Equation Modeling (SEM) approach. To investigate positions of four different supermarkets chain (labeled by A,B,C and, D), they were grouped into two classes as economy class and non-economy class supermarkets according to their customer profile, brand and variety of products. As for the analysis of group (classes of economy vs. non-economy) differences, Kruskal-Wallis Tests were performed following evidence on factorial invariance. Table 8 shows the test results and suitable descriptive statistics of supermarkets.

Table 8. COMPARISONS OF FOUR DIFFERENT SUPERMARKET CHAINS

Index	Groups	N	Mean Rank	Rank Order	Chi-Square	df	p
PSQ	Economy A	405	712.25	4	23.641	3	.000
	Economy B	405	853.86	1			
	Non-Economy C	450	741.34	3			
	Non-Economy D	270	753.10	2			
PPQ	Economy A	405	710.30	4	29.955	3	.000
	Economy B	405	711.06	3			
	Non-Economy C	450	850.88	1			
	Non-Economy D	270	787.66	2			
CS	Economy A	405	836.42	1	17.314	3	.001
	Economy B	405	771.01	2			
	Non-Economy C	450	722.47	4			
	Non-Economy D	270	722.58	3			

According to Kruskal-Wallis Tests, the group differences of PSQ, PPQ and, CS indexes were found statistically significant ($p<0.01$). As seen from the above Table, economy class supermarkets have higher Customer Satisfaction Index while they have lower Perceived Product Quality Index. On the other hand, non-economy class supermarkets with lower Perceived Service Quality Index have lower Customer Satisfaction Index. The second conclusion can be made from the above results that, the single strategy (such as Service Quality or Product Quality going alone) is not enough to achieve customer satisfaction. And it is clear that, some other determinants of customer satisfaction in addition to PSQ and PPQ should be required.

Acknowledgement

This research is fully supported by a grant from the Scientific and Technological Research Council of Turkey (TUBITAK) (Project No.110K098)

References

Bagozzi, R.P., & Yi, Y. (1988). On the evaluation of structural equation models. *Journal of the Academy of Marketing Science*, 16, 74-94

Bentler, P.M, & Bonett, D.G. (1990). Comparative fit indices in structural models. *Psychological Bulletin*, 107 (2), 238-46.

Bloemer, J., & Schroder, G. (2002). Store satisfaction and store loyalty explained by customer and store related factors. *Journal of Consumer Satisfaction, Dissatisfaction and Complaining Behavior*, 15,68-80.

Browne, M. W., & Cudeck, R. (1992). Alternative ways of assessing model fit. *Sociological Methods & Research*, 21, 230-258.

Cattell, R. B. (1978). The scientific use of factor analysis in behavioral and life sciences. New York, NY: Plenum Press

Cronin J. J., Brady, M. K. , Hult G. T. M. (2000). Assessing the Effects of Quality, Value and Customer Satisfaction on Consumer Behavioral Intentions in Service Environments, *Journal of Retailing*. 76 (2), 193-218.

Fornell, C. (1992). A national customer satisfaction barometer: *The Swedish experience, Journal ofMarketing*, 56(1), 1–18.

Fornell, C., Johnson, M., Anderson, E.W.,Cha, J.,& Bryant, B.E. (1996). The American Customer Satisfaction Index: Nature, purpose, and findings, *Journal of Marketing* 60(4), 7-18.

Glorfeld, L.W. (1995). An improvement on Horn's parallel analysis methodology for selecting the correct number of factors to retain. *Educational and Psychological Measurement*, 55, 377-393

Gómez, M.I., McLaughlin, E.W., & Wittink, D.R. (2004).Customer satisfaction and retail sales performance: an empirical investigation, *Journal of Retailing*, 80(4): 265-278.

Guttman, L. (1954). Some necessary conditions for common-factor analysis. *Psychometrika*, 19, 149–161.

Horn, J. L. (1965). A rationale and test for the number of factors in factor analysis. *Psychometrika*, 30, 179-185.

Jöreskog, K.G., & Sörbom, D. (1993). *LISREL 8: A guide to the program and applications*. Chicago, IL: Scientific Software International.

Kaiser, H. F. (1960). The application of electronic computers to factor analysis. *Educational and Psychological Measurement*, 20, 141–151.

Lovelock, C. (2001). A retrospective commentary on the article new tools for achieving service quality *Cornell Hotel Restaurant Administration Quarterly*, Vol. 42 (4).

Mak, B.L., & Sockel, H. (2001). A confirmatory factor analysis of IS employee motivation and retention, *Information and Management*, 38, 265-76.

Menon, K., & Dubé, L. (2000). Engineering effective interpersonal responses to consumer emotions for higher satisfaction, *Journal of Retailing*, 76 (3), 285–307.

Noyan, F.,& Şimşek,G.G. Structural Determinants of Customer Satisfaction in Loyalty Models: Turkish Retail Supermarkets. *Procedia-Social and Behavioral Sciences Journal* (Accepted for publication purpose).

O'Connor, B. P. (2000). SPSS and SAS programs for determining the number of components using parallel analysis and Velicer's MAP test. *Behavior Research Methods, Instruments, & Computers*, 32, 396-402.

Okumuş A., & Temizler, Z. (2006). Süpermarket müşterilerinin mağzaya olan bağımlılık derecelerine göre pazar bölümlerinin tanımlanması ve bölümler arasındaki farklılıkların incelenmesi. *Yönetim*,17(54), 46-61.

Oliver, Richard L. (1989). Processing of the Satisfaction Response in Consumption. *Journal of Consumer Satisfaction, Dissatisfaction and Complaining Behaviour*, 2, 1-16.

Preacher, K.J., & MacCallum, R.C. (2003). Repairing Tom Swift's electric factor analysis machine. *Understanding Statistics*, 2, 13-43

Sirohi N., Mclaughlin E.W., Wittink D.R.(1998). A Model of Consumer Perceptions and Store Loyalty Intentions for a Supermarket Retailer. Journal of Retailing. 74(2).223-245.

Şimşek, G. G., & Noyan, F. (2012). McDonald's ω_t, Cronbach's α, and generalized θ for composite reliability of common factors structures. *Communication in Statistics: Simulation & Computation*, accepted.

Velicer, W. F. (1976). Determining the number of components from the matrix of partial correlations. Psychometrika, 41, 321-327.

Wood, J. M., Tataryn, D. J., & Gorsuch, R. L. (1996). Effects of under- and overextraction on principal axis factor analysis with varimax rotation. Psychological Methods, 1, 254-365.

Zwick, W. R., & Velicer, W. F. (1982). Factors influencing four rules for determining the number of components to retain. *Multivariate Behavioral Research*, 17, 253-269.

Zwick, W. R., & Velicer, W. F. (1986). Comparison of five rules for determining the number of components to retain. *Psychological Bulletin*, 99, 432-442.

Asymmetric Encryption / Decryption with Pentor and Ultra Pentor Operators

Artan Luma, Bujar Raufi, Xhemal Zenuni

Faculty of Contemporary Sciences and Technologies, South East European University
Ilindenska nn, 1200, Tetovo, Macedonia
{a.luma, b.raufi, xh.zenuni}@seeu.edu.mk

Abstract: Finding new approaches for asymmetric encryption / decryption process represents a milestone in cryptographic research and development. In this paper we introduce new algorithm for asymmetric encryption by utilizing two mathematical operators called Pentors and Ultra Pentors. The public and private key in this algorithm represent a quadruple of parameters which are directly dependent from the above mentioned operators.
The strength of the algorithm resides in the inability to find the respective Pentor and Ultra Pentor operator from the mentioned parameters.

Keywords: Asymmetric encryption, Asymmetric decryption, pentor

Introduction

The introduction of public-key cryptography is often attributed to Diffie and Hellman, presented in ”new directions in cryptography” (Diffie & Hellman, 1998), where they described the usage of one way functions, and notions of trapdoor permutations in cryptography to which group belongs the public-key cryptosystem as well where there is a hidden trapdoor which enables the decryption to the legitimate party (Vaudenay, 2006).
A cryptosystem which is consisted of set of enciphering transformations $\{E_e\}$ and of deciphering transformations $\{D_g\}$ is called a public-key cryptosystem or an asymmetric cryptosystem if for each particular key pair $(e; d)$, the enciphering key e is publicly available called the public key, whilst the deciphering key d, called the private key, is being kept secret. The mentioned cryptosystem must satisfy the fundamental property of infeasibility to compute d from e (Mollin, 2007).
In (Luma & Raufi, 2009) and (Luma & Raufi, 2010) we have introduced two new operators as mathematical models that can be used in cryptography
and in many other ideas as well. The contribution of this paper is that through these mathematical operators we are capable of creating and implementing powerful asymmetric encryption/decryption algorithm that can be utilized in many security systems such as banking systems, database security etc. We coin these two operators as Pentor and Ultra Pentor accordingly.

Pentor Operator

We can introduce the Pentor of an integer number n with base B. For every integer number n there exists one Pentor for the given base B. For representing this operator mathematically, we are going to start from modular equation for Pentor of an integer number n with base B that fulfills the condition $\gcd(n, B) = 1$.
Considering the above mentioned conditions we could have:

$$B^m \cdot P(n) \equiv 1 (mod\ n) \qquad (1)$$

Where B is the base of the integer number n, $P(n)$ is the Pentor for the integer number n and m represents the order of the Pentor $P(n)$ for the integer number n. The modular expression (1) can be also transformed to the equality expressions of the form:

$$B^m \cdot P(n) = 1 + n \cdot k \qquad (2)$$

$$P(n) = \frac{1 + n \cdot k}{B^m} \qquad (3)$$

where k is an integer number that fulfils the condition for the fraction to remain an integer number. For example if we want to find the Pentor of the first order than, $m = 1$ the Pentor of the second order $m = 2$ and so on.

Ultra Pentor Operator

The definition of Ultra Pentor of a number n with base B is that for every natural number n there exist an Ultra Pentor operator for the given base B. The mathematical definition of an Ultra Pentor operator begins from modular equation of Ultra Pentor of integer number n with base B that satisfies the condition $gcd(n, B) = 1$. Considering the above mentioned conditions, the modular equation of Ultra Pentor is given as (Luma & Raufi, 2009):

$$B^m \equiv 1(mod\ n) \qquad (4)$$

where m is an integer number. From the modular expression 4, a transformation to equality expression is possible by applying logarithmic operations on both sides and finding the Ultra Pentor given in the form as:

$$B^m \equiv 1 + n \cdot l \mid \cdot log_B \qquad (5)$$

$$log_B B^m = log_B(1 + n \cdot l) \qquad (6)$$

$$m \cdot log_B B = log_B(1 + n \cdot l) \qquad (7)$$

where we will have :

$$m = log_B(1 + n \cdot l) \qquad (8)$$

If $m = UP(n)$, then Ultra Pentor of integer number n with base B can be written as:

$$UP(n) = log_B(1 + n \cdot l) \qquad (9)$$

In the above mentioned equation, l is an integer number that fulfils the condition for $(1 + n \cdot l)$ to be written as B^a, where a is also an integer number. The rest of the work is organized as follows: In section 2 a mathematical outline of the new asymmetric encryption algorithm is being outlined. In section 3, a case study of the functioning of the proposed algorithm with an example is depicted and finally, section 4 concludes this paper with some future directions and proposals.

New Asymmetric Encryption/Decryption Algorithm

Let us chose at the beginning a natural number n, from which we generate the Pentor and Ultra Pentor by using equations 3 and 9. Now, a prime number p is chosen from which we find its primitive root and name it as α.
Let us define a function γ written as:

$$\gamma = n \cdot p \cdot UP(n) \qquad (10)$$

The resulted value from the function γ is being checked by the number of digits it has and its digits are chopped" by the value of Ultra Pentor. All the "chopped pieces" are summed between each other and if the sequence is again longer than the value of Ultra Pentor the process is repeated until the sequence's length is less or equal to the value of Ultra Pentor. The digits of the produced sequence are right shifted by one place, resulting in non-repeating combination of sequences out of which we generate a block with length no greater than that of the value of Ultra Pentor.
Let us choose a value a which represents one of the sequences taken from the above mentioned block. Now, we define a function β written as:

$$\beta \equiv \alpha^a(mod\ p) \qquad (11)$$

After the above mentioned apparatus we define the public key as quadruples $(p, \alpha, \beta, P(n))$ while the secret key as $(n, UP(n), \gamma, a)$.
The overall process of communication through a secure line with above proposed approach goes as follows:

1) Adam sends to Eve the public key with quadruples $(p, \alpha, \beta, P(n))$.
2) Eve calculates a parameter:
$$r \equiv \alpha^{P(n)}(mod\ p)$$
3) Eve also calculates the ciphertext:
$$t \equiv \beta^{P(n)} m(mod\ p)$$
where m is the message.
4) Now, Eve sends a pair (r, t) to Adam.
5) Adam, after receives the pair (r, t) by using its secret key finds the message as:

$$m \equiv t \cdot r^{-a} (mod\ p)$$

Proof:

$$t \cdot r^{-a} \equiv \beta^{P(n)} \cdot m \cdot (\alpha^{P(n)})^{-a} \equiv$$
$$\equiv (\alpha^{a})^{P(n)} \cdot m \cdot (\alpha^{-a})^{P(n)} \equiv$$
$$\equiv \alpha^{a \cdot P(n)} \cdot m \cdot \alpha^{-a \cdot P(n)} \equiv m\ (mod\ p)$$

A Case Study

Let us illustrate the above stated algorithm through a real life example. Initially, let us adopt the value of $n = 13$. We find the value of $P(n)$ and $UP(n)$ as stated in equations 3 and 9 as follows:

$$P(13) = \frac{1 + 13 \cdot 3}{10} = 4$$
$$UP(13) = log_{10}(1 + 13 \cdot 76923) = 6$$

Now, if we adopt a prime number $p = 22621$ and by finding the primitive root of p to be $\alpha = 2$, the γ function, as seen from equation 10, can be calculated as:

$$\gamma = n \cdot p \cdot UP(n) = 13 \cdot 22621 \cdot 6 = 1764438$$

By taking the value of function γ and by "chopping" its digits from the right side by the value of $UP(n)$ which in our case is 6.

$$1 \mid 7\ 6\ 4\ 4\ 3\ 8$$

After we perform addition of these two blocks we get:

$$1 + 764438 = 764439$$

The non-repeating combination of the above presented value by doing a right shift as given in the algorithm above, results in a block as given below:

$$\begin{pmatrix} 7 & 6 & 4 & 4 & 3 & 9 \\ 6 & 4 & 4 & 3 & 9 & 7 \\ 4 & 4 & 3 & 9 & 7 & 6 \\ 4 & 3 & 9 & 7 & 6 & 4 \\ 3 & 9 & 7 & 6 & 4 & 4 \\ 9 & 7 & 6 & 4 & 4 & 3 \end{pmatrix}$$

By taking one of these combination and assigning to a, in a concrete case $a = 397644$ and calculating the function β as given in equation 11 we will have:

$$\beta \equiv \alpha^{a} \equiv 2^{397644} \equiv 17011 (mod\ 22621)$$

If we return to the above elaborated steps of encryption/decryption with calculated values here, for a simple message like **"art"**, which has been converted to numbers based on letters from English alphabet (Luma & Zeqiri, 2008) the process will go as follows:

1) Adam sends to Eve the public key through quadruple $(22621, 2, 17011, 4)$.
2) Eve calculates a parameter:

$$r \equiv 2^{4} \equiv 16 (mod\ 22621)$$

3) Eve also calculates the ciphertext:

$$17011^{4} \cdot 11820 \equiv 588 (mod\ 22621),$$

where $m = 11820$ is the message.

4) Now, Eve sends a pair $(16, 588)$ to Adam.
5) Adam, after receives the pair $(16, 588)$ by using its secret key finds the message as:

$$m \equiv 588 \cdot 16^{397644} \equiv 11820 (mod\ 22621)$$

The strength of this algorithm consists in the secret key because of the parameter a which is dependent from the function γ, while function is dependent from the Ultra Pentor itself. If an intruder intersects the encrypted line, he does not possess the parameter a which in our case, as explained in step 5 of our algorithm is a private key which only Eve possesses.

Conclusion and Future Work

In this paper we have introduced new algorithm for asymmetric encryption / decryption by utilizing two mathematical operators called Pentors and Ultra Pentors. The strength of the proposed algorithm lies in the quadruples of parameters used as public as well as private keys.
Future work and development would involve the creation of electronic certificate which can be used in many aspects of everyday life such as: e-commerce, banking transactions, electronic signatures etc.

References

Diffie, W, & Hellman, M (1998). New directions in cryptography. *IEEE Transactions on Information Theory*,
Luma, A, & Raufi, B (2009). New data encryption algorithm and its implementation for online user authentication. *Security and Management*, 81-85.
Luma, A, & Raufi, B (2010). Relationship between fibonacci and lucas sequences and their application in symmetric cryptosystems.*4th International Conference on Circuits, Systems and Signals*, 146-150.
Luma, A, & Zeqiri, N (2008). Data encryption using an algorithms implemented in RSA algorithm. *International Conference in Information Systems Security*, 146-149.
Mollin, R.A (2007). *An Introduction To Cryptography*. Chapmann & Hall.
Vaudenay, S (2006). *Classical introduction to cryptography: Applications for Communications Security*. Springer Science & Business Media, Inc.

Demonstration of an Electrospray Injection System

Mahmut Can Karakaya [1], M. Ragıp Abdullahoğlu [2], Onur Tunçer [1], Hüseyin Kızıl[2], Levent Trabzon[3]

[1] Istanbul Technical University, Faculty of Aeronautics and Astronautics
[2] Istanbul Technical University, Faculty of Chemistry and Metalurgy
[2] Istanbul Technical University, Faculty of Mechanical Engineering
karakayama@itu.edu.tr, mragipabdullahoglu@gmail.com, tuncero@itu.edu.tr,
kizilh@itu.edu.tr, levent.trabzon@itu.edu.tr

Abstract: The use of liquid hydrocarbons as a chemical energy source is promising for the actualization of high energy density power sources in the near future. Electrospray injection method is a unique technique that provides equal droplet size distribution at very low flow rates. Therefore it is quite suited for the atomization of liquid hydrocarbon fuels in miniature energy conversion devices. This study reports the design and characterization of an electrospray system. First, the electrospray phenomenon is briefly discussed from an historical perspective. An experimental test rig is built and a proof-of-concept demonstration is provided. For the experiments methanol is used as the liquid fuel. Flow visualization is performed to identify the electrospray mode. Results suggest that a Taylor cone is cone formed when voltage is applied to the system. After a certain voltage threshold electrostatic forces overcome the surface tension forces and droplets begin to separate from the Taylor cone. For voltage values higher than 6 kV certain instabilities are observed. Starting voltage for the current configuration is measured to be 2.2 kV. This value is in close agreement the theoretical calculations which suggest that the starting voltage would be 2.5 kV. This 12% discrepancy can be attributed to experimental uncertainty. Flow rate from a single injector is found to be on the order of 2 ml/h. Therefore in order to utilize electrospray injection in practical power conversion devices manufacturing of high nozzle density multiplexed emitter arrays are needed.

Key words: Electrosprey, injection system

Introduction

Liquid hydrocarbons have a much higher energy density than conventional batteries. For example; a typical liquid hydrocarbon has an energy density around 42 MJ/kg, on the other hand a lithium battery can only store about 0.6 MJ/kg (Deng et al. 2007). For this very reason, batteries that work with liquid hydrocarbons can make a technological breakthrough in this field. Even if, these systems have low energy conversion efficiency (i.e. thermal to electric), they can produce much more electrical energy per unit battery weight. Thus, these devices would be quite suitable for military and aerospace applications due to their light weight and size.

In micro scale systems, fuel must be in liquid phase, to get the desirable energy density. Gaseous fuel is simply not an option. Liquid fuel must be atomized, be injected into the combustion chamber and mixed with air. Electrospray injection is a suitable method for liquid injection within micro scale devices.

Electrospray injection is a unique technique suited for very low flow rates, which can assure a uniform spray and droplet size distribution. This technique relies on the ionization of conductive liquids under strong electrostatic fields. Meniscus occurs on the conductive liquid's surface whenever the liquid is affected by the presence of an electric field. This in turn causes electrostatic pressure on the free surface of the liquid. The surface tension of the liquid manages to neutralize the effect of electrostatic pressure. For weak electric fields, meniscus effect on the liquid surface is not much pronounced, however when stronger fields are applied, the liquid surface assumes a conical form. Finally, when a sufficiently strong electric field is applied to the system, electrostatic forces overcome surface tension forces, as a consequence separation from tip of the cone occurs. This phenomenon is termed as electrospray ionization (Krpoun, 2009).

Electrospray can be described with two different phenomena. The first one is a phenomenon where an electric field is used to charge pneumatically or mechanically sprayed droplets. The second one results from the use of the electric field in order to generate a spray from the fluid surface. This latter phenomenon has been given the name "electro-hydrodynamic spraying" (Cloupeau and Prunet-Forch, 1994). This paper deals with electro-hydrodynamic spraying.

First observations of this electro-hydrodynamic spraying phenomenon were conducted by John Zeleny in 1914. His experiments were done in air and he used a single glass capillary for spraying. He used diluted hydrochloric acid, ethanol and glycerin as the conductive liquid.

Later on in the 1930's, Macky conducted research about behavior of water droplets in strong electric fields. In 1965, Taylor found the semi vertical angle of cone at the tip of capillary to be about 49^{o}.

Zeleny's phenomenon was first fully described by Dole in 1968. Furthermore, in 1992, Fernandez de la Mora's solution explains the observed departure of the liquid cone angles from the spray-free value of 49^o and predicts the droplet density as a function of position.

Practical applications are quite new. For example, in 1989 Fenn et al. used electrospray technique in mass spectrometry. This invention won the Nobel Prize for J. B. Fenn in 2002. Besides, electrospray technique is also used in aerospace applications, such as thrust and orbital control (Valesquez-Garcia, BGLF et al., 2008).

For many applications a single electrospray emitter cannot provide the required flow rate alone. Therefore it is often necessary to multiplex emitter arrays. Manufacturing of high density nozzle arrays is possible through state-of-the-art MEMS technology. For example, Kegi Tang et al. (2001) manufactured a multiplexed electrospray system with silicon micro fabrication and used it for mass spectrometry applications. Bocagnera et al. fabricated and tested an electrospray system with 115 source/cm^2 density using a conventional CNC drilling method in 2005. This study proves that, there is no difference of flow rates between a single electrospray and a nozzle of multiplexed electrosprays. 1024 emitters within an area of 0.64 cm^2 were manufactured and tested by Valesquez-Garcia for satellite thruster applications. Deng et al. (2007) manufactured a miniaturized ceramic combustor which has the same order of magnitude volumetric heat release rate with conventional gas turbines. This device is only 0.22 cm^3 in volume. In 2009, Deng et al. fabricated an electrospray system with 11,547 nozzles/cm^2 density. To date this value is highest nozzle density value reported in the open literature.

This paper is organized as follows; first the electrospray theory is briefly presented, and then a proof-of-concept demonstration is provided. Thereafter, the experimental results are compared against theoretical predictions. Finally, the paper concludes with a discussion section.

Mathematical Model

Taylor explained the behavior of liquids issuing from the end of a thin tube due to electrostatic forces. He is the first to observe a conical form at the tip of the capillary needle when the charged liquid is attracted towards a ground electrode. This conical tip is named after him as the "Taylor cone". Taylor experimentally found that the cone half angle was 49.29^o (Taylor, 1964). Later on he mathematically proves that, this angle is independent of fluid properties, applied voltage or the distance between the capillary and the ground electrode (Taylor, 1964).

Should a sufficiently strong electric field be applied to the system, electrostatic forces overcome the surface tension forces, as a consequence separation from tip of the Taylor cone occurs. The resulting flow is the so called cone jet. Starting voltage corresponding to this condition is provided in Eqn. (1).

$$V_{OC} = \sqrt{\frac{\gamma r_t}{\in_0}} \ln\left(\frac{4d}{r_t}\right) \tag{1}$$

In the above expression (Eqn. 1), γ is the surface tension, r_t the radius at the tip of a hyperboloid needle and $\in_0$ is the permittivity of free space. Note that the free space permittivity constant is 8,854x10^{-12} C^{2}N^{-1}m^{-2}. Finally, d is the distance between tip of the capillary and the ground electrode. This mathematical relationship provides the minimum voltage needed to separate droplets from the tip of the Taylor Cone. When these droplets separate from the Taylor cone and fly towards the ground electrode the circuit is completed.

The minimum flow rate to start the electrospray operation is provided by Eqn. (2). Here ϵ denotes the dielectric constant, K the conductivity and ρ the density of the liquid. This is the flow rate corresponding to the starting voltage.

$$Q_{\min} = \frac{\gamma \in \in_0}{\rho K} \tag{2}$$

The current of the system can be obtained with Eqn. (3). Inversely by measuring the electrospray current the flowrate can be obtained as well. Note that this releationship has been experimentally verified by Fernandez de la Mora (1994).

$$I = f(\in)\sqrt{\frac{\gamma Q K}{\in}} \tag{3}$$

The function f appearing in Eqn.3 is the derivative of the dimensionless spray current with respect to the dimensionless flow rate variable. It turns out that this derivative is only a function of the dielectric constant. Consequently, results from different liquids can all be collapsed into a single line. This result is quite important as it allows the indirect measurement of the electrospray flow rate via the current whose measurement is rather trivial. For further discussion reader is kindly referred to the extensive study of de la Mora (1994).

Experimental Setup

A photographic view of the experimental setup is provided in Figure 1. A glass capillary tube of 0.1 mm inner diameter was used for electrospray injection. A syringe pump is utilized for bringing the liquid towards the tip of the needle. 1/8" O.D. tubing is used for connections between the capillary tube and the syringe pump. The liquid is positively charged by a high voltage DC power supply. The applied voltage is varied between 0-8 kV throughout the experiments. A ground electrode made of a conductive sheet metal is placed within a distance from the capillary needle.

Images of electrospray injection are recorded by a CCD camera. A far field microscope with a focal length of approximately 20 mm is mounted in front of the camera in order to increase the spatial resolution of the images. In this study, 10x and 20x magnification lenses are mounted onto the far field microscope. Also note that, the CCD camera was mounted onto a two axis traverse. Another traverse can be used for vertical adjustments (i.e. the distance between the capillary tube and the ground electrode). Therefore, the camera can move in all three directions for capturing desired images.

A digital multimeter is used to measure the electrospray current. A 10 kΩ control resistance is connected between the negative electrode and the ground (see Figure 2). Voltmeter is shunted to this resistance (see Figure 2). The electrospray current is inferred from the voltage drop across this control resistance. The experiments were carried out with methanol as the dielectric liquid. Physical properties of methanol are summarized in Table 1.

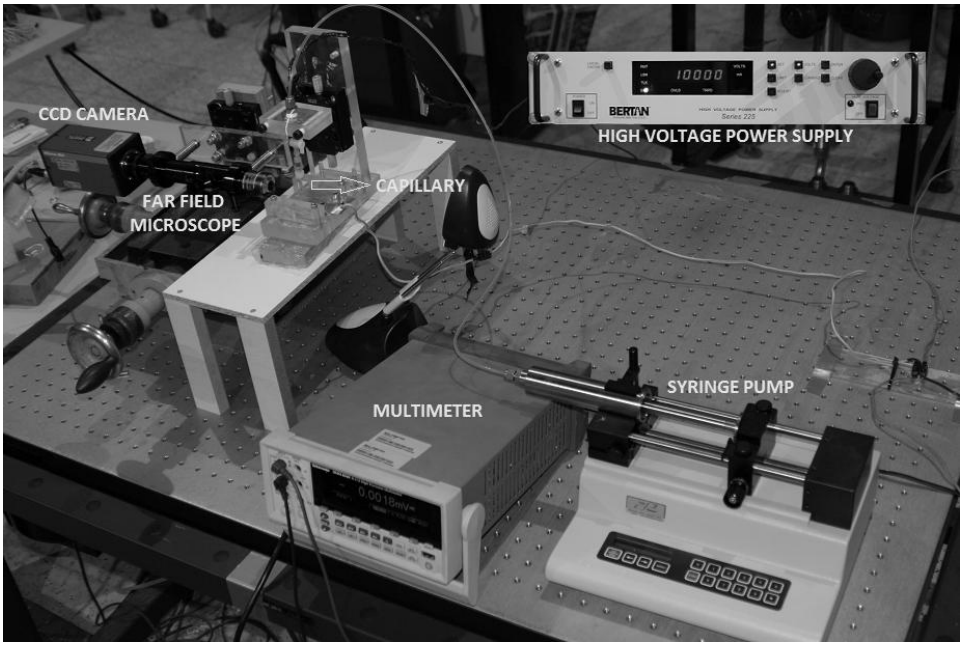

Figure 1 Experimental setup

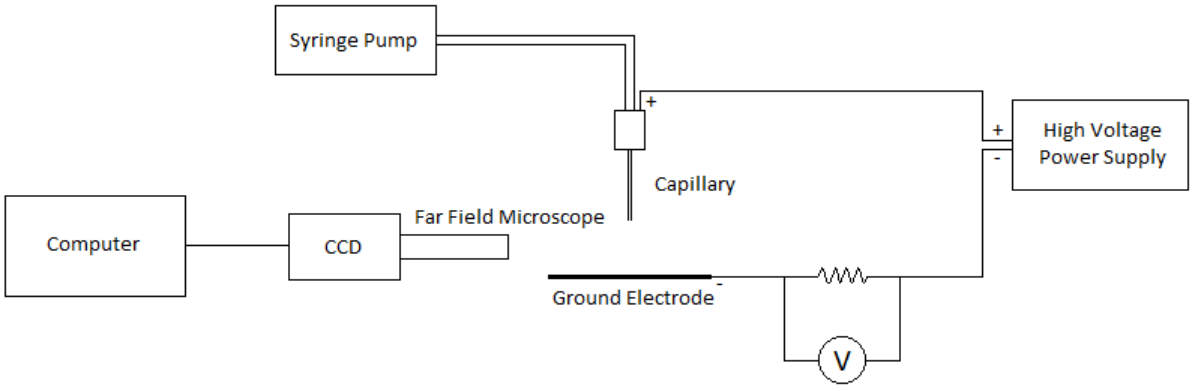

Figure 2 Schematic view of the experimental setup

Table 1. Physical properties of methanol

Density (kg/m^3)	Surface Tension (N/m)	Relative Permittivity	Conductivity ($S.m^{-1}$)
791.3	0.023	33.1	2.1×10^{-7}

Results

Note that as mentioned previously the syringe pump in the test rig is only utilized to bring the liquid towards the tip of the capillary tube. Consequently, electrospray occurs without infusion from the syringe pump, only with the applied potential difference.

Theoretical starting voltage value is calculated via Eqn. 1 for 15 mm distance between the tip of the capillary tube and ground electrode and methanol as the dielectric liquid. The theoretical value for the current configuration is 2.5 kV.

Experiments were carried out with voltage values are applied between 0-6 kV at 0.5 kV intervals. Electrospray views in different voltages are provided in Figure 3. In this experiment syringe pump was adjusted to 1 ml/h flow rate and distance between tip of the capillary and ground electrode is 15 mm. Besides, methanol was used as a fuel. When 1.5 kV was applied to the system, droplets were separated from the Taylor Cone. If the applied voltage is increased, length of the tip of the Taylor Cone approaches to the ground electrode. In our system, Taylor Cone combines at 3.5 kV and flow of electrospray becomes stable. This stabilization can be seen between 3.5 kV and 6 kV in Figure 3. Two sided flow can be seen in 5, 5.5 and 6 kV. The reason is that the ground electrode is rather wider from the diameter of capillary and consequently the shape of the consisted magnetic field is affected. In the frames corresponding to 6.5 and 7 kV test cases the image resolution turns out to be somewhat poor, since the capillary tube which is secured to the test rig like a cantilever beam cannot stand the electrical forces and starts to vibrate.

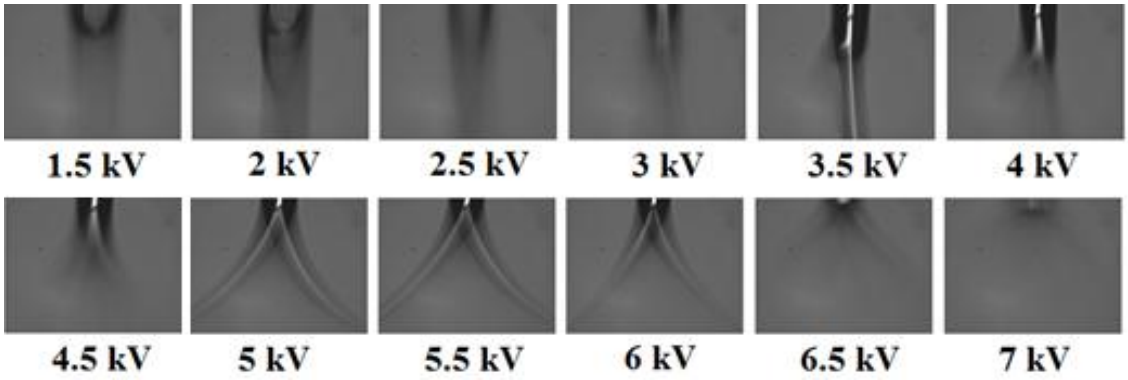

Figure 3 Electrospray views for diferent electric field intensities

In Figure 4, the electrospray current is plotted as a function of potential difference between the charged liquid and the ground electrode. Results indicate a linear trend between the applied voltage and the electrospray current. A trend line is also plotted in Figure 4. The correlation coefficient of the line fit is R^2=0.99. The intersection point of curve fit and x-axis corresponds to the starting voltage of the system. As seen in the figure this value is about 2.2 kV. Note that when the electrospray initializes there is a sudden jump in the voltage drop across the shunt resistance. It is also possible to infer the starting voltage from this sudden jump.

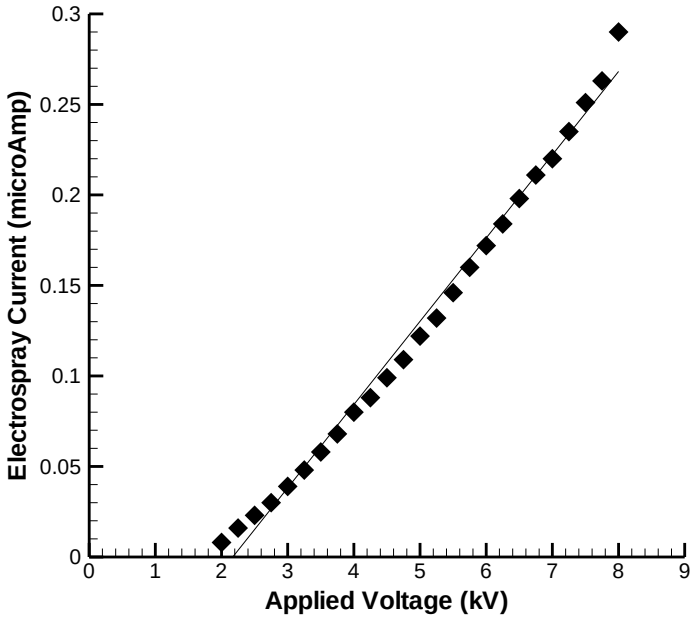

Figure 4 Electrospray Current versus Applied Voltage

Electrospray flow rate was calculated with Eqn. (3). In this equation, all values, expect $f(\in)$ is known from Table 1. $f(\in)$ values vs. $\in$ for pure solvents is plotted by Fernandez de la Mora in 1994. Relative static permittivity for methanol is 33.1, and this value corresponds to $f(\in)$ =15. Thus, electrospray current vs. electrospray flow rate is plotted in Figure 5.

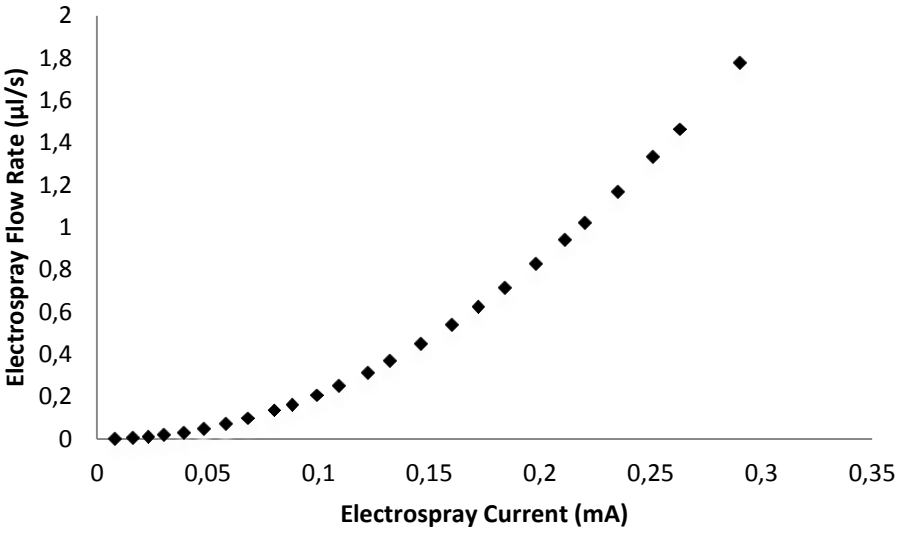

Figure 5 Electrospray Current vs. Electrospray Flow Rate

Discussion

Starting voltage for methanol was found 2.5 kV theoretically and 2.2 kV experimentally. This 12% difference can be attributed to experimental uncertainty. Electrospray views in Figure 3 proves that the experimental system works properly and concludes the proof-of-concept demonstration of an electrospray injection system. Prospective studies shall focus on the manufacturing of dense electrospray emitter arrays. This experimental setup will be used and a similar set of experiments shall be performed for a compact multiplexed electrospray array manufactured with MEMS technology.

Flow rate from a single emitter is on the order of 2 ml/h. This barely corresponds to 17 W of thermal power for a typical liquid hydrocarbon fuel. Typical energy conversion efficiencies of thermoelectric generators are about 4% with the current state of the art. This would correspond to 0.67 W of electric power from a single emitter. For a 100 W electric power output, one would need about 150 emitters. Therefore it is imperative to use a multiplexed array of fuel emitters. Manufacture of high

density nozzle arrays is possible with the utilization of MEMS technology. Ongoing efforts at the ITU-MEMS laboratory aims at manufacturing electrospray emitter arrays at a density of 1000 nozzle/cm2. This suggests that for one centimeter square area of the emitter array 17 kW of thermal power can be generated. This thermal power can then be converted to electric power via a thermoelectric energy conversion system.

Acknowledgement

The authors would like to express their sincere gratitude to the Turkish Scientific and Technological Research Council (TÜBİTAK) for funding this research activity under Contract No: 109M449. The support received from Istanbul Technical University Institute of Science and Technology (İTÜ FBE) is also gratefully acknowledged.

Nomenclature

d	Distance between tip of capillary and ground electrode [m]
Q	Volumetric flow rate [m^3/s]
K	Conductivity [S/m]
r_t	Radius at the tip of a hyperboloid needle [m]
V	Voltage [V]
V_{oc}	Electrospray starting voltage [V]

Greek Letters

γ	Surface tension [N/m]
$\in$	Dielectric constant
$\in_o$	Permittivity of the free space [C^2/Nm2]
ρ	Density [kg/m^3]

References

Bocanegra R., Galan D. Marquez M., Loscertales I.G., Barrero A., (2005), "Multiple electrosprays emitted from an array of holes", *Journal of Aerosol Science*, **36**, 1387-1399

Cloupeau, M. and Prunet-Foch, B. (1994), "Electrohydrodynamic spraying functioning modes: a critical Review", *Journal of Aerosol Science*, **25**, 1021.

Deng, W., Klemig, J.F., Xiaohui,L., Reed, M.A., Gomez,A., (2007), "Liquid Fuel Microcombustor Using Microfabricated Multiplexed Electrosprey Sources", *Proceedings of the Combustion Institute*, **31**, 2239-2246.

Deng, W., Waits, C.M., Morgan, B., Gomez, A., (2009), "Compact Multiplexing of Monodosperse Electrosprays", Aerosol Science, 40, 907-918.

Dole, M., Mach, L.L., Hines, R.L., Mobley, R.C., Ferguson, L.D., Alice, M.B., (1968), "Molecular Beams of Macroions", *J. Chem. Phys*., **49**, s. 2240-2247

Fenn, J. B., Mann, M., Meng, C.K., Wong S.F., Whitehouse, C.M., (1989), "Electrospray Ionization for Mass Spectroscopy of Large Molecules", *Science*, **246,** 64-71

Fernandez de la Mora, J. (1992)," The effect of charge emission from electrified liquid cones", *J. Fluid Mech*. **243**, 561–574.

Fernandez de la Mora, J., Loscertales I. G. (1994), "The current emitted by highly conducting Taylor cones", *J. Fluid Mech.*, **260**, 155-184

Javorek A. (1998), "Main modes of electrohydrodynamic spraying of liquids", Third International Conference on Multiphase Flow, Lyon, France. Retrieved from: http://www.imp.gda.pl/fileadmin/old_imp/ehd/lyon-98s.pdf

Krpoun, R. (2009), "Micromachined Electrospray Thrusters for Spacecraft Propulsion" (Doctoral dissertation), École Polytechnique Fédérale de Lausanne

Lozano P., Martinez-Sanchez M., (2003), "Studies on the Ion-Droplet Mixed Regime in Colloid Thrusters" (Doctoral dissertation), Massachusetts Instutude of Technology

Macky, W. A. (1931), "Some investigations on the deformation and breaking of water drops in strong electric fields", Proceedings of the Royal Society of London. Series A **133(822)**, 565–587.

Smith, K. L., (2005), "Characterization of Electrospray Properties in High Vacuum with a View to Application in Colloid Thruster Technology", (Doctoral dissertation), University of London

Tang K., Lin Y., Matson D. W., Kim, T., Smith R.D., (2001), "Generation of Multiple Electrosprays using microfabricated emitter arrays for improved mass spectrometric sensitivity", *Anal. Chem*., **73**, 1658-1663

Taylor, G. (1964), Desintegration of water drops in an electric field, Proceedings of the Royal Society of London. Series A, *Mathematical and Physical Sciences* **280(1382)**, 383–397.

Velasquez-Garcia, L. F., Akinwade, A. I., Martinez-Sanchez, M., (2006), A Micro-Fabricated Linear Array of Electrospray Emmiters for Thruster Applications, *Journal of Microelectromechanical Systems*, **15**, 1260-1271

Velasquez-Garcia, L. F., Akinwade, A. I., Martinez-Sanchez, M., (2006), "A planar array of micro-fabricated electrospray emitters for thruster applications", *Journal of Microelectromechanical Systems*, **15**, 1272-1280

Valesques-Garcia BGLF, Akinwande, A., Martinez-Sanchez, M., (2008), Fabrication of a Fully Integrated Electrospray Array with Applications to Space Propulsion, 21st IEEE International Conference on Micro Electro Mechanical Systems (MEMS 2008), 976-979.

Zeleny, J. (1914), The electrical discharge from liquid points and a hydrostatic method to measure electric intensity at their surface, *Phys. Rev*., **3**, 69–91.

Effect of H_2 Reduction on Carbon Nanotube Synthesis

Nazlı Çınar, Neslihan Yuca, Nilgün Karatepe

Energy Institute, Istanbul Technical University, 34469 Maslak, Istanbul, Turkey
nazlicinar2004@yahoo.com, nyuca@itu.edu.tr, kmnilgun@itu.edu.tr

Abstract: Carbon nanotubes (CNTs) with their high mechanical, electrical, thermal and chemical properties are regarded as promising materials for many different potential applications. Chemical vapor deposition (CVD) is a common method for CNT synthesis especially for mass production. There are important parameters (synthesis temperature, catalyst and calcination conditions, substrate, carbon source, synthesis time, H_2 reduction, etc.) affecting the structure, morphology and the amount of the CNT synthesis. In this study, CNTs were synthesized by CVD of acetylene (C_2H_2) on magnesium oxide (MgO) powder substrate impregnated by iron nitrate ($Fe(NO_3)_3 \cdot 9H_2O$) solution. The synthesis conditions were as follows: at catalyst calcination temperatures of 400 and 550°C, calcination time of 0, 15 and 30 min, hydrogen concentrations of 0, 5, 10, 20, 50 and 100 % vol, synthesis temperature of 550°C and synthesis time of 30 minutes. The synthesized materials were characterized by thermal gravimetric analysis (TGA), transmission electron microscopy (TEM), and Raman spectroscopy. Effect of H_2 reduction on catalyst calcination and CNT synthesis were investigated.

Key words: H_2, reduction, carbon nanotubes, CVD, synthesis, fluidized bed

Introduction

Since the carbon nanotubes discovery of by Iijima in 1991 (Iijima,1991), Carbon nanotubes (CNTs) have attracted much attention due to their exceptional electrical, optical and mechanical properties. Therefore, they can be implicated to many fields such as electronics, chemicals, sensors, energy storage, and biotechnology. However, currently major obstacles are present in the application of carbon nanotubes. Specifically, the exact growth mechanism of CNTs and their resulting properties are not yet well understood. Hence, there has been an ungoing effort to understand the growth of CNTs. Various methods were used for carbon nanotubes growth, both single-walled and multi-walled nanotubes (SWNTs and MWNTs), including arc-discharge (ADE) (Maiti et al., 1994), laser beam evaporation (LBE) of graphite (Guo et al. ,1996) and chemical vapor deposition (CVD) of carbon through catalytic decomposition of hydrocarbons (Hernadi et al.2000; Trimm,1977) . The catalytic chemical vapor deposition method is a very efficient technique for the large-scale and low-cost synthesis of carbon nanotubes. Recently, several groups have started academic and engineering researches on the CVD in the fluidized bed reactor process (Pérez-Cabero et al., 2003; Corrias et al., 2003; Qian et al., 2004) based on the catalytic decomposition of carbonaceous gases on a catalytic material that contains transition-metal nanoparticles. For large-scale production, the use of a fluidized bed reactor has been proposed as an alternative to avoid obstruction of the carbon deposited and damage to fixed bed reactor walls (Pérez-Cabero et al., 2003). There are different parameters (synthesis temperature, catalyst and calcination conditions, substrate, carbon source, synthesis time, H_2 reduction, etc.) affecting the structure, morphology and the amount of the CNT synthesised. In the growth of CNTs, it is clear that hydrogen is an essential element having been implicated in a number of surface morphology change of the catalyst. The activity of hydrogen with the hydrocarbon gas is also important. During recent decades, many studies have been reported in this subject (Chang Chung et al., 2004; Kim et al., 2006). In a study conducted with the effect of H_2 addition on synthesis yield of CNT was investigated and the relation between the reduction degree and reaction temperature, the ratio of H_2/CO concentration in the synthesis was observed. It was reported that the high reduction degree of catalyst before synthesis is an essential condition for high yield of CNTs because low reduction degree means the insufficiency of an active catalyst required to make CNTs. Optimum gas flow rate of H_2 on CNT synthesis was determined. Also it was found that when content of H_2 was higher this critical value, the shapes of CNTs became worse due to transition into inactive surface of catalyst (Chang Chung et al., 2004). In another study, the effect of growth temperature on the CNT synthesis was examined with H_2 reduction. It was found that the H_2 reduced the iron oxide to different oxidation states, depending on the time of H_2 introduction. When H_2 was introduced at 200°C, very little growth was achieved. As the H_2 was introduced at 400°C and 600°C, the growth was curbed with very little CNTs resulting on the samples. When H_2 was introduced at 600°C, CNTs were seen only on the edges of the subsrate (Kim et al., 2006).

In this study, the effects of H_2 reduction on catalyst calcination and multi-walled carbon nanotubes (MWCNTs) synthesis were investigated. MWCNTs were produced by CVD of (C_2H_2) on magnesium oxide (MgO) powder substrate impregnated by iron nitrate ($Fe(NO_3)_3 \cdot 9H_2O$) solution. While catalyst calcination and CNTs synthesis, parameters such as calcination temperature and time,H_2% concentration in catalyst calcination and CNT synthesis were optimized to investigate the effects on the carbon efficiency and quality of CNTs. The synthesized materials were characterized by thermal gravimetric analysis (TGA), transmission electron microscopy (TEM), Raman spectroscopy.

Experimental Study

Synthesis of Carbon Nanotubes

Multi-wall carbon nanotubes were synthesized by the fluidized-bed CVD synthesis of acetylene (C_2H_2) on a magnesium oxide (MgO) powder impregnated with an iron nitrate ($Fe(NO_3)_3 \cdot 9H_2O$) solution which has MgO to Fe weight ratio of 5%. The system was composed of a "Protherm" furnace that can operate up to 1100ºC and a quartz reactor with a diameter of 2.5 cm and length of 94.5 cm .In the middle of the reactor is a nano porous silica disc allowing gas flow. The furnace is placed vertically and the quartz reactor is placed in it with the nano porous silica disc placed in the middle of hot region of the furnace. MWCNT synthesis was held on the 5 to 10 cm length region around the quartz disc of the reactor. To fluidize the bed a certain flow rate of gas was necessary for a given substrate catalyst mixture. For this purpose argon was used as carrier and inert gas and acetylene was used as carbon source. The gas was fed to the system through the bottom of the reactor and it left the system from the top. A magnesium oxide (100 $m^2.g^{-1}$) supported iron oxide powder produced by impregnation in an iron nitrate ethanol solution is used as precursor powder. To get a precursor with a MgO to Fe weight ratio of 5%, MgO were suspended in ethanol and iron nitrate ($Fe(NO_3)_3 \cdot 9H_2O$) previously dissolved in 100 ml ethanol was stirred together and sonicated for 20 min in order to homogenize the mixture. Afterwards the precursor was dried and grinded into a fine powder. The catalyst and substrate mixture was placed homogeneously on the disc. For MWCNT synthesis while heating the system to calcination temperatures of 400ºC and 550ºC by an increase of 10°C/min, 100 ml/min argon was fed to the system to maintain inert atmosphere and to make flow of other gases existing in the system. As the temperature reached calcination temperature, H_2 flow started with argon to form reduction on iron oxide catalyst. To investigate the effect of H_2reduction in calcination, hydrogen concentrations in gas mixture were varied as 0, 5, 10, 20, 50 and 100 % vol. Calcination times were selected as 0, 15 and 30 min. After calcination, the furnace was heated to the synthesis temperature (550 °C). The synthesis was started with the introduction acetylene mixed with argon and different H_2 concentrations (0,5, 20 and 50 % vol) for 30 min. After synthesis, the MWCNTs were cooled in inert gas (argon). The total experimental time varied from 2 to 3 h with duration of actual growth stage 45 min. All experimental conditions were given in Table 1.

Table 1. Calcination and synthesis experimental conditions

	Calcination Experiments					Synthesis Experiments			
Exp. No	Ar flow rate (ml/min)	H_2 flow rate (ml/min)	Calcination temp. (°C)	Calcination time (min)	C_2H_2 flow rate (ml/min)	Ar flow rate (ml/min)	H_2 flow rate (ml/min)	Synthesis time (min)	Synthesis temp. (°C)
1	410	0	400	30	41	369	0	30	550
2	410	0	550	30	41	369	0	30	550
3	0	0	550	0	41	369	0	30	550
4	410	0	550	15	41	369	0	30	550
5	369	41	550	15	41	369	0	30	550
6	328	82	550	15	41	369	0	30	550
7	205	205	550	15	41	369	0	30	550
8	0	410	550	15	41	369	0	30	550
9	369	41	550	30	41	369	0	30	550
10	328	82	550	30	41	369	0	30	550
11	205	205	550	30	41	369	0	30	550
12	0	410	550	30	41	369	0	30	550
13	369	41	400	15	41	369	0	30	550
14	328	82	400	15	41	369	0	30	550
15	205	205	400	15	41	369	0	30	550
16	0	410	400	15	41	369	0	30	550
17	369	41	400	15	41	369	0	30	550
18	328	82	400	15	41	369	0	30	550
19	205	205	400	15	41	369	0	30	550
20	0	410	400	15	41	369	0	30	550
21	0	410	550	30	41	348,5	20,5	30	550
22	0	410	550	30	41	287	82	30	550
23	0	410	550	30	41	164	205	30	550
24	0	0	550	30	41	348,5	20,5	30	550
25	0	0	550	30	41	287	82	30	550
26	0	0	550	30	41	164	205	30	550

Characterization of Materials

The synthesized MWCNTs were characterized by transmission electron microscopy (TEM) -FEI-Tecnai-G2 F-20 instrument, raman spectroscopy-Horiba Jobin-YVON HR 800UV instrument and thermogravimetric analyzer (TGA)-TA-Q600 SDT instrument.

Results and Discussion

Structure Characterization of Multi Wall Carbon Nanotube

By the synthesis temperature of 550°C at a fixed iron content of 5%, a synthesis time of 30 min. and acetylene as carbon source the yield was obtained in multi-wall nanotube type. TEM image of this yield was given in Fig. 1. It has obviously been seen from Fig. 1 that the diameter of the CNTs is 10 nm and their appearance is darker in the picture. One possible explanation for the dark parts is a result of the impurities within the structure. This observation lead to a conclusion: in the temperature of 550°C MWNTs were grown.

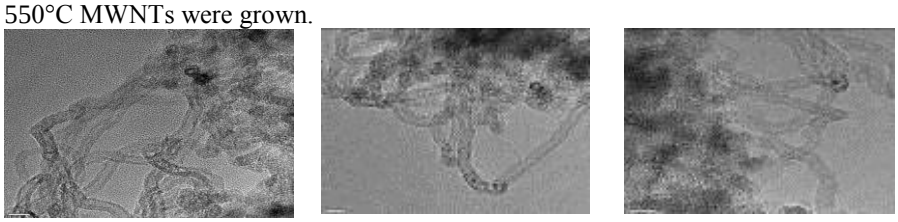

Fig.1. TEM images of MWNTs

Raman spectroscopy is a powerful technique for the characterization of the structure of carbon nanotubes. Fig. 2 shows Raman spectrum for carbon deposits excited by 633 nm laser. As seen from Fig. 2, the spectrum in RBM band which is a characteristic of SWNT was also observed in the sample. The reason of this spectrum which was observed at MWCNT is that the innermost tube diameter was below 2 nm.

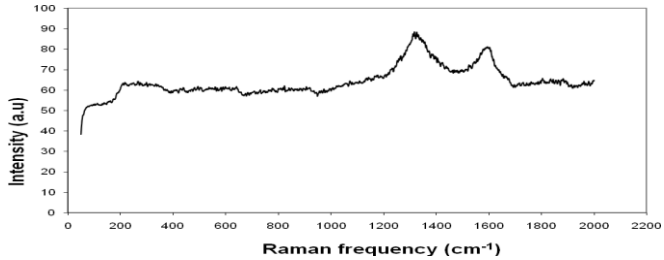

Fig. 2. Raman spectra of MWNT

Effect of Hydrogen Reduction

The effects of H_2reduction were investigated into two parts: catalyst calcination and MWCNT synthesis. The carbon efficiency of the synthesized MWCNTs was calculated according to TGA measurement. In order to eliminate any differences which may be caused due to moisture content of synthesized samples, in the calculations the initial temperature was selected as 200ºC to have the dry weight percent and the final temperature was taken as 800ºC to have the same temperature value for all samples. The formula of carbon efficiency is:

$$Carbonefficiency(\%) = \frac{Weight\%(200^{\circ}C) - Weight\%(800^{\circ}C)}{Weight\%(200^{\circ}C)} \times 100 \quad (1)$$

Thermogravimetric (TG) analysis is used to characterize the total carbon loading and determine the residual metallic catalyst. The amorphous carbon is completely oxidized at temperatures below 350 °C and graphite burns above 750 °C. The oxidation temperatures of the CNTs depend on the nanotube type and MWCNTs is generally oxidized at the temperatures above 400 °C. In this study, the TG analysis of MWNTs was conducted in air atmosphere with a ramp of 10 °C/min between 200 and 800°C. Carbon efficiency (%) of the MWCNTs were obtained from TG analysis. TGA results were given in the Table 2.

Table 2. TGA results of MWCNTs

Exper. No	Calcination Temp. (°C)	Calcination Time (min)	H_2 % in calcination	H_2 % in synthesis	Carbon Efficiency %
1	400	30	0	0	42
2	550	30	0	0	45
3	550	0	0	0	49
4	550	15	0	0	44
5	550	15	10	0	23
6	550	15	20	0	35
7	550	15	50	0	41
8	550	15	100	0	39
9	550	30	10	0	32
10	550	30	20	0	37
11	550	30	50	0	38
12	550	30	100	0	53
13	400	15	10	0	40
14	400	15	20	0	44
15	400	15	50	0	41
16	400	15	100	0	43

17	400	30	10	0	40
18	400	30	20	0	46
19	400	30	50	0	49
20	400	30	100	0	42
21	550	30	100	5	58
22	550	30	100	20	59
23	550	30	100	50	55
24	550	0	0	5	54
25	550	0	0	20	57
26	550	0	0	50	64

Effect of H_2 Reduction on Catalyst Calcination

Calcination Temperature

The effect of calcination temperature on carbon efficiency was examined for 100 % H_2 and two calcination times (15, 30 min). The selected calcination temperatures were 400 and 550ºC. Carbon efficiency (%) of these synthesized materials from TG analysis are shown in Fig. 3. It is seen that there is a tremendous increase in carbon efficiency (from 42% to 53%) of 30 min calcination time whereas there exists a slightly decrease in carbon efficiency of 15 min calcination time (from 43% to 39%).With this result it can be said that with the increase in calcination time there becomes an increase in the carbon efficiency. In summary the order of the carbon efficiency of given temperature of 400ºC for 100% H_2 concentration is 30 min > 15 min , whereas for 550ºC it is 30 min>15 min.

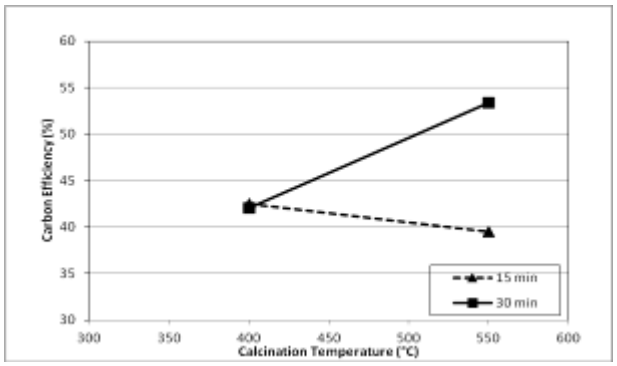

Fig. 3. Calcination temperature vs. carbon efficiency for 100 % H_2

Calcination Time

The effect of calcination time on carbon efficiency was examined for 100 % H_2 and two calcination temperatures (400ºC, 550ºC). The calcination times were selected 15 and 30 min. Carbon efficiency (%) of these synthesized materials from TG analysis are shown in Fig. 4. It is seen that there is a tremendous increase in carbon efficiency (from 39% to 53%) of 550°C calcination temperature whereas there exists a decrease in carbon efficiency of 400°C calcination temperature (from 43% to 42%).With this result it can be said that with the increase in calcination temperature there becomes an increase in the carbon efficiency. In summary the order of the carbon efficiency of given time of 30 min for 100% H_2 is 550°C > 400°C , whereas for 15 min it is 400°C > 550°C.

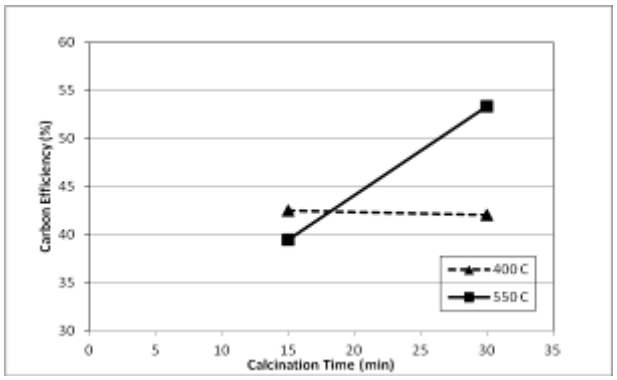

Fig. 4. Calcination time vs. carbon efficiency for 100 % H_2

H_2 Concentration (%) in Calcination

The effect of H_2 concentration on carbon efficiency was examined for calcination time of 30 min and calcination temperatures of 400 and 550ºC. The H_2 concentrations were selected as 10, 20, 50 and 100 %vol. Carbon efficiency of these synthesized

materials from TG analysis are shown in Fig. 5. It is seen that there is a tremendous increase in carbon efficiency (from 32% to 53%) at 550°C whereas there exists an increase in carbon efficiency at 400°C (from 40% to 42%). With this result it can be said that with the increase in H_2 concentration % there becomes an regular increase in the carbon efficiency for 550°C of calcination temperature. Besides this for 400°C calcinations temperature , carbon efficiency increased between 10% and 50% H_2 concentration , then a decrease was found between 50% and 100% H_2 concentration.Depending on these results,it was examined that the highest carbon efficieny % was obtained with 100% H_2 concentration, 30 min calcination time at 550°C calcination temperature.

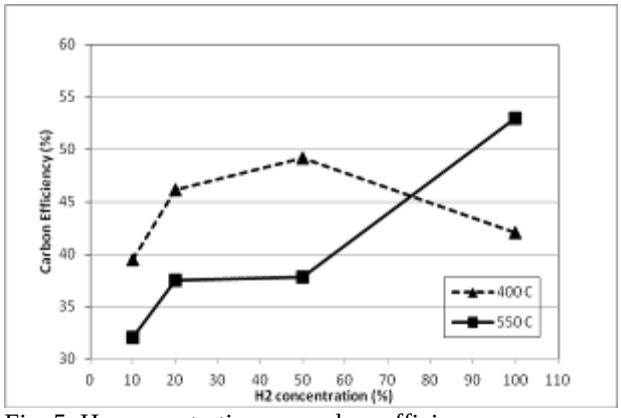

Fig. 5. H_2 concentration vs. carbon efficiency

Effect of H_2 Reduction on CNT Synthesis

According to the TGA results of experiments which were carried out without H_2 reduction (0%) in CNT synthesis, the highest carbon efficieny values were obtained as 49% and 53% at 550°C calcination temperature for 0% and 100% H_2 calcination, respectively (Table 2). To examine the effect of H_2 reduction in CNT synthesis, H_2 was added into synthesis gas with three different concentrations of 5, 20 and 50% vol for 0 and 100% H_2 calcination. Carbon efficiency (%) of these synthesized materials from TG analysis are shown in Fig.6. According to the H_2 concentrations of 5, 20 and 50% vol in the CNT synthesis for 0% H_2 calcination there is a regular increase (from 49 % to 64 %) in carbon efficiency. Also TG analysis showed that for 100% H_2 calcination, there is an increase (from 58% to 59%), then a decrease (from 59% to 55%) in carbon efficiency. As a result of these values, it was found that H_2 concentration (%) in the CNT synthesis is important for increasing of carbon efficiency and this results are consistent with other studies found in literature (Uoo-Chang Chung et al., 2004). In the study of Uoo-Chang Chung et al., they investigated the shapes and structures of CNTs with H_2 addition in CO using a cheap iron oxide catalyst for CNTs synthesis. They found that the synthesized carbon weight increased with H_2 addition, and the value showed maximum in the H_2 gas with a flow rate of 0.7 L/min at 680°C with CO gas of 0,3 L/min. When H_2 value was higher than 0.7 L/min, carbon weight decreased as H_2 contents increase. Also it was found that when content of H_2 was higher than this critical value (0.7 L/min), the shapes of CNTs became worse due to transition into inactive surface of catalyst. It was also found that H_2 addition had an influence considerably on the shape and structure of CNTs.

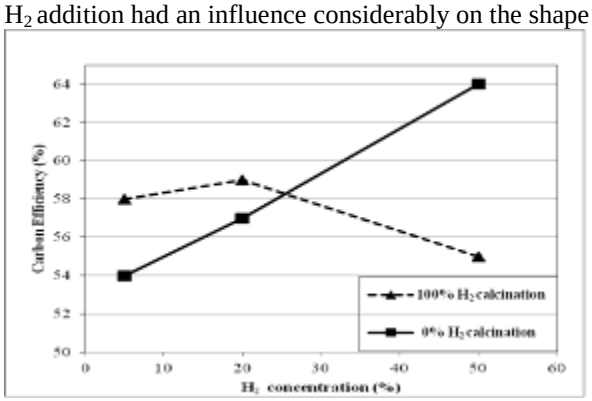

Fig. 6. H_2 concentration vs.carbon efficiency

Conclusions

The present study has shown that calcination temperature, calcination time and H_2 concentration (%) are important parameters in catalyst calcination and MWCNT synthesis. As a result of TGA measurements, at highest calcination temperature (550°C), carbon efficiency (%) was incerased with calcination time (15, 30 min) and H_2 concentrations (10, 20, 50, 100%). In addition to these results, with increase in H_2 concentration (5, 20, 50%) in synthesis gas, higher carbon efficiencies were obtained. Experimental evidences and measurements showed that the carbon efficiencies of synthesized MWCNTs are positively affected with increase the calcination temperature, calcination time and H_2 concentration (%) in CNT synthesis.

References

Chang Chung, Uoo.(2004). Effect of H_2 on formation behavior of carbon nanotubes. *Bull. Korean Chem. Soc*,25,1521-1524
Corrias,M.,Caussat,B.,Ayral,A.,Durand,J.Kihn,Y.,Kalck,Ph.,Serp,Ph.(2003).Carbon nanotubes produced by fluidized bed catalytic CVD: first approach of the process.*Chem. Eng. Sci*,58,4475－4482.
Guo,T., Nikolaev,T.P.,Thess,A.(1996).*Chem.Phys.Lett*,260,471.
Hernadi,K, Fonseca,A., Nagy,J.B.,Siska,A., Kiricsi,I.(2000).*Appl.Catal.A*,199,245.
Iijima, S.(1991).Helical microtubules of graphitic carbon.Nature, 354,56-58
Kim, Jin Suk Calvin.(2006).The role of hydrogen in the growth of carbon nanotubes: a study of the catalyst state and morphology, Massachusetts Institute of Technology,B.Sc.Thesis.
Maiti,A.,Brabec,C.J.,Rol,C.M.,Bernhole,J.(1994).*Phys.Rev.Lett*,73,2468.
Pérez-Cabero,M.,Rodríguez-Ramos, I., Guerrero-Ruíz,A.(2003).Characterization of carbon nanotubes and carbon nanofibers prepared by catalytic decomposition of acetylene in a fluidized bed reactor.*J. Catal*, 215,305-316.
Piao,Lingyu.,Li,Yongdan.,Chen,Jiuling.,Chang,Liu.,Lin,Jerry.Y.S.(2002).Methane decomposition to carbon nanotubes and hydrogen on an alumina supported nickel aerogel catalyst, *Catalysis Today*,74,145-155.
Qian ,W., Liu,T.,Wang,Z.,Wei,F.,Li,Z.,Luo,G.,Li,Y.(2004).Production of hydrogen and carbon nanotubes from methane decomposition in a two-stage fluidized bed reactor. *Appl. Catal. A*,260,223-228.
Trimm, D.L.(1977).*Catal. Rev Sci. Eng*,16,155.
Uoo-Chang C. (2004). Effect of H_2 on Formation Behavior of Carbon Nanotubes. *Bull. Korean Chem. Soc.;25,10:1521*

Effect of Two Lobe Wave Squeeze Film Damper in the Support of an Unbalanced Rigid Rotor

Giovanni Adiletta[a], Erasmo Mancusi[b]

[a]Università degli Studi di Napoli "Federico II", Dipartimento di Ingegneria Meccanica per l'Energetica, Via Claudio 21, 80125 Napoli, Italy
[b]Facoltà di Ingegneria, Università degli Studi del Sannio, Piazza Roma 21, 82100 Benevento, Italy
E-mail: adiletta@unina.it, mancusi@unisannio.it

Abstract: A possible improvement of the performances of squeeze film damper (SFD) for supporting the rotors of high-speed turbomachinery has been sought adopting a two lobe, wave (2LW) geometry of the bearing bore. A statically unbalanced, symmetrical, rigid rotor supported with 2LW-SFD has been theoretically examined through numerical continuation, assuming laminar, isoviscous oil flow within the damping film and incomplete centering action of the retainer springs mounted parallel to the film. Despite nonlinearity which still affects the system, the obtained results highlight the potential of the unconventional geometry as a mean for a possible reduction of the typical drawbacks in the response with conventional SFD, mainly consisting in undesired whirling motions with too large journal orbits and/or nonsynchronous character, so as to assure more safe conditions for the rotor operation. Yet, further theoretical and experimental investigation is desirable in order to confirm such an outcome.

Key words: lubrication, squeeze film damper, rotordynamics, bifurcation.

Introduction

The poor quality and drawbacks which affect the dynamic behaviour of turbomachinery on rigid supports equipped with simple rolling bearings, in terms of forces transmitted to the frame and vibrations, fostered the concept of combining the bearing to an oil film since from the Thirties of the past century (Birmann, 1933). As a device capable to work in this way, in order to assure enough damping to the rotor-system, the squeeze film damper (SFD) has received substantial and systematic scientific attention in the last five decades (Della Pietra & Adiletta, 2002). This huge research work has been mainly addressed to fluid dynamic and structural aspects of the damping device, like oil cavitation and inertia or oil feeding and seals effects, which highly influence the pressure distribution in the film and hence the film forces. The said factors, together with the basic nonlinear character of the film forces, represent a crucial issue as regards the dynamic response of the supported rotor. Here the nonlinearity, possibly exalted under some circumstances, can give rise to undesirable or unexpected whirling motions of the rotor with very large orbits described by the journals within the relative bearings and/or characterized by nonsynchronous nature. General consequences of these effects are high levels of vibrations and force transmissibility, shortening in the life of the bearings, damage of the damper bearing, possible failure of the rotor due to the fatigue mechanism connected to the nonsynchronous whirl. Therefore, a consistent part of the research from literature has been just focused onto the dynamic behaviour of the rotor-support system with SFD, represented by practical or experimental real rotors, often theoretically characterized by very simple flexible or rigid models, provided with supports of the uncentralized or centralized type (Adiletta & Della Pietra, 2002). Regarding to this last option, it is worth mentioning that the rotor journal is let free to whirl within the damping film, i.e. subjected to the only hydrodynamic forces of the squeeze film, or it is further supported by springs which work in parallel to the film and allow a preliminary centering of the journal within the bearing clearance when the rotor is at rest. Nevertheless, the registration of the static position can be carried out in practice with higher or lesser accuracy and the complete, full centering turns out to be only theoretical. Bistable conditions with jump in rigid rotors were investigated, among others, by White (1970) and Hahn (1979). Mohan & Hahn (1974) analyzed the horizontal centralized rotor, where the flexibility of supports is due the spring elements mounted in parallel to the damping film, and pointed out the importance of a critical value of the unbalance beyond which the squeeze film bearing with flexible mount behaved worse than a rigid support. The influence of the initial conditions, when numerical integration is carried out for solving the nonlinear equations of the rotor-support system, was investigated by Taylor & Kumar (1980). They observed on this basis the dominant character of one of the two solutions present in intervals of speed with bistable behaviour. Li & Taylor (1987) showed the coexistence of nonperiodic and synchronous solutions after numerical study of the unbalanced rigid rotor on SFD with centralizing springs. Also, they investigated into the effects of incomplete centering and pointed out the importance of the complex characteristic roots about the degree of attraction of the different coexistent motions. Similar analyses were carried out by Zhao & Hahn (1993) and Zhao et al. (1994) who analyzed the bifurcating behaviour of the rotor system. In the latter paper, successive bifurcations along rotor run up, respectively representing changes from sysnchronous to quasi-periodic, sub-harmonic and again to synchronous whirl, were reported and explained with the study of Floquet multipliers. More recent examples of research works about

nonlinear behaviour of rigid rotors on SFD are represented by Bonello, Brennan, & Holmes (2002), focused onto receptance harmonic balance method that was adopted to determine periodic solutions, and Inayat-Hussain, Kanki, & Mureithi (2003), where the bifurcating dynamics of the nonlinear systems was dealt with by means of a numerical case study and recourse to continuation technique. Besides the rigid rotor case, flexible rotor systems have been extensively study too, especially in the simple symmetrical model with rigid disk, flexible shaft and SFD end supports (Inayat-Hussain, 2009). Furthermore, particular research efforts have been addressed to innovative design of the squeeze damper, in order to improve the dynamic performances of the supported rotor (de Santiago et. al. 1999, El-Shafey & El-Hakim, 2000). In this regard, the present work is aimed to test the adoption of a two lobe, wave (2LW) geometry of the bearing bore, in place of the common circular profile. Such a concept, with adoption of different shapes, is well known in journal bearing design (Pinkus, 1956). The three lobe wave profile, in particular, has been thoroughly investigated for gas bearings application (Dimofte, 1995) putting in evidence its advantages and the present authors have recently focused their attention onto the 2LW geometry for oil lubricated journal bearings (Adiletta, Mancusi, & Strano, 2011). In this case, wave amplitude and angular phase of the profile represent, in respect of the conventional circular geometry, two further parameters that influence the behaviour of the rotor-support system and are possibly at hand to optimize the dynamic response. On this basis, a statically unbalanced, symmetrical, rigid rotor supported with 2LW-SFD has been theoretically examined under the hypotheses of laminar, isoviscous oil flow within the damping film and incomplete centering action of the retainer springs mounted parallel to the film. The analysis has been carried out with use of numerical integration of system equations and continuation algorithm.

The Equations of Motion and the Fluid Film Forces ın the SFD

A statically unbalanced, rigid rotor is in horizontal disposition and supported at each end by roller bearing plus squeeze film damper (SFD) with retaining springs. The whole system is assumed to be symmetrical, so that cylindrical whirl can be assumed for the rotor motion and the following equations are written for a single half of the rotor-support system:

$$\begin{cases} m\ddot{\bar{x}} + \sigma\dot{\bar{x}} + k\,\bar{x} = m\rho\omega^2 \cos\omega t + F_{SFx} \\ m\ddot{\bar{y}} + \sigma\dot{\bar{y}} + k\left(\bar{y} - \bar{y}_S\right) = m\rho\omega^2 \sin\omega t + F_{SFy} \end{cases} \tag{1}$$

Equations (1) are written assuming a reference fixed frame placed in the bearing center, with the $\bar{y}$ axis parallel to the gravity force, upward directed, and $\bar{z}$ direction parallel to the rotor axis. A gravity residual $\bar{y}_S$, due to hypothesized incomplete centering of the springs, is defined as:

$\bar{y}_S = \bar{y}_0 + f_S$,

where f_S represents the static deflection of the spring system, i.e. $f_S = -mg/k$, and $\bar{y}_0$ is the coordinate of journal center of the rotor in the absence of weight. Substitutions:

$$x = \frac{\bar{x}}{C},\ y = \frac{\bar{y}}{C},\ y_S = \frac{\bar{y}_S}{C},\ \omega t = \tau,\ \dot{x} = \frac{dx}{d\tau}\frac{d\tau}{dt} = x'\omega,\ \dot{y} = \frac{dy}{d\tau}\frac{d\tau}{dt} = y'\omega,\ \zeta = \frac{\bar{z}}{L},$$

$$\omega_R = \sqrt{\frac{k}{m}},\quad \Omega = \frac{\omega}{\omega_R},\quad \omega_B = \frac{\mu R L^3}{mC^3},\quad \mathrm{f} = \frac{\omega_B}{\omega_R},\quad U = \frac{\rho}{C},\quad q = \frac{\sigma}{2\sqrt{mk}},$$

$$\lambda = \frac{L}{D},\quad F_{SFx} = \frac{\mu\omega_R L R^3}{C^2} f_{SFx},\quad F_{SFy} = \frac{\mu\omega_R L R^3}{C^2} f_{SFy}, \tag{2}$$

$$f_{SFx} = -\int_{-1/2}^{1/2}\int_{\delta 1}^{\delta 2} \gamma\cos\delta\, d\delta\, d\zeta,\quad f_{SFy} = -\int_{-1/2}^{1/2}\int_{\delta 1}^{\delta 2} \gamma\sin\delta\, d\delta\, d\zeta,\ \gamma = p\Big/\left(\mu\omega_R\frac{R^2}{C^2}\right),$$

$w_1 = x$, $w_2 = y$, $w_3 = x'$, $w_4 = y'$, $w_{2,S} = y_S$,

yield the following system of first order ODEs equivalent to (1):

$$\begin{cases} w_1' = w_3 \\ w_2' = w_4 \\ w_3' = -\dfrac{2q}{\Omega} w_3 - \dfrac{1}{\Omega^2} w_1 + \dfrac{\mathrm{f}}{4\Omega\lambda^2} f_{SFx} + U\cos\tau \\ w_4' = -\dfrac{2q}{\Omega} w_4 - \dfrac{1}{\Omega^2}\left(w_2 - w_{2,\mathrm{S}}\right) + \dfrac{\mathrm{f}}{4\Omega\lambda^2} f_{SFy} + U\sin\tau \end{cases} \quad (3)$$

Components F_{SFx} and F_{SFy} of the fluid film force were obtained from the pressure distribution determined solving the Reynolds equation written for finite SFD, in the presence of non circular bearing profile and incompressible, isothermal, isoviscous, laminar flow:

$$\frac{1}{R^2}\frac{\partial}{\partial\vartheta}\left(\frac{\bar{h}^3}{\mu}\frac{\partial p}{\partial\vartheta}\right) + \frac{\partial}{\partial\bar{z}}\left(\frac{\bar{h}^3}{\mu}\frac{\partial p}{\partial\bar{z}}\right) = -12\left(\dot{\bar{x}}\cos\delta + \dot{\bar{y}}\sin\delta\right) \quad (4)$$

The fluid film region with $\delta \in [0, 2\pi]$, $\zeta \in$[-1/2, 1,/2] was discretized by means of a two-dimensional mesh of N+1 columns by M rows, with cell dimension $\Delta\delta$ x $\Delta\zeta$ and $\Delta\delta = 2\pi/N$, $\Delta\zeta = 1/(M-1)$. Finite differences solution of the Reynolds equation was carried out by means of a forward-time, centered-space FD scheme, with M=5, N=81, and a subsequent SOR algorithm for solving the algebraic system. Ambient pressure was adopted at film borders and to replace sub-ambient values obtained from the FD routine. Equations (3) were numerically integrated with a Runge-Kutta routine. The determination of trajectories and Poincaré sections was carried out together with numerical continuation of periodic solutions after suitable choice about the set of the system parameters.

According to (2), Fig. 1 and Adiletta, Mancusi, & Strano, (2011) the bearing of the damper presented a two-lobe, wave profile characterized by dimensionless amplitude *B* and angular orientation φ. In the present investigation, *B* was given values 0, 0.05, 0.1, 0.15 and 0.2 (the null value was included in the set in order to represent the circular bearing case) while φ was assigned in the set $\pi, -3\pi/2, -\pi/2, -\pi/4, 0, \pi/4, \pi/2, 3\pi/2$. Figure 1a illustrates the modification of the original circular bearing clearance as an effect of *B* and φ. Fig. 1b shows three examples with *B* = 0.2 and $\varphi = \pi$, 0 and $\pi/4$. The geometry of the bearing was further specified by means of a length to diameter ratio λ that was assumed equal to 0.125, as typical of short-bearing aspect.

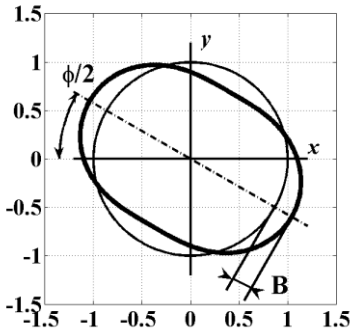

a)

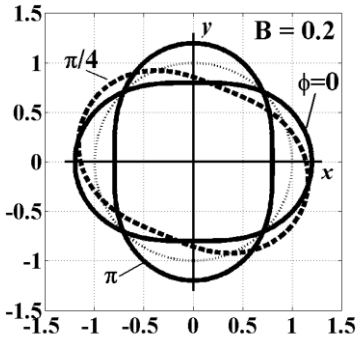

b)

Fig. 1

The effects of damper geometry and orientation onto the dynamic behaviour of the rotor were tested once suitable set-up conditions of the system had been fixed. In this regard, the results from Zhao and Hahn (1995), relative to a common circular bearing case in the presence of severe unbalance, suggested to assign: f = 0.072, *U* = 0.3, w_{2s} = -0.7, given the remarkable nonlinearity which affected the rotor response under these conditions. A specific, dimensional case study was conceived in congruence with the above parameters, fixing *k* = 929752 N/m, *m* = 50 kg, *R* = 0.04 m, *C* = 0.00015 m and *q* = 0.005. The angular speed was given in the interval Iω = [100, 1200] rad/s. Then the remaining quantities ω_R, *L*, μ and Ω could be inferred:

$$\omega_R = \sqrt{\frac{k}{m}} = 136.36 \text{ rad/s}, \quad L = 2R\lambda = 0.01 \text{ m}, \quad \mu = \mathrm{f}\frac{m\omega_R C^3}{RL^3} = 0.0414 \text{ Pa s}, \quad \Omega = [0.733, 8.80] \ .$$

Results of Numerical Analysis

Bifurcation analysis of periodic and *k*-periodic solutions was carried out by means of a continuation algorithm, based onto AUTO 97 (Doedel *et al.*, 1997), which traced the fixed point locus of the discrete-time "equivalent" system constructed via the Poincaré sections. The branches of the fixed points were computed together with Floquet multipliers. These quantities made it possible to check the stability of the branches. On the other hand, numerical integration of Eq. (3) based on Runge-Kutta method made it possible to check some of the results from continuation through direct observation of the journal orbits. Only two significant examples of the obtained numerical results have been reported here below:

a) The resonance curves of the synchronous response (1*T*), respectively obtained for different φ values, when the bifurcation parameter ω varies in the interval Iω. The angular positioning of the damper bearing not only modifies the resulting orbit magnitude, here expressed by means of the maximum orbit radius, but determines too the presence or absence of the saddle-node bifurcation connected to the well known jump effect. In Fig. 2a, the curves obtained with $\varphi = \pi$ and $- 3\pi/4$ are deprived of the "nose" followed by instable branch (not reported) that characterized the curves with $\varphi = - \pi/2$ and $- \pi/4$. In Fig. 3a waterfall picture of the resonance curves has been plot in the whole interval Iω. Fig. 3b shows a from-the-top view of the same plot, evidencing the sub-intervals of Iω where the synchronous motion turns out to be stable (absence of line represents instability).Three examples of the journal orbits about resonance are put in comparison in Fig. 4a-c.

b) Two continuation diagrams of the 1*T*, obtained at given values of *B* and ω, assuming φ as the bifurcation parameter which varies in the interval $[0, 2\pi]$. In Fig. 5a, b the angular speed has been assumed equal to 600 and 500 rad/s, respectively, i.e within a zone of Iω that is generally characterized by instability of the synchronous solution (compare Fig. 3b). Fig. 6 illustrates a particular from Fig. 5b. The plots point out that the existence of the stable motion, at given speed, is conditional on the choice of suitable values for *B* and φ. In the diagrams the response of the circular bearing case has been further reported to allow comparison.

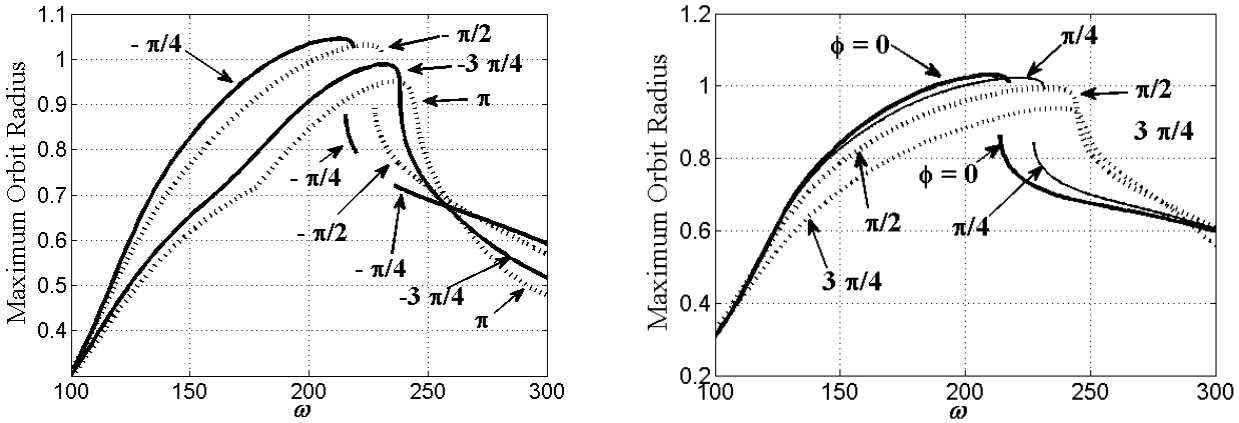

a) b)

Fig. 2

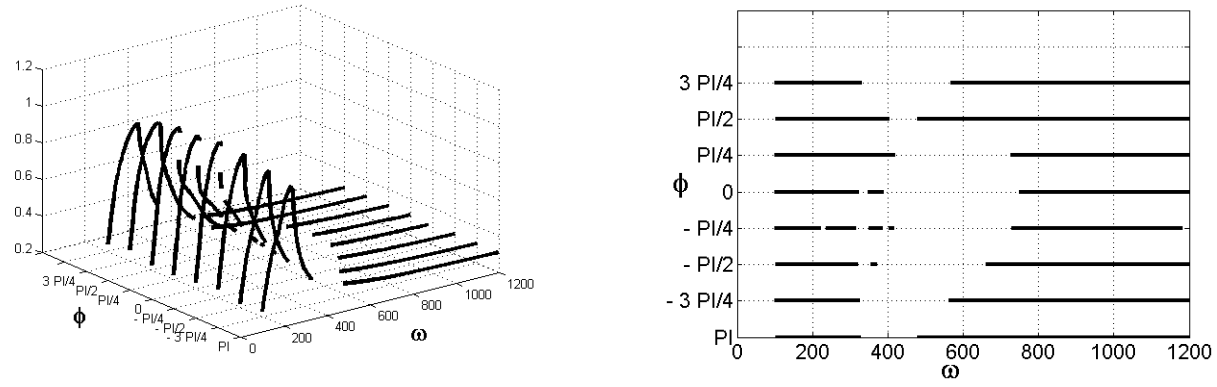

a) b)

Fig. 3

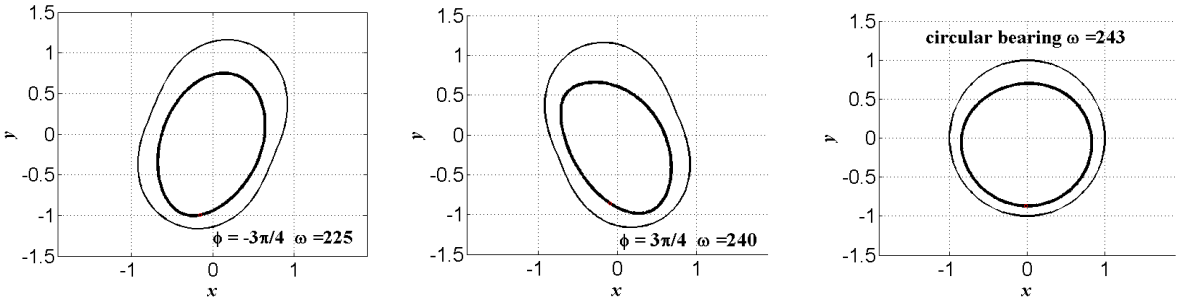

a) b) c)

Fig. 4

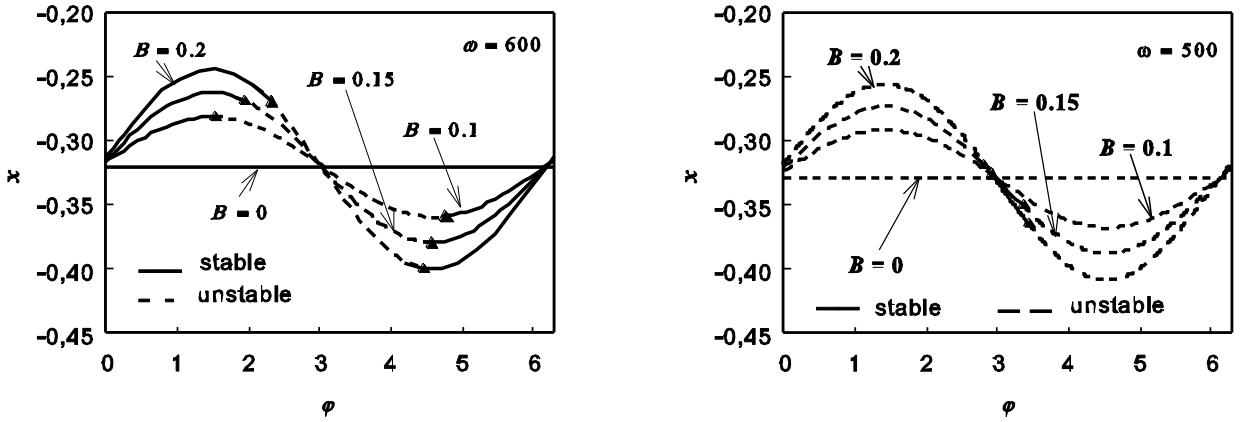

a) b)

Fig. 5

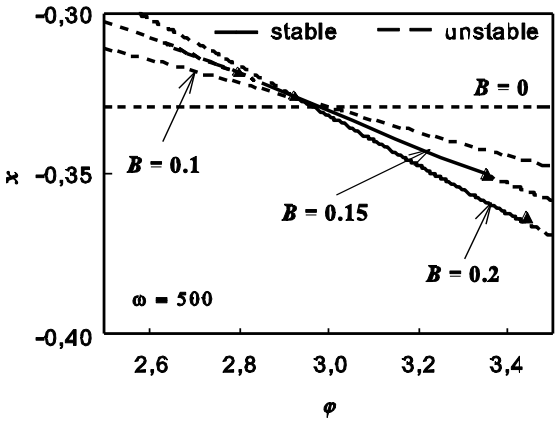

Fig. 6

Conclusions

The use of 2LW-SFD for supporting a rigid unbalanced rotor has been investigated through numerical continuation method, with particular attention to the effects of the bearing geometry onto the synchronous response. A case study with given unbalance, gravity residual, lubricant viscosity, wave amplitude of the bearing profile, and different values for the angular position of the 2LW bearing has been selected for the analysis. The obtained results, despite the restriction of the investigation to the synchronous response, put in evidence the substantial effect of the choice of such a bearing geometry, with particular regard to the jump phenomenon and the recover of stable solutions. Further investigation, both theoretical and experimental, is desirable in order to assess possible practical benefits of the device.

Nomenclature

C,L,D,R	= reference radial clearance, axial length, reference diameter and radius of the bearing
F_{SFx}, F_{SFy}	= fluid force component, in function of dimensional coordinates and velocities
m	= half rotor mass
φ	= angular orientation of the 2-lobe bearing (2LB)
U	= (ρ/C) dimensionless static unbalance
ω	= angular speed of rotor
k	= stiffness of the SFD restraining springs
μ	= lubricant viscosity

References

Adiletta, G., & Della Pietra, L. (2002). The Squeeze Film Dampers Over Four Decades of Investigations. Part II: Analyses With Rigid and Flexible Rotors. *The Shock and Vibration Digest*. *34* (2), 97-126.

Adiletta, G., Mancusi, E., & Strano, S. (2011). Nonlinear behavior analysis of a rotor on two-lobe wave journal bearings. *Tribology International*, *44(1)*, 42-54.

Birmann, R. (1933). US Patent 1,926,225, "Turbo Compressor".

Bonello, P., Brennan, M.J., Holmes, R. (2002). Non-linear modelling of rotor dynamic systems with squeeze film dampers- An efficient integrated approach. *Journal of Sound and Vibration*, *249(4)*, 743-773.

Della Pietra L., & Adiletta G. (2002). The Squeeze Film Dampers Over Four Decades of Investigations. Part I: Characteristics and Operating Features. *The Shock and Vibration Digest*. *34* (1), 3-26.

de Santiago, O., San Andrés, L., & Oliveras, J.. (1999). Imbalance Response of a Rotor Supported on Open-Ends Integral Squeeze Film Dampers. *ASME J. Engineering for Gas Turbines and Power*, *121*, 718-721.

Dimofte, F. (1995). Wave journal bearing with compressible lubricant - part I: the wave bearing concept and a comparison to the plain circular bearing. *STLE Tribology Transactions*, *38(1)*, 153-160.

El-Shafei, A., & El-Hakim, M. (2000). Experimental Investigation of Adaptive Control Applied to HSFD Supported Rotors. *ASME J. Engineering for Gas Turbines and Power*, *122*, 685-692.

Hahn, E.J. (1979). Stability and Unbalance Response of Centrally Preloaded Rotors Mounted in Journal and Squeeze Film Bearings. *ASME J. Lubrication Technology*, *101*, 120-128.

Inayat-Hussain, J.I., Kanki, H., & Mureithi, N.W. (2003). On the bifurcation of a rigid rotor response in squeeze-film dampers. Journal of Fluids and Structures, 17, 433-459.

Inayat-Hussain, J.I. (2009). Bifurcations in the response of a flexible rotor in squeeze-film dampers with retainer springs. Chaos, Solitons and Fractals, 39, 519-532.

Li Xuehai, & Taylor, D.L. (1987). Nonsyncronous Motion of Squeeze Film Damper Systems. *ASME J. Tribology*, *109*, 169-176.

Mohan, S., & Hahn, E.J. (1974). Design of Squeeze Film Damper Supports for Rigid Rotors. *ASME J. Engineering for Industry*, *96*, 976-982.

Pinkus, O. (1956). Analysis of Elliptical Bearings. *Trans. ASME*, *78*, 965-973.

Taylor, D.L., & Kumar, K. (1980). Nonlinear Response of Short Squeeze Film Dampers. *ASME J. Lubrication Technology*, *102*, 51-58.

White, D.C. (1970). Squeeze Film Journal Bearings. *Ph.D. Dissertation*, Cambridge University.

Zhao, J.Y., & Hahn, E.J. (1993). Subharmonic, Quasi-Periodic and Chaotic Motions of a Rigid Rotor Supported by an Eccentric Squeeze Film Damper. *IMechE, Proc Inst Mech Engrs, Part C: J. Mechanical Engineering Science*, *207*, 383-392.

Zhao, J.Y., Linnet, I.W., & McLean, L.J. (1994). Subharmonic and Quasi-Periodic Motions of an Ecccentric Squeeze Film Damper-Mounted Rigid Rotor. *ASME J. Vibration and Acoustics*, *116*, 357-363.

Zhao, J. Y., & Hahn, E. J. (1995). Eccentric Operation and Blade-Loss Simulation of a Rigid Rotor Supported by an Improved Squeeze Film Damper. *ASME J. Tribology*, *117*, 490-497.

Inhibition Action of Lawsone on the Corrosion of Mild Steel in Acidic Media

S.H.S. Dananjaya, M. Edussuriya and A.S. Dissanayake

Department of Chemistry, University of Ruhuna, Matara, Sri Lanka

Email: shsdananjaya@gmail.com, madurani@chem.ruh.ac.lk, arunasd@chem.ruh.ac.lk

Abstract: The use of inhibitors is one of the most practical methods for protection against corrosion. Lawsone, 2-hydroxy-1,4-naphthoquinone, the main active ingredient of Henna (*Lawsonia inermis*) plant was extracted, isolated and subjected to several studies. The corrosion inhibition of lawsone on the corrosion of mild steel in 1.0 M hydrochloric acid was studied using weight loss method. It was found that lawsone acts as a good corrosion inhibitor for mild steel in 1.0 M HCl medium. The inhibition efficiency increases with increasing of lawsone concentration. The inhibitive action was addressed in view of adsorption of lawsone molecules on the metal surface. It was found that this adsorption follows Langmuir adsorption isotherm in all tested systems and the adsorption is not activated.

Key words: Corrosion inhibition, Hydrochloric acid, Mild steel, 2-hydroxy-1,4-napthoquinone

Introduction

Corrosion problems have received a considerable attention because of the attack on materials. The use of inhibitors is one of the most practical methods for protection against corrosion. A corrosion inhibitor is a substance which is added in small amounts to a corrosive medium to reduce its ability for corrosion. Mild steel is an alloy of iron with carbon (carbon content 0.16-0.25%) which undergoes corrosion easily in acidic medium.The study of mild steel corrosion phenomenon has become important particularly in acidic media because of the increased industrial applications of acid solutions and also elevated levels of hydrogen ions in the atmosphere due to pollution. As an example, the refining of crude oil results in a variety of corrosive conditions. Refinery corrosion is generally caused by a strong acid attacking the equipment surface (Scattergood, 1992).The majority of well-known inhibitors are organic compounds containing heteroatoms, such as O, N or S, and multiple bonds, which allow an adsorption on the metal surface (Ali et al., 2003). These compounds can adsorb on metal surface and block the active surface sites to reduce the corrosion rate. Four types of adsorption may take place by organic molecules at metal/solution interface: (a) electrostatic attraction between the charged molecules and the charged metal, (b) interaction of uncharged electron pairs in the molecule with the metal, (c) interaction of p-electrons with the metal and (d) combination of (a) and (c) (Shorky et al., 1998).However, the stability of the inhibitor film on the metal surface depends on some physicochemical characteristics of the molecule, related to its functional groups, aromaticity, possible steric effects, electronic density of donors, type of corrosive medium, structure, charge of metal surface and nature of interaction between the p orbital of inhibitors with the d-orbital of iron (Machnikova et al., 2008).

Although many synthetic compounds show good anticorrosive action, most of them are highly toxic to both human beings and the environment. These inhibitors may cause temporary or permanent damage to organ systemssuch as kidneys or liver, or to disturb a biochemical process or an enzyme system at some sites in the body (Raja et al., 2008). The toxicity may manifest either during the synthesis of the compound or during its applications. These drawbacks lead investigations to focus on the use of naturally occurring substances in order to find low-cost and non-hazardous inhibitors. Plant extracts have become important as an environmentally acceptable, readily available and renewable source of materials for wide range of corrosion prevention.Therefore, finding of naturally occurring substances as corrosion inhibitors is a subject of great practical significance (El-Etre, 1998, 2001, 2003)

Henna is the Persian name of a shrub known as ***Lawsonia inermis Linn***. It is native to Asia and the Mediterranean coast of Africa, However, now it is spread to other parts of the world with warmer climate also. Henna leaves are harvested throughout the year, dried and ground to a fine powder for different applications including medicinal but largely as a cosmetics (Bhuvaeshwari et al., 2002). The extracted lawsone, 2-hydroxy-1,4-napthoquinone, is the main active ingredient of Henna (Thomso,1970). Two oxygen atoms are attached to the naphthalene carbons at positions 1 and 4 to form 1,4-naphthoquinone and a hydroxyl (–OH) group is present at position 2. In the present work, inhibition action of lawsone, 2-hydroxy-1,4-napthoquinone, isolated from Henna extract as a cheap, eco friendly and naturally occurring substance on corrosion behavior of mild steel in 1 M HCl has been investigated using weight loss measurements.

Materials and Method

Isolation of Lawsone from Henna : Powder of dried Henna leaves (40 g) was placed in a large beaker and distilled water (2 L) was added. The suspension was stirred with a magnetic stirrer with heating up to 70 ^{0}C. After 4 h, solid $NaHCO_3$ (8.4 g) was added. The suspension was filtered under gravity overnight using three large glass funnels with filter papers. The filtrate was acidified to pH 3 by adding of 0.12 M HCl. The resulting solution was extracted with diethyl ether (4 x 200 mL) .The combined ethereal phases were washed with water (3 x 50 mL) and dried over anhydrous $MgS0_4$. Ether was removed completely in a rotary evaporator to leave a reddish brown solid (760 mg) as the crude product.

The crude lawsone was purified by column chromatography, conditions: column 40 x 3 cm; stationary phase, silica gel 60; eluent ethanol-ethyl acetate (1:2 v/v). Initially fractions of 10 mL were taken and in the region of the lawsone zone the fraction size was reduced to 3 mL. The composition of all fractions was tested by TLC. The combined desired fractions contained a small amount of a less polar impurity and were recrystallized from glacial acetic acid to yield 78 mg of brown crystals. The recrystallized sample was identified as lawsone by melting point of 193-195 ^{0}C (lit. 195 ^{0}C) and its UV- visible spectrum.(Berger and Sicker, 2009)

Specimen Preparation: The mild steel sheets of 70 x 10 x 0.5 mm dimension were used for weight loss measurements. They were mechanically abraded with 200, 400, 800 and 1000 grades of emery papers. They were first washed with distilled water followed by acetone and dried using a stream of air and stored in moisture free desiccators before use.

Solution Preparation: 1 M HCl solution was prepared by diluting of 37 % HCl (Merck) using distilled water. The concentration of lawsone solution employed was varied from 10-500 mg L^{-1} in 1.0 M hydrochloric acid.

Weight Loss Measurements: After weighing accurately, the specimens were immersed in test tubes which contained 50 mL 1 M HCl with and without addition of lawsone of different concentrations. After 4 h, the specimens were taken out, washed, dried and weighed accurately. Then the tests were repeated at the temperatures, 30, 35, 40 and 45 ^{0}C. The inhibition efficiency (E %) of lawsone for the corrosion of mild steel was calculated using the following equation (Singh, I., Singh, M., 1987)

$E = (W_0 - W) / W_0 \times 100\%$

where W_0 and W are the weight loss of mild steel in the presence and absence of the inhibitor, respectively.

Results and Discussion

The melting point of the isolated, pure 2-hydroxy-1,4-napthoquinone was in the range of 193-195 ^{0} C which is same as the literature value, 195 ^{o}C (Krishnaswamy, 2003).

As it can be seen from the UV-vis spectrum of lawsone in 0.1 M HCl (Figure 1, a), absorption maximum appears at 334 nm. This spectrum of the isolated lawsone had a close resemblance with the spectrum reported in the literature (Berger and Sicker, 2009). The long tail of the band (Figure 1, a) at 334 nm that is reaching far into the visible region, is responsible for yellowish colour of lawsone. If one removes the acidic proton and measures the UV spectrum in 0.1 M NaOH, lawsone gives an orange colour solution with the spectrum band at about 453 nm (Figure 1, b),

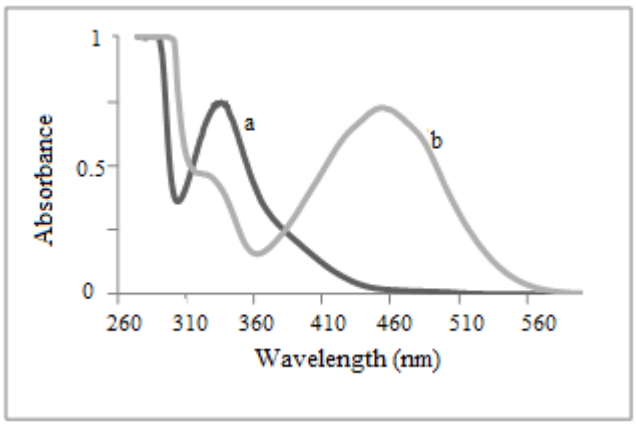

Figure 1. Absorption spectrum of lawsone (a) in 0.1 M HCl (b) in 0.1 M NaOH

The values of inhibition efficiencies (E) obtained from the weight loss for different concentration of lawsone in 1M HCl are given in Table 1. It is clear that inhibition efficiencies increases with increasing the inhibitor concentration.

Assuming that the corrosion inhibition was caused by the adsorption of lawsone, and the degree of surface coverage (θ) for different concentrations of lawsone in 1M HCl was evaluated from weight loss measurements using the Sekine and Hirakawa's method (Sekine ,1987).

$\theta = (W_0 - W)/(W_0 - W_m)$

where W_m is the smallest weight loss.

For the value of θ (Table 1), it can be seen that the values increased with increasing lawsone concentration as a result of adsorption of more lawsone molecules on the surface of steel at high concentrations.

Table 1: Corrosion parameters obtained from weight loss of mild steel in 1 M HCl containing various concentrations of lawsone at different temperatures.

Lawsone in 1M HCl (ppm)	Temperature, Inhibition efficiency (E %) and surface coverage (θ)							
	30 ^{0}C		35 ^{0}C		40 ^{0}C		45 ^{0}C	
	E (%)	θ	E (%)	θ	E (%)	θ	E (%)	θ
10	64.66	0.693	55.66	0.617	47.50	0.493	19.96	0.402
25	79.55	0.853	68.48	0.806	58.40	0.716	26.66	0.635
50	86.17	0.924	74.18	0.898	63.30	0.843	33.79	0.786
100	89.91	0.964	77.40	0.952	66.00	0.925	41.25	0.892
150	91.23	0.978	78.54	0.972	67.00	0.956	41.91	0.934
250	92.31	0.99	79.47	0.988	67.80	0.982	42.75	0.970
500	93.14	0.999	80.18	1.000	68.40	1.000	44.20	1.000

Assuming that lawsone adsorbed on the surface of mild steel forming a monolayer and ignoring the lateral interactions between the adsorbed lawsone molecules, the Langmuir adsorption isotherm was used to investigate the adsorption mechanism by the following equation (Zhao and Mu,1999)

$$c/\theta = 1/K + c$$

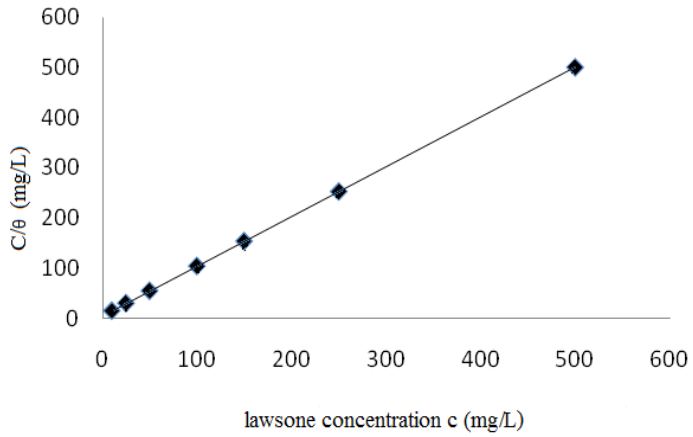

Figure. 2. The plot c/θ (mg L^{-1}) vs. c (mg L^{-1}) at 35 ^{0}C (R^2 = 1.000)

Figure 2 is the relationship between c/θ and c at 35 ^{0}C. The results given in the Table 2 show that linear correlation coefficient of 1.000 within the temperature range of 30 to 45 ^{0}C and the slopes were 0.992,0.9870.976 and0.970. The data

indicate that the assumption and the deduction were correct and at all temperatures of the experiment lawsone formed a chemical bond on the adsorption sites of mild steel surface. It could be found that the adsorption coefficient (K) decreased with increasing temperature. Lawsone gave higher values of K at lower temperatures, indicating that it was adsorbed strongly on the steel surface at lower temperatures and the adsorption process was not activated.

Table 2: Some parameters extracted from the linear regression between c/θ and c

Temperature (^{0}C)	K (mg^{-1} L)	Slope	Linear correlation coefficient
30	0.222	0.992	1.00
35	0.158	0.987	1.00
40	0.095	0.976	1.00
45	0.066	0.970	1.00

Mechanism of Inhibition : Lawsone is a ligand that can chelate with various metal cations to form metal complexes. Therefore, the formation of insoluble complexes, by chelating of the metal cations with the lawsone molecules adsorbed on the metal surface, is a probable interpretation of the observed inhibition action of lawsone. The formation of metal complexes with stoichiometric ratio of 1:1 and 2:1 are shown in Figure. 2.

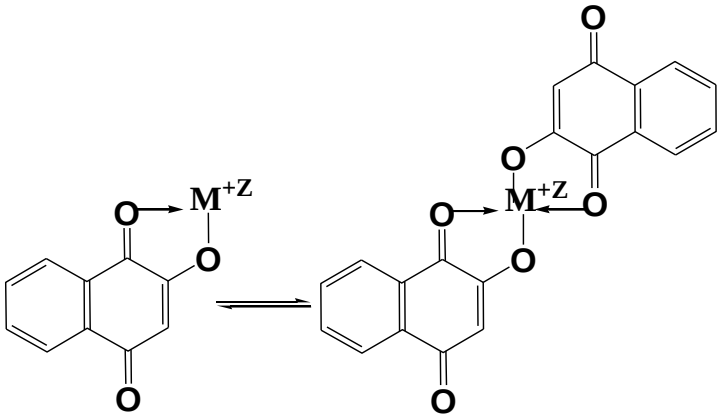

(a) 1 : 1 (b) 2 : 1

Figure 3. Forms of metal ion-lawsone complexes.

In the acidic medium, protonation of 2-hydroxy-1,4-napthoquinone takes place resulting in the rearrangement (tautomerization) as shown in the Figure 4 to give 4-hydroxy-1,2-napthoquinone. Such rearrangement, in the presence of metal cations, may enhance the complex formation ability. This could be the reason for the high inhibition efficiency in acidic media for mild steel.

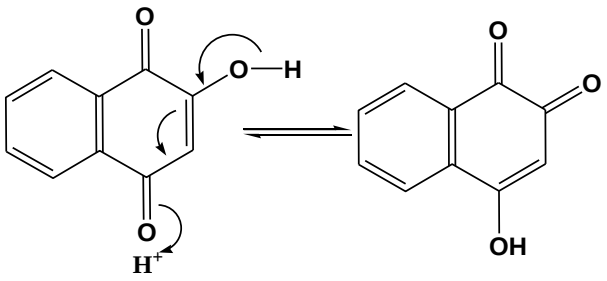

Figure.4. Forms of lawsone due to protonation.

Conclusion

Lawsone was found to be an effective inhibitor for corrosion of mild steel in 1M HCl, and inhibition efficiency increased with decreasing temperature. The adsorption of lawsone on the mild steel surface from 1 M HCl obeys the Langmuir adsorption isotherm and the adsorption is not activated.

References

Ali, Sk.A.,Saeed, M.T and Rahman, S.U. (2003). The isoxazolidines: a new class of corrosion inhibitors of mild steel in acidic medium. Corros. Sci. 45, 253–266.
Berger, Sand Sicker. D (2009) Classics in spectroscopy: isolation and structure elucidation of natural products, WILEY-VCH,Weinheim ± New York ± Chichester ± Brisbane ± Singapore ± Toronto
Bhuvaeshwari, K.,Poongothai,S.G.,Kurvilla,A. and ,Raju,B.A., (2002) .Inhibitory Concentration of *LawsoniaInermis* Dry powder for Urinary Pathogens,Indian J Pharmacol,34,260-263
El-Etre, A.Y., (1998).Natural honey as a corrosion inhibitor for metals and alloys. I. Copper in neutral aqueous solution, Corros. Sci. 40, 1845.
El-Etre, A.Y., (2001) Inhibition of acid corrosion of aluminum using vanillin, Corros. Sci. 43, 1031– 1039.
El-Etre, A.Y., (2003). Inhibition of aluminum corrosion using Opuntia extract, Corros. Sci. 45, 2485–2495.
Krishnaswamy, N.R., (2003). Chemistry of Natural Products,a Laboratory Handbook, India, Universities Press Private Limited.
Machnikova, E, Whitmire, K.H. and Hackerman, N., (2008). Corrosion inhibition of carbon steel in hydrochloric acid by furan derivatives, Electrochim. Acta, 53, 6024–6032.
Raja, P.B. and Sethuraman,M.G., (2008). Natural products as corrosion inhibitor for metals in corrosive media – a review, Mater. Lett.62 ,113–116.
Scattergood, G.L. Corrosion inhibitors for crude oil refineries, corrosion, ASM Handbook, vol. 13, ASM International, 1992.
Sekine, I. and Hirakawa, Y. (1986). Corrosion 42, 272.
Singh, I. and Singh, M. (1987). Corrosion 43, 425.
Shorky. H ,Yuasa.M, Sekine. I, Issa.R.M, El-Baradie.H.Y and Gomma, G.K, (1998). Corrosion inhibition of mild steel by schiff base compounds in various aqueous solutions: part 1, Corros. Sci. 40, 2173.
Thomson, R.H. (1970).Naturally Occurring Quinones, Academic Press, London, New York 1971.
Zhao, T.P. and Mu, G.N. (1999). Corrosion Science 41, 1937-1944.

LAND USE AND LAND COVER (LULC) CLASSIFICATION USING SPOT-5 IMAGE IN THE ADAPAZARI PLAIN AND ITS SURROUNDINGS,TURKEY

Cercis Ikiel (cikiel@sakarya.edu.tr) , Ayse Atalay Dutucu (aatalay@sakarya.edu.tr) ,

Beyza Ustaoglu (bustaoglu@sakarya.edu.tr) , Derya Evrim Kilic (dkilic@sakarya.edu.tr)

Sakarya University Arts and Science Faculty Department of Geography, Sakarya, Turkey

Abstract:

The objective of the study is determination of land use and land cover patterns of Adapazari plain and its surroundings by image classification. The study area is located in northwest of Turkey between coordinates of 40°37′- 40°57′ N and 30°12′- 30°46′ E and approximately 140 km east of Istanbul. Plain has become by the accumulation of sediments carried by Sakarya River and its tributaries. Adapazari Plain is a fertile agricultural area because of its favourable natural conditions. However, because of its closeness to Istanbul, population stress has gradually increased, so industrialization and urbanization has been accelerated in the plain. In this study, SPOT-5 satellite image is used to determination of land use and land cover characteristics of research area. The image is analyzed by using data images processing techniques in ERDAS Imagine© 10.0 and ArcGIS© 10.0 software. Land cover nomenclature is classified according to the CORINE (Coordination of Information on the Environment) Level 2 Classification (1-Urban fabric, 2-Heterogeneous agricultural areas, 3-Forests and 4-Inland wetlands) and Level 3 Classification (1-Industrial units, 2-Roads) . Furthermore, the image analysis results are confirmed by the field research.

Keywords: Land use and land cover (LULC), CORINE, SPOT 5, The Adapazari plain.

1. INTRODUCTION

Land use and land cover (LULC) classes characterize important information of natural landscape and human activities on the Earth's surface (Gong et al. 2011). In recent decades, remotely sensed data have been widely used to provide the land use and land cover information such as degradation level of forests and wetlands, rate of urbanization, intensity of agricultural activities and other human-induced changes. More recently, imagery from high spatial resolution satellite systems such as IKONOS, QuickBird, and SPOT-5 has become available. High resolution satellite imagery offers new opportunities for potentially more accurate identification and area estimation than traditional satellite imagery (Yang et al. 2010). In this study we used SPOT-5 data with 10 meter spatial resolution. Land use/land cover classification is a time-consuming and expensive process. There are various methods that can be used in the collection,analysis and presentation of resource data but the use of remote sensing and geographic information system (RS/GIS) technologies can greatly facilitate the process (İkiel and Ustaoglu, 2011). In remote sensing technology, classification as a common image processing technique is implemented to derive data regarding land cover types. In classification process, supervised classification with the maximum likelihood method which is also used in this study has been widely used in remote sensing applications (Yuksel et al. 2008). In this study, land use and land cover classification standards of Coordination of Information on the Environment (CORINE) Land Cover were used in the process classification system. The study area, Adapazari Plain, is located in northwest of Turkey approximately 140 km east of Istanbul (Figure 1). The plain has become by the accumulation of sediments carried by Sakarya River and its tributaries (Bilgin,1984: 2). Adapazarı plain has an intensive and varied agriculture because of its favorable natural conditions (Erinc and Tuncdilek, 1952) and the largest plain in the Marmara region (Tuncel, 2005). The research area is involved in Euxine province of Euro-Siberian phytogeographical region. This region is the most important area with its forest formation (Humid-Mild Deciduous Forests) (Kilic and Ikiel 2010). However, because of its closeness to Istanbul, population stress has gradually increased, so industrialization and urbanization has been accelerated in the plain. In recent years, change has been observed in the natural land use and land cover. The objective of the study is determine the land use and land cover (LULC) patterns of Adapazari plain in 2010 using an integrated approach of remote sensing and GIS.

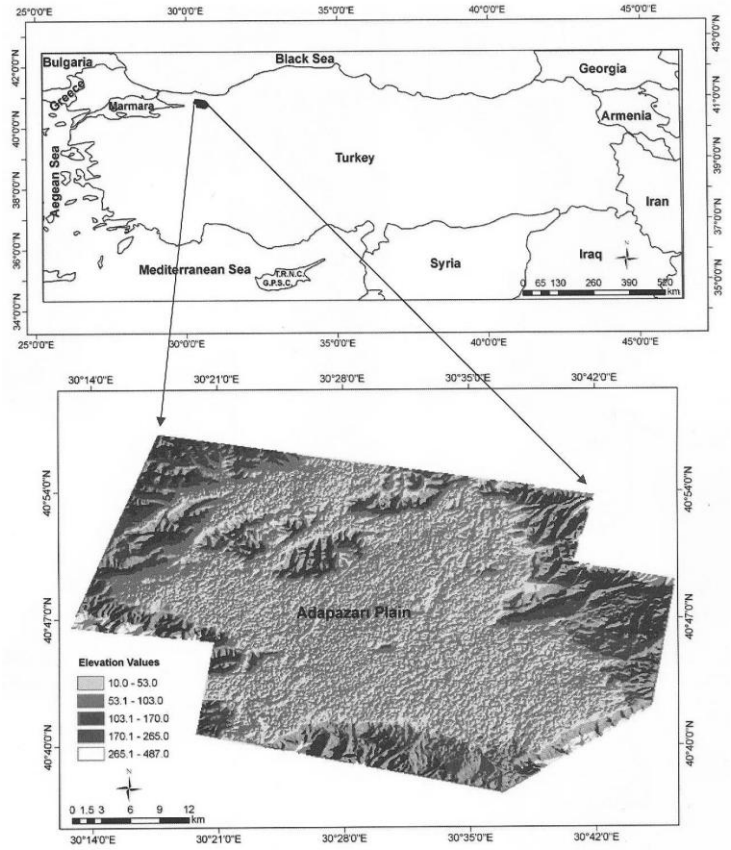

Figure 1: The Location map of study area.

2. DATA AND METHOD

2.1 Data

A Spot 5 image acquired on December 7, 2010 with 10 meter spatial resolution and four spectral bands: B1 (green: 0.50–0.59 μ m), B2 (red: 0.61–0.68 μ m), B3 (near infrared NIR: 0.79–0.89 μ m) and B4 (short-wave infrared SWIR: 1.58–1.75 μ m) was used to classify the land use land cover (LULC) in our study area. The image was provided by a commercial data provider. The image was also required to have less than 20 % cloud cover. With thiscriteria the image was cloud cover of 0 %. The characteristics of the image data are presented in Table 1. The other data used in this study for reference and analyses mainly include: (1) topographic maps at a scale of 1/100.000; (2) detailed vegetation map obtained from TR Forestry and Water Affairs Minister belongs to 2002; (3) detailed environment plan obtained from Sakarya Metropolitan Municipality; (4) ground reference data obtained from land survey with hand held GPS (5) demographic data of Sakarya from 1990 to 2010 which obtained from TurkStat, Turkish Statistical Institute (6) ERDAS Imagine© 10.0 and ArcGIS© 10.0 software were used for image classification and data analyses.

Type of imagery	Date	Spatial resolution (m)
Spot 5	07.12.2010	10

Table 1: Characteristics of the satellite data used for land cover change mapping in the study area.

2.2 LULC classification and mapping

LULC classification and mapping was performed in four stages: 1) Preprocessing of the images 3) Determination of land cover types 3) Supervised classification of the image into LULC classes 4) Accuracy assessment. These applications were performed using ERDAS Imagine 10.0 software. This research primarily used theory and methodology from geography, remote sensing and geographic information science to analyze the land cover dynamics in the study area.

2.2.1 Preprocessing of the images

Image was clipped out according to the location map by using subset function (Figure 2). The radiometric corrections, systematic errors and SPOT 5 geometric correction were carried out by data set providers. The image was geo-referenced into the Universal Transverse Mercator-UTM, WGS-84.

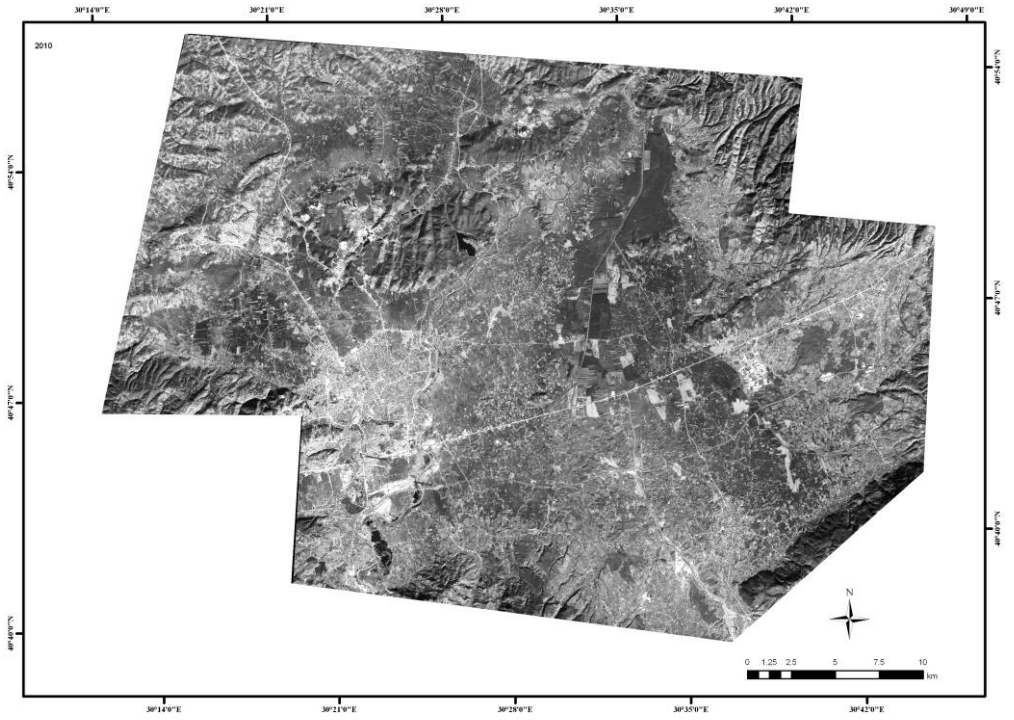

Figure 2: SPOT 5 satellite image with 10 meter resolution (07.12.2010)

2.2.2 Determination of land cover types

The CORINE land cover nomenclature/ classification system was chosen and referred for the classification system for this study. The field work supported the image interpretation of land cover types defined in the classification. The Coordination of Information on the Environment (CORINE) land cover determination program, which is mainly operated by member countries of the European Union, was started by the European Commission of the Union and can be summarized as 'environmental knowledge formation'. The legend of the CORINE land cover nomenclature/ classification is standard for the whole of Europe, which as a result is quite extensive with 44 classes describing land cover (and partly land use) according to a nomenclature of 44 classes organized hierarchically in three levels (Sonmez et.al, 2009). In this study land cover legends include six classes. Some of those are classified at level 2 (1-Urban fabric, 2-Heterogeneous agricultural areas, 3-Forests and 4-Inland wetlands) and others are classified at level 3 (1-Industrial units, 2-Roads).

2.2.3 Supervised classification of the image into LULC classes

A good knowledge of the study area was achieved by a suitable image enhancement and related literature. Furthermore Richards and Jia (1999) suggest fieldwork that develops knowledge of the area with interviews, photography of characteristic surfaces, ground truth data in order to validate a classification. In this study, all images were independently classified using the supervised classification method of maximum likelihood algorithm. Although many different methods have been devised to implement supervised classification, the maximum likelihood is still one of the most widely used supervised classification algorithms (Jensen, 1996). In supervised classification, spectral signatures are collected from specified locations in the image by digitizing various polygons overlaying different land cover types. The spectral signatures are then used to classify all pixels in the scene. "user defined polygon" were selected from the whole study area by drawing area of interest (aoi). In supervised classification process, .aoi function reduces the chance of underestimating class variance since it involved a high degree of user control. After the classification process, all signature sample points were grouped as a class by "recode" function according to the determined land cover classification types in this study. In this study, the supervised classification method detected over 50 homogenously distributed sample areas from 6 classes in total according to the maximum likelihood algorithm (aoi).

2.2.4 Accuracy assessment

Accuracy assessment tool was performed to evaluated of the accuracy of the classified images. It is based on random sampling method which selected the points from referenced map. After the application, obtained a report which show error matrix of the results. Error matrix is in the most common way to present the accuracy of the classification results. Overall accuracy, user's and producer's accuracies, and the Kappa statistic were then derived from the error matrices. The overall accuracy and a KAPPA analysis were used to perform classification accuracy assessment based on error matrix analysis. Using the simple descriptive statistics technique, overall accuracy is computed by dividing the total correct (sum of the major diagonal) by the total number of pixels in the error matrix. KAPPA analysis is a discrete multivariate technique used in accuracy assessments. KAPPA analysis yields a Khat statistic (an estimate of KAPPA, equation 1) that is a measure of agreement or accuracy (Jensen, 1996, Guler et al, 2007). The Khat statistic is computed as:

$$\frac{N\sum_{i=1}^{r} x_{ii} - \sum_{i=1}^{r}\left(x_{i+}x_{+i}\right)}{N^2 - \sum_{i=1}^{r}\left(x_{i+}x_{+i}\right)} \quad (1)$$

Where r is the number of rows in the matrix, x_{ii} is the number of observations in row i and column i, x_{i+} and x_{+i} are the marginal totals for row i and column i respectively and N is the total number of pixels. Independently classified images were compared with each other to determine the changes of land cover types. Accuracy levels of more than 80 % are considered adequate enough for reliable classification of land cover types (Alrababah and Alhamad, 2006).

3. RESULTS AND DISCUSSIONS

The supervised classification method detected over 50 homogenously distributed sample areas from 6 classes in total according to the maximum likelihood algorithm (aoi). Accuracy analysis was applied to the classified satellite image (2010) with an aim to confirm the accuracy of the classification. To do this, over 50 random reference control points were identified on the study area map for 6 classes. The point distributions were made in proportion to the field distributions of the classes. Total accuracy rate (total number of accurate pixels / number of pixels taken as reference) was detected 94.00% and kappa statistics value was 92.30%. Both Producer's accuracy and User's accuracy (accuracy rate generated by the user) are over 80% in all classes (Table 2). According to the high accuracy assessment results up to 80%, LULC classification is correct statistically.

Class Name	Reference Totals	Classified Totals	Number Correct	Producers Accuracy (%)	Users Accuracy (%)	Kappa (%)
Heterogenous agricultural areas	20	20	19	95,0	95,0	91,6
Forests	5	5	4	80,0	80,0	77,7
Urban Fabric	6	5	5	83,3	100,0	100,0
Industiral Units	5	5	5	100,0	100,0	100,0
Inland Wetlands	5	5	5	100,0	100,0	100,0
Roads	4	5	4	100,0	80,0	100,0
Totals	50	50	47			78,2
Overall Classification Accuracy: 94.00 %		94,00%		Overall Kappa Statistics =	92,30%	

Table 2: Results of accuracy assessment of the 2010 land use and land cover classification map produced from SPOT 5 data.

The highest classification accuracy was obtained in industrial units and inland wetlands due to their homogenous character. Structural character of the land (homogeneous-heterogeneous) and spatial resolutions of the satellite image put a direct effect on the obtained result. According to LULC classification results, land cover distributed as heterogeneous agricultural areas 78.4 %, forests 14.8%, urban fabric 5.1%, industrial units 0.3%, inland wetlands 0.5% and roads 0.9%. Based on the results, heterogeneous agricultural area is the largest land use and land cover classes in the plain (Table 3). Major agricultural areas and industrial units are located around the settlements according to the map (Figure 3).

Class Name	Area (hectare)	Area (%)
Heterogenous agricultural areas	145798	78,4
Forests	27476	14,8
Urban Fabric	9419	5,1
Industiral Units	609	0,3
Inland Wetlands	1014	0,5
Roads	1671	0,9
Totals	185987	

Table 3: Results of the land use and land cover classification table for 2010 image showing area of each class.

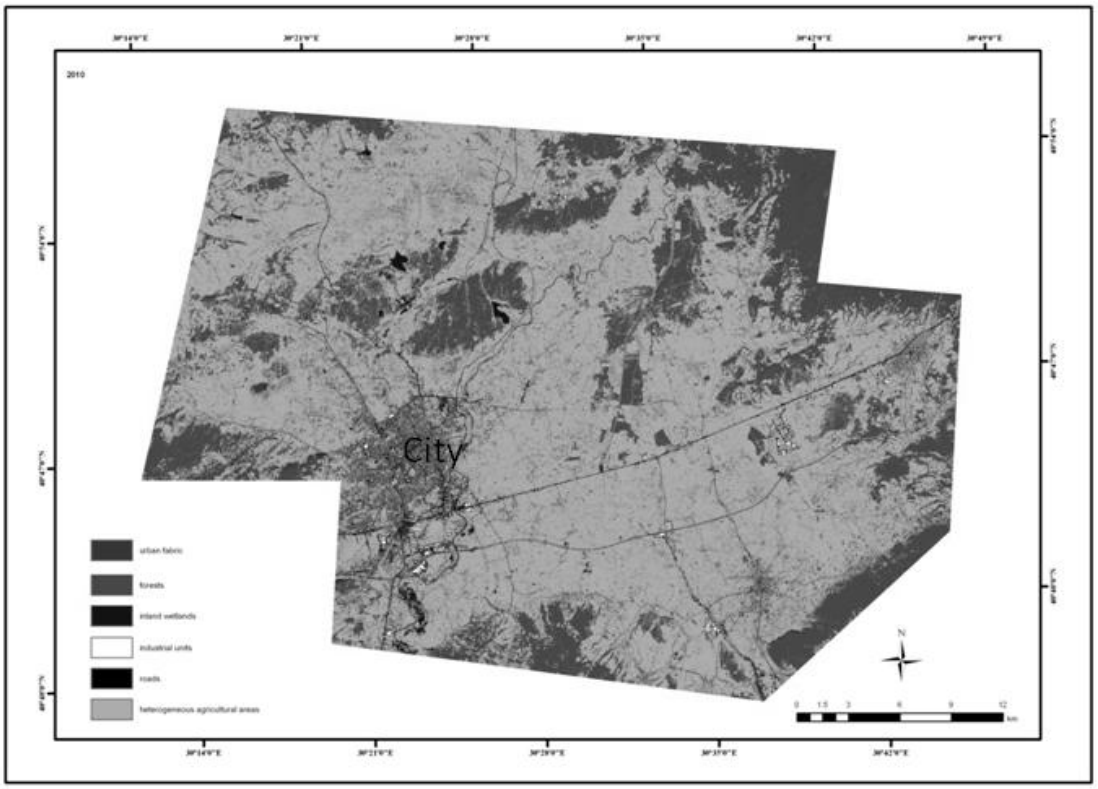

Figure 3: Land use and land cover (LULC) classification map (2010) derived from SPOT -5.

Adapazari plain is close to major roads every period of history. Because of this advantage geographic positon, settlements on the plain have developed up to now (Doldur, 2006). Today the city of the Adapazari consisted of the expansion of settlement around the old Adapazari area. Other settlements are Hendek and Akyazı which are the town center in the plain.

Years	Total Population	Accrual	Population Growth Rate (%)
1990	683,061		
2000	756,168	73,107	10,7
2007	835,222	79,054	10,5
2008	851,292	16,070	1,9
2009	861,570	10,278	1,2
2010	872,872	11,302	1,3

Table 4: Population growth of the Sakarya city between 1990 and 2010 according to TurkStat 2011.

Therefore, the population is increasing in Adapazari which has become a center of attraction for the near and far around (Table 4). Particularly urban population has greater share increasing in this population. For example, while the central town of Adapazari according to 1955 census, 74% of the population living in villages (İnandık, 1956), this ratio decreased 5.1% while the urban population ratio increased % 94.9 according to the results the 2010 census calculation of the data obtained from

TurkStat, Turkish Statistical Institute (Table 4). Therefore, urban fabric is changing and urban settlements area is growing continuously.

4. CONCLUSIONS

We obtained classified land use and land cover classification in the Adapazari Plain, Turkey (2010) with analysing SPOT-5 satellite image. According to LULC classification results, land cover distributed as heterogeneous agricultural areas 78.4 %, forests 14.8%, urban fabric 5.1%, industrial units 0.3%, inland wetlands 0.5% and roads 0.9%. Based on the results, heterogeneous agricultural area is the largest land use and land cover classes in the plain. Although industrialization and urbanization is increasing in the study area, the Adapazari Plain is still an important agricultural area in Turkey. As a results of this study, high accuracy of land use and land cover classification map was obtained. Relatively homogeneous structural character of the plain and high spatial resolutions of the SPOT-5 with 10 meter put a direct effect on the obtained result. Accurate LULC maps can play an important role in aiding land use and land cover management as well as helping in deciding what sort of lands are best suited for sustaining land use and land cover and in what manner this land use and land cover should be practiced.

Acknowledgement

The authors are grateful to Scientific Research Fund of Sakarya University for financially supported to this work. They are also grateful to the Istanbul Technical University (ITU) - Center for Satellite Communications and Remote Sensing (ITU-CSCRS) for providing the necessary SPOT-5 data for the study.

References

Alrababah MA, Alhamad MN. Land use/cover classification of arid and semi-arid Mediterranean landscapes using Landsat ETM. Int J Remote Sens 2006;27:2703-2718.

Bilgin (1984), *Adapazarı Ovası ve Sapanca Oluğunun Alüvyal Morfolojisi ve Kuaternerdeki Jeomorfolojik Tekamülü*, İstanbul Üniv. Edebiyat Fak. Yayını, No: 2572, İstanbul.

Doldur (2003), *Tarımdan Sanayiye Bir Ova Şehri: Adapazarı*, İstanbul Üniv.Sosyal Bilimler Enst. Coğrafya Anabilim Dalı Doktora Tezi, İstanbul.

Erinc and Tuncdilek (1952), *The agricultural regions of Turkey*, Geographical Review Vol. X L I I, No. 2, April 1952 New York s. 193.

Guler, Yomralıoğgu and Reis (2007), *Using Landsat Data to Determine Land Use/ Land Cover Changes in Samsun, Turkey*, Environ Monit Assess (2007) 127:155–167, DOI 10.1007/s10661-006-9270-1.

Gong, Im, Mountrakis (2011). *An artificial immune network approach to multi-sensor land use/land cover classification*. Remote Sens Environ.m115:600-614.

Ikiel and Ustaoglu (2011), *Sakarya Deltasının Doğu Kesiminde Kıyı Çizgisi Değişiminin Coğrafi Bilgi Sistemleri ve Uzaktan Algılama Yöntemleriyle Analizi*, Fiziki Coğrafya Araştırmaları: Sistematik ve Bölgesel, Türk Coğrafya Kurumu Yayınları, Sayı:6, 485-494, İstanbul.

Inandık (1956), *Adapazarı Ovası ve Çevresinde Nüfus ve Yerleşme*, İstanbul Üniv. Coğrafya Enst. Dergisi Cilt 4 Sayı 7, S.66-91, İstanbul.

Jensen (1996), *Introductory Digital Image Processing: A Remote Sensing Perspective*. 2ndEdition, Prentice-Hall, Upper Saddle River, NJ.

Kilic and Ikiel (2010), *Vegetation Features of Western Part of Elmacik Mountain*. International Symposium on Geography, Environment and Culture in Mediterranean Region, 2-7 June 2010, Antalya-Turkey.

Richards and Jia (1999), *Remote Sensing Digital Image Analysis: An Introduction*, 3rd Edition, Berlin/Heidelberg/New York: Springer.

Sonmez, Onur, Sarı and Maktav (2009), *Monitoring changes in land cover/use by CORINE methodology usingaerial photographs and IKONOS satellite images: a case study for Kemer, Antalya, Turkey*, International Journal of Remote Sensing Vol. 30, No. 7, 1771–1778.

Tuncel (2005), *Adapazarı Yöresinin Coğrafyası, Sakarya İli Tarihi*, Cilt 1, Sakarya İli Tarih Araştırmaları Projesi, Sakarya.

Yang, Everitt and Murden (2010), *Evaluating high resolution SPOT 5 satellite imagery for crop identification*, Computers and Electronics in Agriculture Volume 75, Issue 2, February 2011, Pages 347-354.

Yuksel, Akay and Gundogan (2008), *Using ASTER Imagery in Land Use/cover Classification of Eastern Mediterranean Landscapes According to CORINE Land Cover Project*, Sensors 2008, 8, 1237-1251.

Lethal Effect of Salts on the Terrestrial Snail *Monacha Cantiana*

Mohamed M. Y. El-Shazly

Plant Prot. Dept. Fac. of Agric. (Saba Basha), Alexandria Univ., Egypt
e-mail: doctors_ag@yahoo.com

Abstract: The lethal effect of ten salts,on the terrestrial snail *Monacha cantiana*, was examined in laboratory. Tested salts were: sodium chloride, potassium sulphate, ferrous sulphate hepta hydrate, magnesium sulphate hepta hydrate manganese sulphate tetra hydrate, zinc sulphate hepta hydrate, ammonium sulphate, calcium nitrate, di ammonium phosphate and ammonium nitrate.

LC_{50} values of the previous salts after 72 hours were; 2.09 %, 3.70 %, 0.27 %, 11.65 %, 3.38 %, 0.13%,1.36 %, 1.85 %, 0.90 % and 0.20 %, respectively.

LC_{90} values of the previous salts after 72 hours were ; 10.27 %, 4.82 %, 0.67 %, 25.45 %, 5.00 %, 0.18 %, 5.87%, 7.59 % , 4.68 % and 0.83 %, respectively.

Each of Lc_{50} and Lc_{90} values correlated negatively with E.C. values of 1 % solutions of the tested salts but correlated positively with pH values of 50 % solutions of the examined salts. In other words each of Lc_{50} and Lc_{90} values correlates negatively with each of salinity and acidity of salts.

Each of Lc_{50} and Lc_{90} values were found to be correlated positively with the molecular weights of the examined salts.

Key words: Lethal salts terrestrial snail *Monacha cantiana*

Introduction

Slugs are a serious pest in floriculture, horticulture and agriculture in many parts of the world. *Deroceras reticulatum* is generally the most destructive species (Grewal *et al.*, 2001).

Different investigators examined different agents to be used to control snails; Bullock *et al.*(1992) found that control of terrestrial slugs and snails can be achieved by some common metals as contact-action poisons acquired passively by crawling animals and they were acting more efficiently than the currently used bait-delivery method.

Trent *et al.* (1997) tested thirteen molluscicides containing metaldehyde, three molluscicides containing metaldehyde plus carbaryl, one molluscicide containing metaldehyde plus methiocarb and one molluscicide containing methiocarb alone for their efficacy against the brown slug, *Vaginula plebeia* Fischer, and the two-striped slug, *Veronicella cubensis* (Pfeiffer). With the exception of corry's liquid slug, snail and Insect killer against *V. plebeia*, all the tested molluscicides caused significant mortalities against both species. In a separate study, physical barriers composed of copper or fiberglass screens repelled both slug species.

David *et al*. (2001) stated that feeding inhibition by diluted tuber peel extracts of the variety Homeguard was greater than that elicited by comparable authentic glycoalkaloid solutions suggesting additional inhibitory compound(s) in the peel of this variety.

Grewal *et al.* (2001) found that the beneficial nematode, *Phasmarhabditis hermaphrodita,* has potential for the biological control of slugs and application rates of 3.0×10^9 infective juveniles (IJs)/ha are usually required for effective plant protection.

Schuder *et al.* (2003) tested certain products that have irritant, antifeedant, physical barrier, chemical repellent, or molluscicidal effects or a combination of more than one effect against slugs. Garlic, ureaformaldehyde and cinnamamide were the three best products for controlling snails. In 7 day bioassay trials, these products had mortality rates between 20% and 95% which was significantly higher than the untreated.

Shmuel *et al.*(2004) tested two formulations of water dispersible granules contained 61.4% and 53.8% of copper hydroxide. The 0.1% concentration of either formulation was sufficient for the management of the land snails *Monacha syriaca* and *Theba pisana* populations.

Der *et, al.* (2005) stated that morpholine which is a solvent of apple wax was very effective in suppressing hatching of the snail *Pomacea canaliculata* eggs at a concentration of 60%.

Ravindra *et al.* (2008) proofed that saponin concentration in rice water at 9 and 11 ppm gave seedling protection of 93% and 95%, respectively after 48 h against different sizes of the snail *Pomacea canaliculata*.

Youssef (2011) tested four plant species used as a dry powder of their leaves against *Biomphalaria alexandrina* snails. The bioassay tests revealed that the plants *Datura stramonium* and *Sesbania sesban* were more toxic to the snails than the other two tested ones.

Snails are found tremendously beside irrigation or drainage canals where moisture is abundant .They are more active after irrigation. Snails destroy the vegetative parts of plants therefore, the aim of the present study is to determine the most suitable substance to ban snails from passing through. These substances may be useful and can be used to surround fields to protect them from snails for their molluscicidal effects as contact-action poisons.

Modeling of Residual Stresses in TBC Coated Gas Turbine Blades

Yaşar KAHRAMAN *, Sedat İRİÇ, İmdat TAYMAZ

Sakarya University, Engineering Faculty, Serdivan - Sakarya, Turkey
kahraman@sakarya.edu, siriç@sakarya.edu.tr, taymaz@sakarya.edu.tr

Abstract: Ceramic thermal barrier coatings have been developed for advanced gas turbine and diesel engine applications to improve engine reliability and fuel efficiency. Blades and vanes of the high-pressure turbine stages of aero-engines are the most highly stressed parts in engineering components. The blade geometry was objected to airflow at the temperatures about 800°C. These high gas turbine temperatures can only be maintained through advanced cooling techniques like electro-beam physical vapor deposition (EB-PVD) and thermal barrier coatings (TBCs). Such TBCs consist of thin ceramic layers of low thermal conductivity, yttrium stabilized zirconia (YSZ) which are applied on the blade surface. The coating imparts good adhesion of the ceramic to the substrate.

In this study, 3-D finite element structural and thermal analyses were carried out on both uncoated (without coating) and ceramic-coated turbine blade using ANSYS code. A 150 micron super alloy bond coating (NiCrAlY) was first applied to the turbine blade. Then, the blade was covered by 350 micron thickness of Mullit ($3Al_2O_3.2SiO_2$) as a top coating. These analysis were performed for detecting the possible thermally problem spots. Finally, the blade's thermal stressed problematic areas were determined by the finite element simulations which were important for the improving blade and TBC.

Key words: TBC, Turbine Blade, Finite Element Analysis, Residual Stresses, Modeling

Introduction

For the protection of the blade in hot working conditions by thermal stresses and other effects, TBC was applied on to the geometry. Different types of coating technologies widely used on the turbine blades. Thermal barrier coating (TBC) systems, consisting of yttria partially stabilized zirconia (YSZ), thermally grown oxide (TGO) and a metallic bond coat are used in applications for thermal protection of hot-section parts in gas turbine engines. (R.A. Miller 1987, D.J. Wortman at all 1989, S.M. Meier at all 1991, R.T. Jones at all 1996, R.D. Jr. Sisson at all 1995, Y.H. Sohn at all 2001)

When the turbine blades are considered, some affects are more important than the others. The important research areas related to heat transfer of a gas turbine blade include external and internal heat transfer coefficient predictions, metal temperature distributions, blade cooling methods, rotation effects, and ceramic coatings amongst others. External convection depends upon the development of the boundary layer on the blade surface, which is a complex phenomenon, and there is considerable uncertainty associated with both numerical predictions and experimental measurements (] N. Asok Kumar , S.R. Kale 2001).

The thermal barrier coating provides a temperature drop of up to 200°C, due to its low thermal conductivity, which is enhanced further by the intentionally porous microstructure (Marcin Białas 2008).

Although the composition of the TBC was created many protective abilities for the blades, some insufficient and troubled behaviors are still alive. A major weakness of TBC systems is the interface between the metallic bond coat and the ceramic TBC. At this interface an in-service degradation is observed often leading to a macroscopic spallation of the ceramic layer (R.A. Miller, C.E. Lowell 1982). The interface regions undergo high stresses due to the mismatch of thermal expansion between BC and TBC. Additionally, growth stresses due to the development of thermally grown oxide (TGO) at the interface and stresses due to interface roughness are superimposed. Stress relaxation leads generally to reduce stress levels at high temperature, but can give rise to enhanced stress accumulation after thermal cycling resulting in early crack initiation at the bond coat/alumina interface and spallation failure afterwards (A.G. Evans at all 2001, G. Fleury at all 1997, F. Schubert at all 2000)

In this study, finite element simulations of uncoated turbine blade model and also thermal barrier coated turbine blade geometry were performed with the ANSYS code. For the TBC used geometry, the turbine blade was covered with a super alloy bond coating (NiCrAlY). Over the bond coating layer, Mullit ($3Al_2O_3.2SiO_2$) was used as a top coating. For the coated turbine blade; hot air flow was applied to the all top coating layer surfaces and for the uncoated geometry; hot air flow was applied to the turbine blade surfaces. The results of the thermal simulations were compared, initially with the temperature distribution of the coated and uncoated turbine blades. Then the equivalent stress profiles of coated and uncoated turbine blade were matched and evaluated. As a final decision, TBC for the blade geometry is a supporting material for reducing the blade's temperature and equivalent stress value.

Materials

For the base blade material, steel substrate was used. As a bond coating material NiCrAlY was preferred. Mullit was selected for the top coating layer. See table 1 for materials' details. Up to the selected materials, thermal and structural properties affect the turbine blades behaviors. For an appropriate protection; which was originated from the selected materials, chemical and structural behaviors, coating material types and usage will differ.

For the TBC used geometry, the turbine blade was covered with a 150 micron thickness of a super alloy bond coating (NiCrAlY). For over the bond coating layer, 350 micron thickness of Mullit ($3Al_2O_3.2SiO_2$) was used as a top coating.

Table 1. Material properties of substrate, bond coat and top coating

Material	Thermal conductivity [W/m°C]	Thermal expansion 10^{-6} [1/°C]	Density [kg/m^3]	Specific heat [J/kg°C]	Poisson's ratio	Young's modulus [GPa]
Steel Substrate	16,2	17,2	7850	434	0,3	200
NiCrAlY	16	15	7710	520	0,25	16,8
Mullit	1,2	5,2	2608	760	0,25	21

Modeling and Analysis

For the thermal and structural simulations of the turbine blades, solid CAD models were used. Solid models of the two different finite element models of the uncoated and coated turbine blades were modeled in Pro_Engineer CAD program. Simplified solid models of the turbine blades were sent to ANSYS code directly, for easy control of finite element model. To prepare the fine meshed and simple based finite element models, unchanging one section area was applied to the turbine blades.

Two types of solid elements were used for the thermal and structural analysis in ANSYS code. Each solid element has 20 nodes. "*Solid 90"* element for the thermal analysis and "*Solid 186"* element was applied for the structural analysis. In figure 1, the meshed model of the coated turbine blade can be observed. For the uncoated turbine blade 2900 elements and 13428 nodes; for the coated model 1100 elements and 5959 nodes were used.

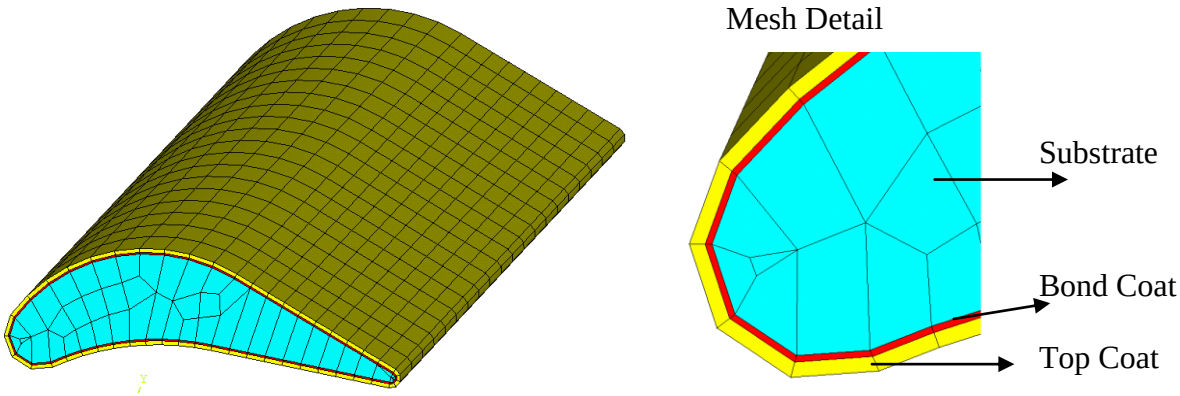

Figure 1. Meshed model of the coated blade

Initially, thermal analysis was processed for each turbine blade. During the thermal analysis, 800°C air flow was applied to the top coating surface for a while. For comparing the blades, in the uncoated model, same 800°C air flow was applied on to the turbine blade surfaces. The simulations were solved under these circumstances. The results of the thermal simulations were imported into the structural analysis set up data of the turbine blades.

During the structural analysis preparation process, transferred data of all the thermal simulation results was adapted to the structural finite element models. The thermal element "solid 90" was switched in to the structural element "solid 186" in ANSYS; but the mesh structure and distribution were not changed. Not changed mesh structure gives valuable advantage for

the comparison between coated and uncoated turbine blades. All the comparisons were made from the same attitude of the elements and nodes of the mesh structure. The results of the analysis can be matched between the same node and the same element numbers for the base turbine blade geometry.

In the structural analysis, thermally simulated models were hold in All DOF from one flat side surface of the turbine blade geometry. The imported temperature distributions in the turbine blades and the coatings were reflected to the material behavior to find the stresses of the thermal simulation results. For the imported thermal simulation data, of the coated and the uncoated turbine blades, were solved. Finally, stress results for the thermally originated structural analysis can be determined for each turbine blade.

Results and Discussion

After the analysis, results are satisfactory for the evaluation and comparison for the uncoated and coated turbine blades. The thermal simulation results for the models can be determined from the figure 2. Evaluation of the figure 2 is showed that coating material was decreased the turbine blade surface temperature from 440°C to 360°C during the process of 800°C air flow. For the last steps of the analysis of, about 80°C profit was held. Using Mullit as a top coating material, 18% thermal protection was received for the turbine blade.

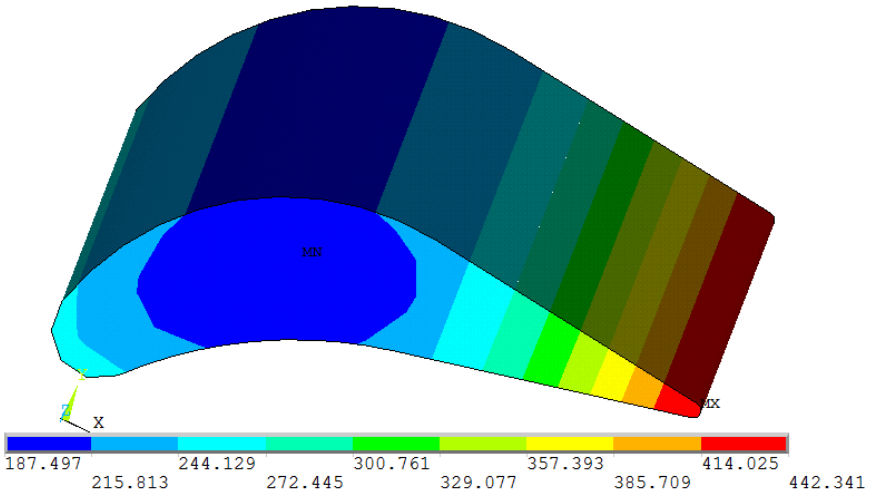

Figure 2.a. The thermal simulation results in temperatures (°C) for the uncoated blade

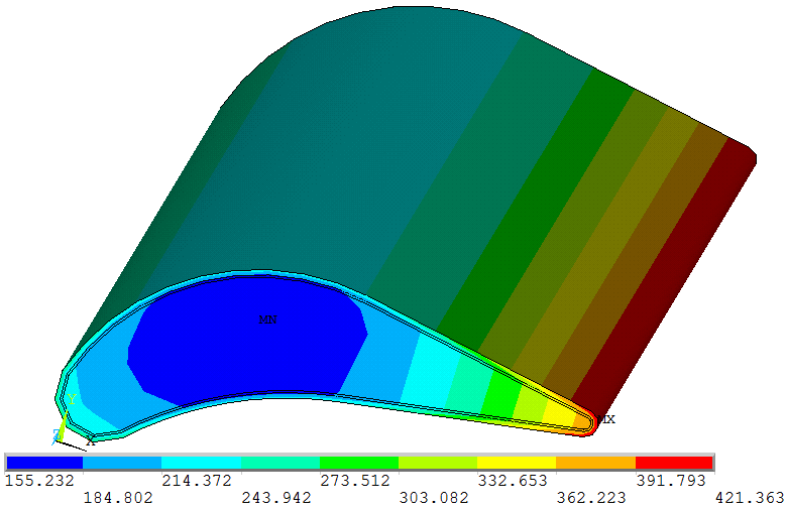

Figure 2.b. The thermal simulation results in temperatures (°C) for the coated blade

For the evaluation of the Temperature-Distance and Equivalent Stress-Distance curves, a distance profile was defined on the edge of the blade. The distance profile is started at the point which is defined in the figure 3 and 5, below the curves. As it is mentioned on the figure 3 and 5, arrows define the distance's trajectory.

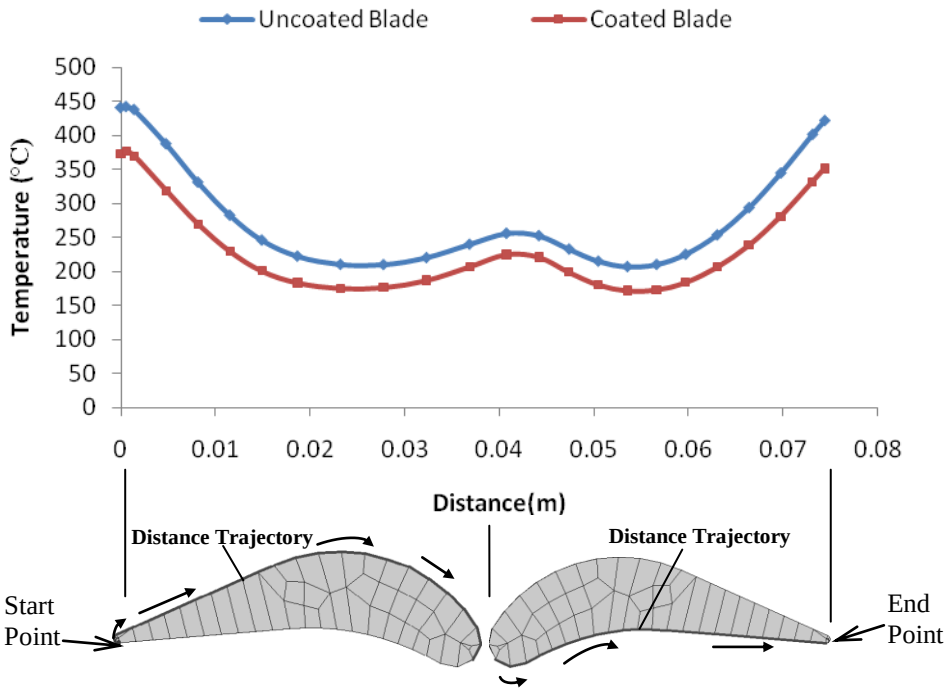

Figure 3. The temperature distribution (°C) of the uncoated and coated blades

In the figure 3, the temperature distribution could be observed through the whole process. During the thermal process coated turbine blade temperature is always smaller than the uncoated one, as it is wanted from the coated turbine blade geometry. For the critical trajectory, TBC was reduced the blade's mean temperature about 48°C. To understand the general thermal behavior of the blades, maximum, minimum and the mean temperature values for the distances of the uncoated and coated turbine blades are given in table 2.

Table 2. The maximum, minimum and mean temperature values for the trajectory distances of the uncoated and coated blades

	Max. Temp. (°C)	Min. Temp. (°C)	Mean Temp. (°C)
Uncoated Blade	442,29	206,68	290,88
Coated Blade	376,35	171,93	242,93

When the figure 4 is considered, stress curves of the uncoated and coated turbine blades can be compared. The uncoated turbine blade's maximum equivalent stress value was 3270MPa and the coated one's maximum equivalent stress value was 2550MPa. Used TBC was reduced the blade geometry's stress distribution in considerable values as 720MPa which was given the 22% equivalent stress reduction. More detailed evaluation of the stress behaviors of the uncoated and coated turbine blades' stress curves can be observed in figure 5.

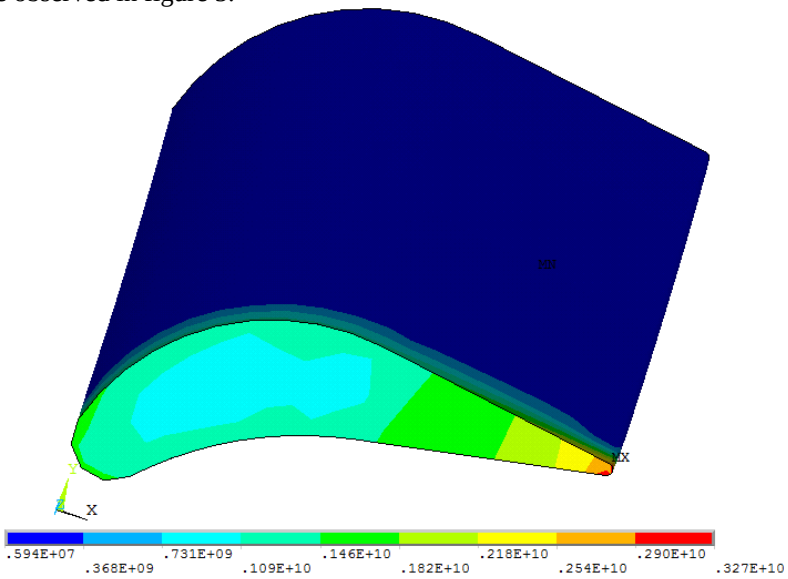

Figure 4.a. The structural simulation of equivalent stress results (Pa) for the uncoated blade

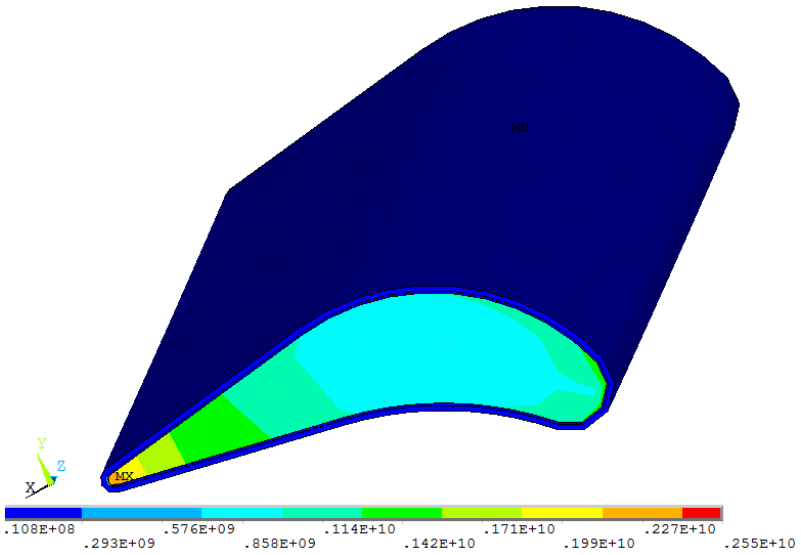

Figure 4.b. The structural simulation of equivalent stress results (Pa) for the coated blade

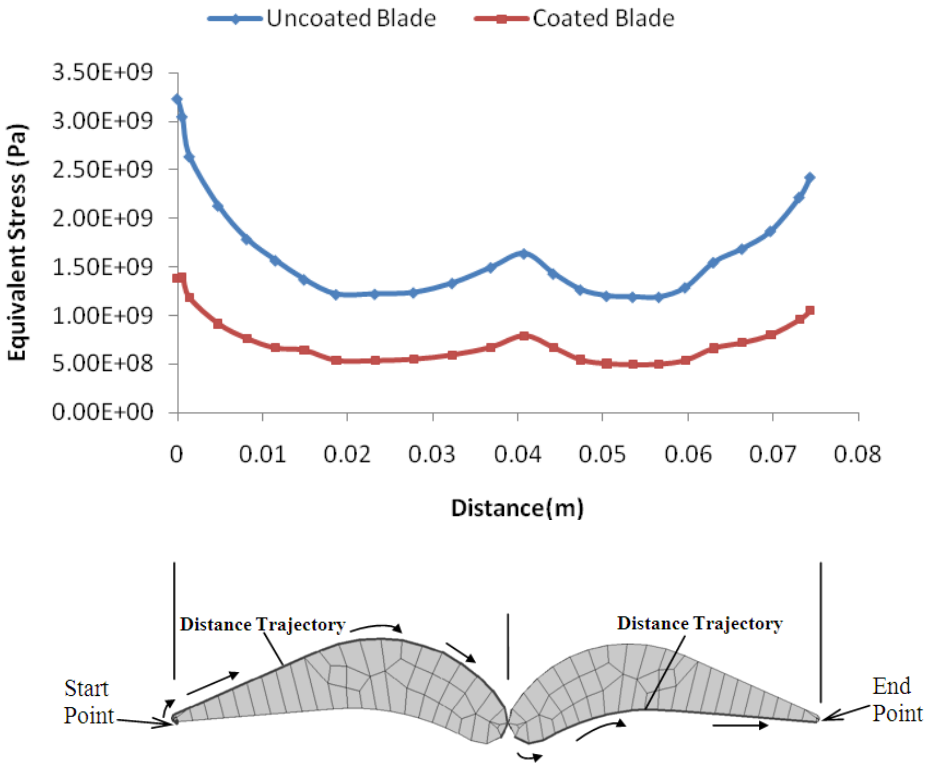

Figure 5. The equivalent stress distribution (Pa) of uncoated and coated blade for trajectory distance

As in the figure 3, figure 5 shows that the equivalent stress distribution of the coated turbine blade is always smaller than the uncoated turbine blade during the process. Little fluctuations can be observed from the curves. For the critical trajectory of the thermal barrier coated blade was reduced only blade's mean stress about 963MPa (29.4% equivalent stress reduction). To determine the stress distribution of the blades, maximum, minimum and mean stress results for the distances of the uncoated and coated turbine blades are shown in table 3.

Table 3. The maximum, minimum and mean equivalent stress values for the trajectory distances of the uncoated and coated blades

	Max. Stress (Pa)	Min. Stress (Pa)	Mean Stress (Pa)
Uncoated Blade	3,24e9	1,19e9	1,72e9
Coated Blade	1,4e9	4,95e8	7,53e8

Finally, in this study, used thermal barrier coated blade geometry, with the help of finite element technique, is proved that the coating decreases the temperatures and the stresses of the turbine blade.

Conclusions

From the present study following results can be drawn:

- In the present study, used TBC reduced the whole blade geometry's mean temperature about 80°C. Using Mullit as a top coating material, 18% thermal protection is received for the turbine blade.
- For the critical trajectory, TBC was reduced the blade's mean temperature about 48°C.
- TBC used blade geometry's reduced mean stress value of 720MPa was given 22% equivalent stress reduction. The indicated level of stress reduction is considerable and protects the blade from the thermal stress more than expected.
- For the critical trajectory of the thermal barrier coated blade was reduced only the blade's mean stress about 963MPa (29.4% equivalent stress reduction).
- This study showed that; after thermal and structural finite element simulations for the uncoated and coated turbine blade, the reduction of the temperatures and stresses are satisfactory and can be determined easily.

References

A.G. Evans, D.R. Mumm, J.W. Hutchinson, G.H. Meier, F.S. Pettit, 2001, Prog. Mater. Sci. 46 , 505.

D.J. Wortman, B.A. Nagaraj, E.C. Duderstadt, 1989 "Mater. Sci. Eng.A", 121, 433.

F. Schubert, G. Fleuri, T. Steinhaus, 2000 "Modelling of the mechanical behaviour of the SC alloy CMSX-4 during thermomechanical loading, Modelling Simul". Sci. Eng. 8, 947.

G. Fleury, F. Schubert, Anisotrope Stoffgesetze für dasviskoplastiche Verformungsverhalten der einkristallinen Superlegierung CMSX-4, Dissertation, RWTH Aachen, Jül-3436 (1997) ISSN 0944-2952.

Marcin Białas, Surface & Coatings Technology 202 (2008) 6002–6010

N. Asok Kumar , S.R. Kale, 2002, " International Journal of Heat and Mass Transfer" 45, 4831–4845

R.A. Miller, C.E. Lowell, 1982, "Thin Solid Films" 95, 265

R.A. Miller, 1987, "Surf. Coat. Technol". 30, 1.

R.D. Jr. Sisson, E.Y. Lee, Y.H. Sohn, in: K.S. Shin, J.K. Yoon, S.J. Kim (Eds.), 1995, "Proceedings of the 2nd Pacific Rim InternationalConference on Advanced Materials and Processing, TheKorean Institute of Metals and Materials", p. 1203.

R.T. Jones, Thermal barrier coatings, in: K.H. Stern (Ed.),1996, "Metallurgical and Ceramic Protective Coatings, Chapman &Hall", London, p. 194.

S.M. Meier, D.M. Nissley, K.D. Sheffler, T.A. Cruse, J. 1991, "Eng.Gas Turbines Power Trans. Am. Soc. Mech. Eng". 114 258.

Y.H. Sohn, E.Y. Lee, B.A Nagaraj, R.R. Biederman, R.D. Sisson Jr.,2001, " Surface and Coatings Technology"146 –147, 132–139

Simulation and Optimization of Ethyl Acetate Reactive Packed Distillation Process Using Aspen Hysys

Abdulwahab GIWA and Süleyman KARACAN

Ankara University, Faculty of Engineering, Department of Chemical Engineering, 06100, Ankara, TURKEY
E-mail: agiwa@eng.ankara.edu.tr, karacan@eng.ankara.edu.tr

Abstract: The simulations and optimizations of a reactive packed distillation process for the production of ethyl acetate, water being the by-product, from the esterification reaction between acetic acid and ethanol has been carried out in this work using Aspen HYSYS 3.2 process simulator. The main column, apart from the condenser and the reboiler, was divided into five sections: rectification, acetic acid feed, reaction, ethanol feed and stripping sections. In the simulations, Non-Random Two-Liquid model was used as the fluid package and the reaction occurring in the reaction section of the column was modeled as an equilibrium one. In order to validate the results of the simulator, experiments were carried out in a reactive packed distillation pilot plant. The data input and output of the experiments were done with the aid of MATLAB/Simulink via electronic modules. The results of Aspen HYSYS simulations were compared with those obtained from the experimental studies.

Key words: Reactive packed distillation; Esterification reaction; Aspen HYSYS; Simulation; MATLAB/Simulink.

Introduction

In recent years, integrated reactive separation processes have attracted considerable attentions in academic research and industrial applications, (Völker, Sonntag, and Engell 2007). One of these processes which is known as "reactive distillation" is potentially attractive whenever conversion is limited by reaction equilibrium (Balasubramhanya and Doyle III, 2000).

Reactive distillation is a process that combines both separation and chemical reaction into one unit. It has a lot of advantages for those reactions occurring at temperatures and pressures suitable for the distillation of the resulting components. Its main advantages are derived from the elimination of equipment and the constant removal of products (Sneesby, Tade, Datta, and Smith 1997). It is known that increased overall conversion can be achieved in equilibrium reactions if the products are continuously removed from the reaction zone. Its other advantages include reduced investment and operating costs, environmental impacts (Pérez-Correa, González, and Alvarez 2008), higher conversion, improved selectivity, lower energy consumption, scope for difficult separations and avoidance of azeotropes (Jana and Adari, 2009).

However, due to the occurrence of both reaction and separation in a single unit, reactive distillation exhibits complex behaviors (Khaledi and Young, 2005) such as steady state multiplicity, process gain sign changes (bidirectionality) and strong interactions between process variables (Jana and Adari 2009). These complexities have made the modeling of the process extremely difficult especially when the column type is a packed one and the reaction is solid-catalyzed. Thus, the representation of this process in the form of a model is still a challenge to chemical engineers because the reactive distillation process, especially one involving continuous flows of feeds, is never truly at steady state. Feed and environmental disturbances, reboiler fouling and catalytic degradation continuously upset the conditions of the smooth running of the process. One approach discovered for the representation of the behavior of a process like this (reactive distillation) is the use of Aspen HYSYS process simulator.

Aspen HYSYS is a process simulation environment designed to serve many processing industries. It is an interactive, intuitive, open and extensible program. It also has many add on options to extend its capabilities into specific industries. With this program, rigorous steady state and dynamic models for plant design can be created. Apart from this, monitoring, troubleshooting, operational improvement, business planning and asset management can be performed with the HYSYS simulator. Through the completely interactive HYSYS interface, process variables and unit operation topology can be easily manipulated (Aspen, 2003).

Therefore, this paper is aimed to develop, simulate, optimize and validate, using experimental studies, an esterification process for the production of ethyl acetate using reactive packed distillation column with the aid of Aspen HYSYS.

Procedures

Experimental Procedure

The experimental pilot plant in which the experiments were carried out was a reactive packed distillation column set up as shown in Figures 1a and b. The column had, excluding the condenser and the reboiler, a height of 1.5 m and a diameter of 0.05 m. The column consisted of a cylindrical condenser of diameter and height of 5 and 22.5 cm respectively. The main column section of the plant was divided into three parts of 0.5 m each. The upper, middle and lower sections were the rectifying, the reaction and the stripping sections respectively. The rectifying and the stripping sections were packed with raschig rings while the reaction section was filled with Amberlyst 15 solid catalyst (the catalyst had a surface area of 5300 m^2/kg, a total pore volume of 0.4 cc/g and a density of 610 kg/m^3). The reboiler was spherical in shape and had a volume of 3 Litre. The column was fed with acetic acid at the top (between the rectifying and the reaction sections) while ethanol was fed at the bottom (between the reaction and the stripping sections) with the aid of peristaltic pumps which were operated through a computer via MATLAB/Simulink program. All the signal inputs (reflux ratio (R), feed ratio (F) and reboiler duty (Q)) to the column and the measured outputs (top section temperature (T_{top}), reaction section temperature (T_{rxn}) and bottom section temperature (T_{bot})) from the column were sent and recorded respectively on-line with the aid of MATLAB/Simulink computer program and electronic input-output (I/O) modules that were connected to the equipment and the computer system. At each case of the experimental studies, the operating parameters were fixed based on the conditions being investigated. The reaction taking place in the packed column is given as:

$$CH_3COOH + C_2H_5OH \xleftrightarrow{K_{eq}} CH_3COOC_2H_5 + H_2O \qquad (1)$$

(a) (b)

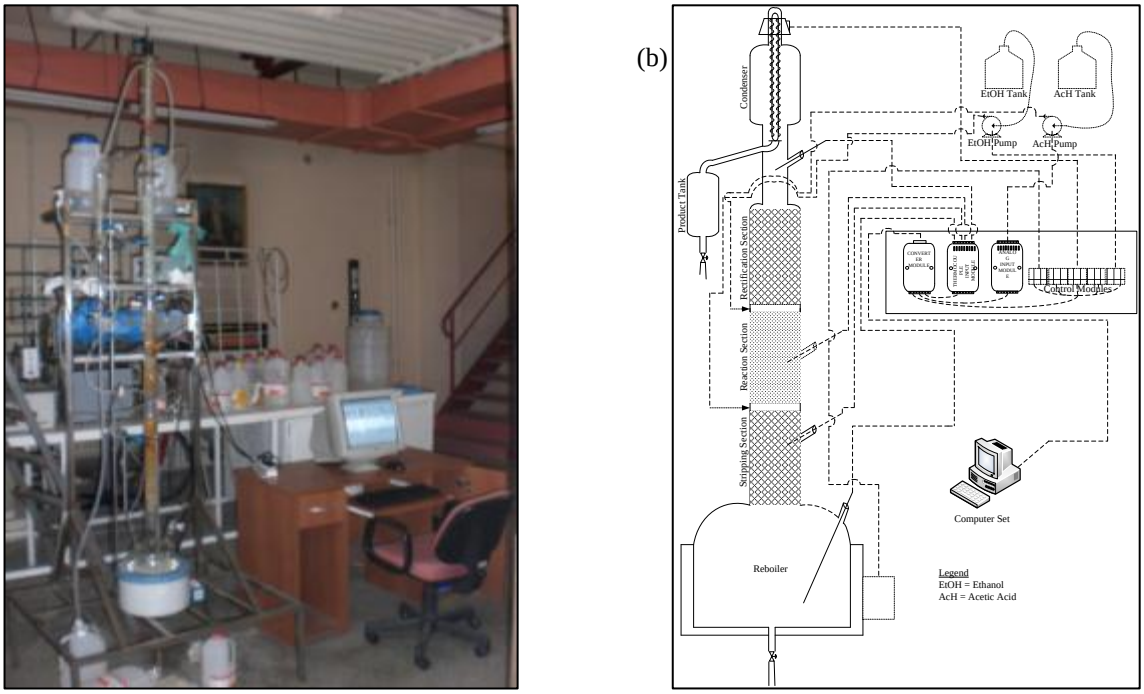

Figure 1 Reactive packed distillation pilot plant: (a) Pictorial view; (b) Sketch view

HYSYS Modeling Procedure

Figure 2 below shows the flowsheet of the reactive packed distillation column built and modeled in HYSYS 3.2 environment. The column consists of a condenser, a rectifying section, an acetic acid feed section, a reaction section, an ethanol feed section, a stripping section and a reboiler. The steady state operating parameters used for the HYSYS model formulation and simulation are as shown in Table 1.

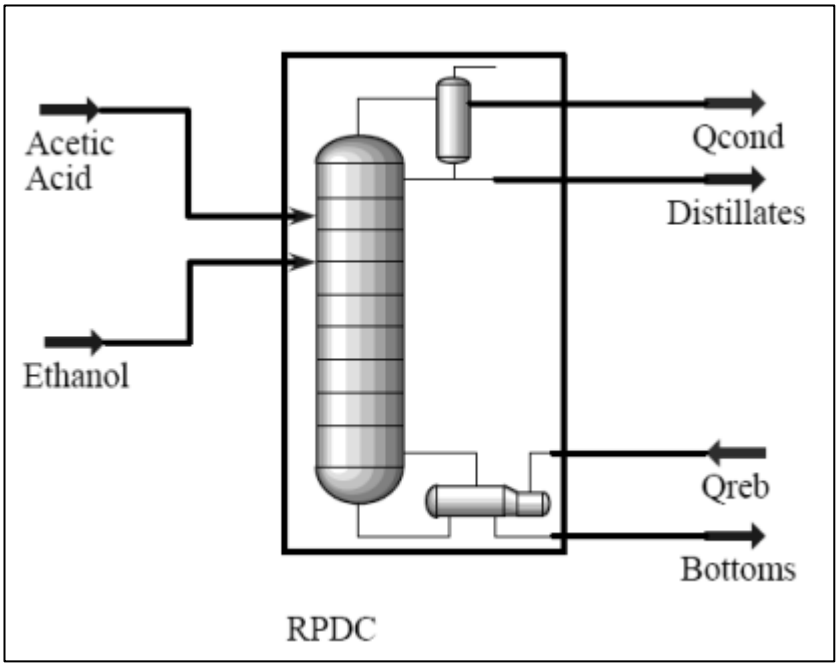

Figure 2 Aspen HYSYS reactive packed distillation steady state simulation flowsheet

Table 1 Steady state operating parameters

Parameter	**Value**
Fluid Package	General NRTL
Reflux ratio (kmol s^{-1} recycle/ kmol s^{-1} distillate)	1
Feed ratio (mL s^{-1} acetic acid/mL s^{-1} ethanol)	1
Reboiler duty (kJ/s)	0.250
Condenser	
Type	Cylindrical
Height (m)	0.225
Diameter (m)	0.05
Rectifying Section	
Packing type	Raschig rings
Height (m)	0.4412
Acetic Acid Feed Section	
Packing type	Raschig rings
Height (m)	0.0882
Reaction Section	
Packing type	Amberlyst 15
Height (m)	0.4412
Ethanol Feed Section	
Packing type	Raschig rings
Height (m)	0.0882
Stripping Section	
Packing type	Raschig rings
Height (m)	0.4412
Reboiler	
Type	Spherical
Volume (L)	3
Level	50%

HYSYS Optimization Procedure

After the steady state simulation, the optimization of the plant was carried using the same HYSYS 3.2 process simulator by incorporating an optimizer into the flowsheet (see Figure 3). Three different algorithms were used for the optimization; they are: Fletcher-Reeves, Quasi-Newton and Successive Quadratic Programming (SQP) algorithms. The objective function of the optimization was taken as maximizing the mole fraction of ethyl acetate in the distillate (top segment) stream. The ranges of the adjusted variables used for the optimizations are as shown in Table 2 below.

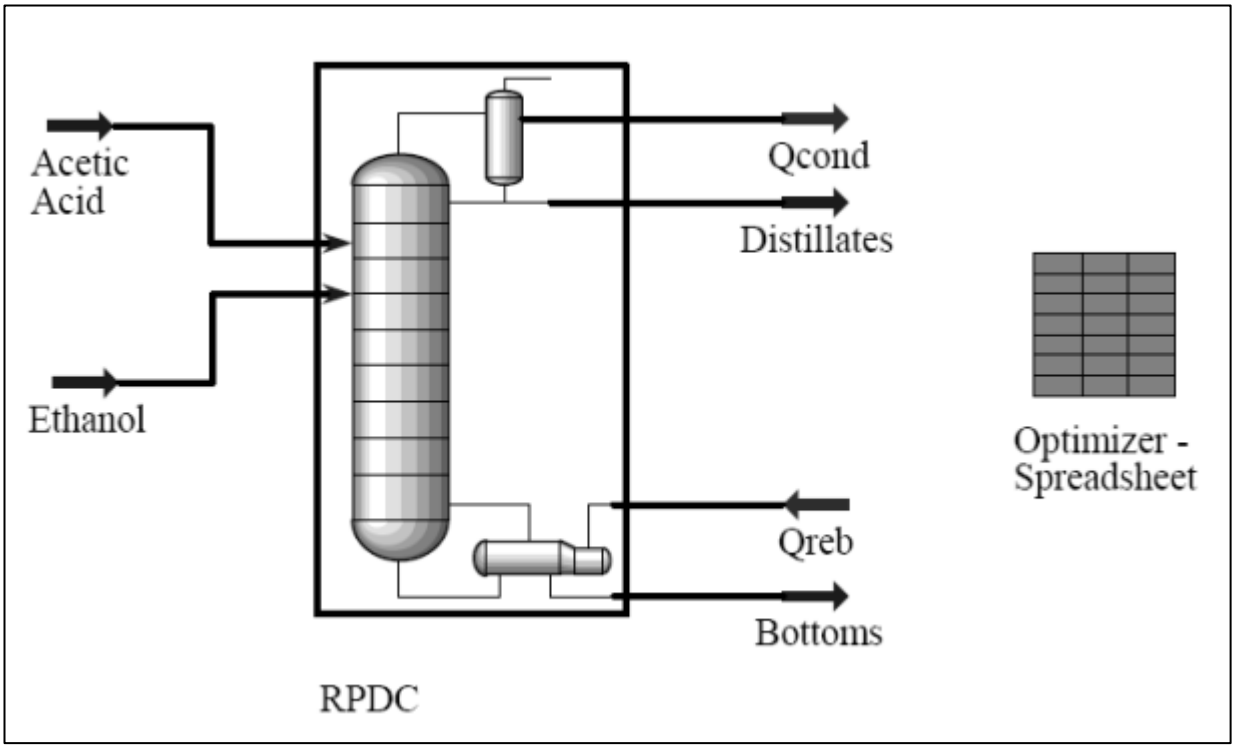

Figure 3 Aspen HYSYS reactive packed distillation optimization flowsheet

Table 2 Parameters used for running the optimizations

Parameter	Low bound	High bound
Reflux ratio (kmol s^{-1} recycled liquid/kmol s^{-1} liquid distillate)	1	9
Feed ratio (mL s^{-1} acetic acid/mL s^{-1} ethanol)	0.5	5
Reboiler duty (kJ/s)	0.050	0.600

After running the HYSYS optimizer, the optimized values of the parameters obtained from one of the algorithms were then used to run the experimental set-up again for validation.

Results and Discussions

To simulate and optimize a reactive packed distillation column for the production of ethyl acetate using Aspen HYSYS 3.2 process simulator in this work, the entıre column was divided into 17 segments excluding the condenser and the reboiler and its steady state study was carried out by simulating the prototype plant built using the simulator under the conditions of reflux ratio of 1, feed ratio of 1 and reboiler duty of 0.250 kJ/s. The other parameters used for the simulation can be found in Table 1. After the simulation, the temperature and composition profiles obtained are as shown in Figures 4 and 5 respectively.

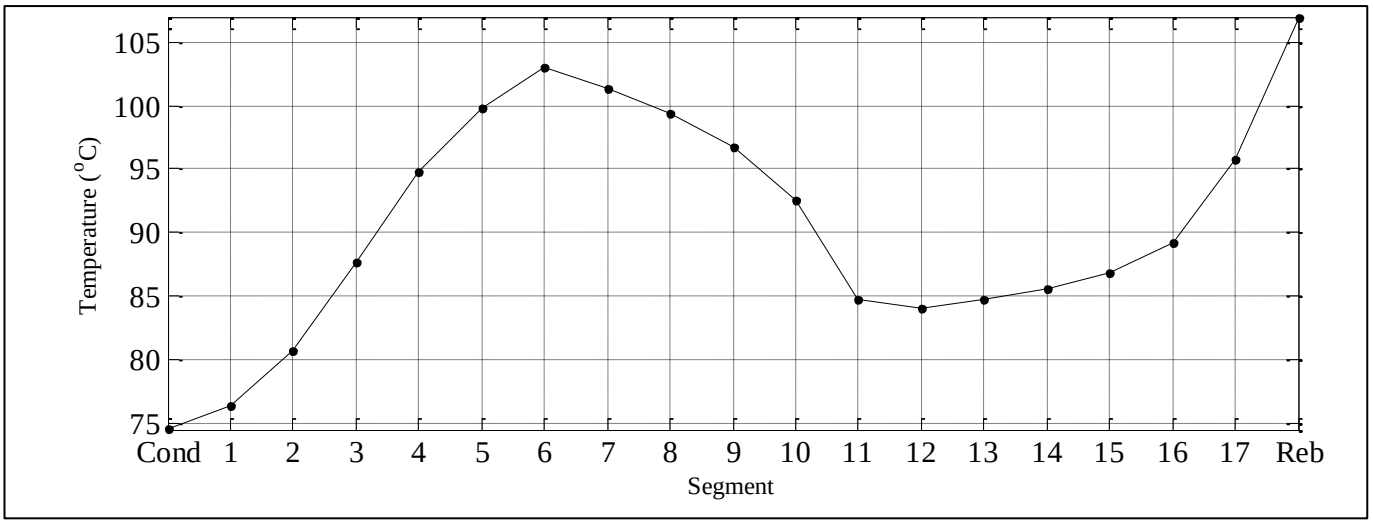

Figure 4 Aspen HYSYS reactive packed distillation column steady state temperature profile

As can be seen from the temperature profile shown in Figure 4, the temperature of the segment near the acetic acid feed section was found to be very high. This was due to the combined effects of the exothermic nature of the reaction occurring in the reaction section of the column, the upward movement of ethanol vapor from the ethanol feed section and the mixed vapor moving upward from the reboiler.

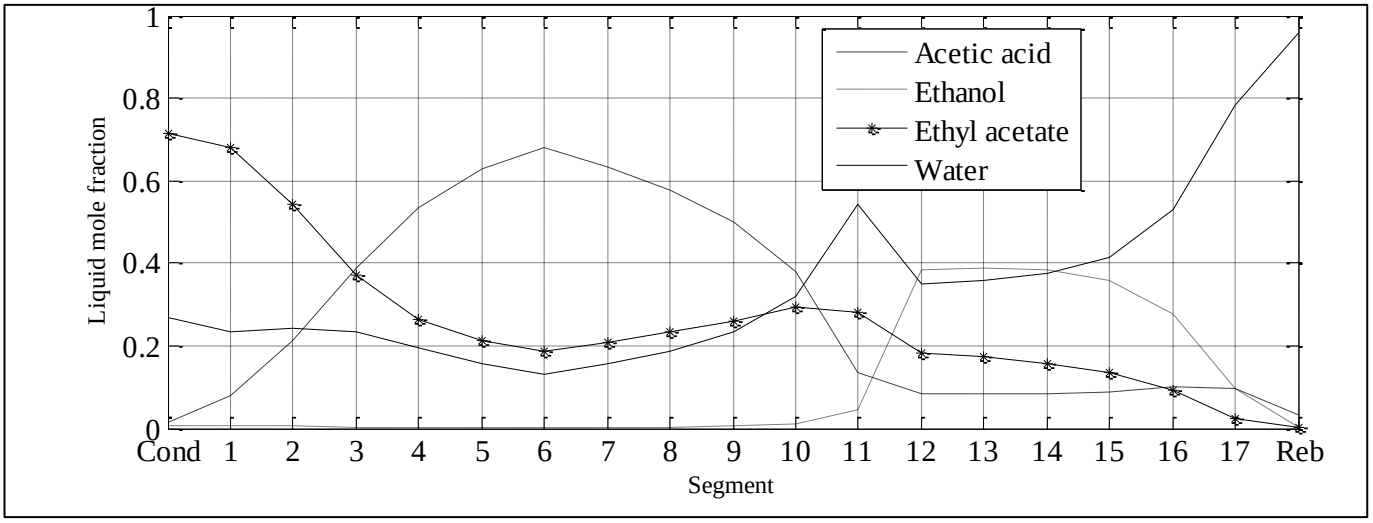

Figure 5 Aspen HYSYS reactive packed distillation column steady state composition profiles

From the composition profile (Figure 5), ethyl acetate (the desired product), as expected, was found to have the highest mole fraction of 0.7132 in the top segment of the column followed by water with a mole fraction value of 0.2665. The mole fractions of the other two components (acetic acid, 0.0141 and ethanol, 0.0062), as expected, were found to be very low in the top segment. This was an indication that effective reaction conversion and separation were achieved in the column.

Considering the mole fractions of the various components in the reboiler, water was found to have the highest mole fraction of 0.9597 followed by acetic acid with mole fraction of 0.0332. The mole fractions of ethanol and ethyl acetate in the reboiler were 0.0043 and 0.0028 respectively. The very small values of the mole fractions of acetic acid and ethanol in the reboiler were due to high reaction conversion occurring in the column.

When the experimental set-up was run using the same parameters as those used for the HYSYS simulation, taking the top temperature as the point of interest to infer composition because it is the one indicating the state and kind of the product obtained from the column, a good relationship was observed from the results of the two (HYSYS simulation and experimental study) cases. For instance, the steady state top segment temperature obtained from HYSYS simulation was 74.5338 ^{o}C while that of the experimental study was measured to be 74.6600 ^{o}C. This is an indication of the fact that the HYSYS model developed for the reactive packed distillation process is a good representation of the real process.

Having carried out the steady state simulation of the Aspen HYSYS RPDC and validated using an experimental study, the process was optimized using three different optimization algorithms. The maximization of the mole fraction of ethyl acetate in the column top segment was set as the objective function of each of the optimizations. The results obtained from the optimizations of the process are as shown in Table 3 below.

Table 3 Optimum parameters

	Value			
Parameter	**Steady-State**	**Fletcher-Reeves**	**Quasi-Newton**	**SQP**
Reflux ratio (kmol s^{-1} recycle/ kmol s^{-1} distillate)	1.0000	2.8995	3.0881	2.6103
Feed ratio (mL s^{-1} acetic acid/mL s^{-1} ethanol)	1.0000	3.3251	3.4565	2.0011
Reboiler duty (kJ/s)	0.2500	0.1076	0.0951	0.1070
Objective function (Top ethyl acetate mole fraction)	0.7132	0.7628	0.7624	0.7608
Top segment temperature (^{o}C)	74.5338	74.3335	74.3356	74.3260

It can be observed from the results shown in Table 3 that the increase (due to the maximization) in the mole fraction of ethyl acetate in the column top segment has resulted in a decrease in the top section temperature. Also, as can be seen from the table, among the three algorithms used for the optimization of the process, Fletcher-Reeves algorithm was found to give the highest mole fraction of ethyl acetate in the top segment of the column by maximizing the objective from the steady state simulation value of 0.7132 to 0.7628. Quasi-Newton algorithm yielded a very very close value (0.7624) of ethyl acetate mole fraction to that of the Fletcher-Reeves algorithm. The optimized ethyl acetate mole fraction (0.7608) gave by SQP algorithm was also found not to be too different beyond acceptation from those of the other two. The differences in the objective functions given by the three algorithms were accounted for by the differences in the optimized operating conditions given by them. For instance, the optimized reflux ratio obtained from the three algorithms can be approximated to one significant figure of 3.

However, the situation is not the same in the case of the feed ratio because the approximations to one significant figure of each of the feed ratios obtained from the Fletcher-Reeves and Quasi-Newton algorithms were both 3 while that of the SQP was 2. Considering the optimum reboiler duty, the values given by Fletcher-Reeves and SQP algorithms were found to be very close to each other than when each of them is compared to the result given by Quasi-Newton.

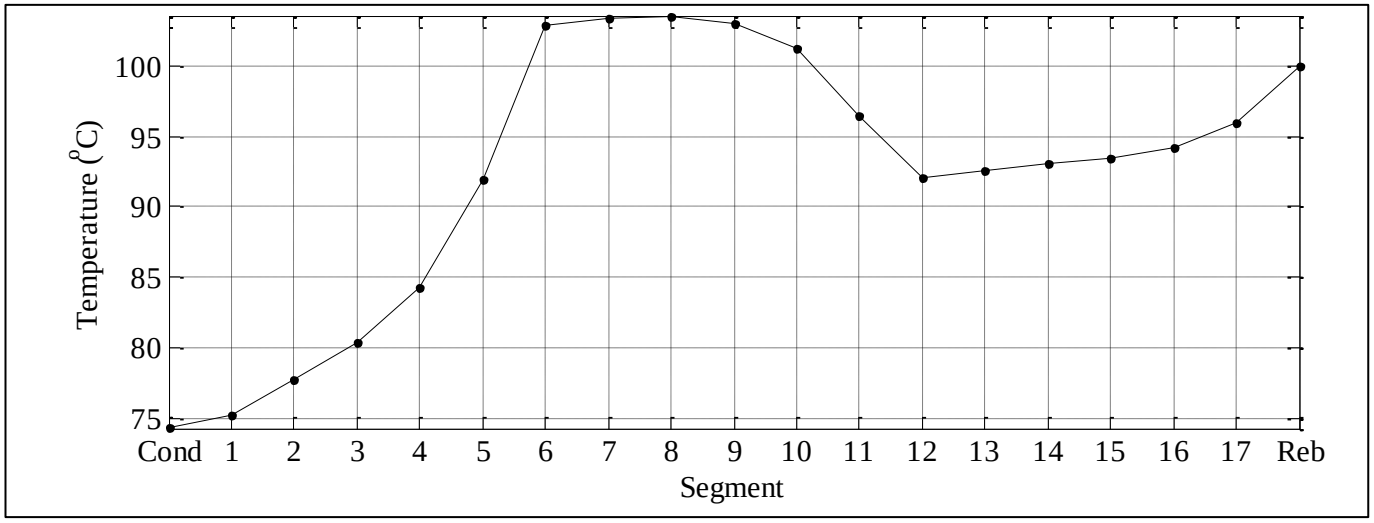

Figure 6 Aspen HYSYS reactive packed distillation column optimization temperature profile

Furthermore, an experiment was carried out for the validation of the optimization using the optimized operating conditions obtained from one of the algorithms. In this case, the optimized operating conditions of SQP was used because the value of its objective function was discovered to be close to those of the other two and it had the lowest feed ratio among the three. Choosing it (SQP) was considered as an effort to reduce cost. After the experiment was carried out using the selected optimum operating conditions, it was discovered from the results that there is a good conformity between the optimized top segment temperature of the process using HYSYS 3.2 and the one measured from the experiment because the HYSYS 3.2 optimized value was 74.3260 ^{o}C while the experimental one was 74.5200 ^{o}C.

From the temperature and composition profiles of the optimized case of the process shown in Figures 6 and 7 respectively, it was noticed that there are changes between the profiles and those of the steady-state simulation shown in Figures 4 and 5. That is to say that, while trying to maximize the composition of the ethyl acetate in the product stream, the changes that occurred in the composition profiles of the components have caused a change in the temperature profile also.

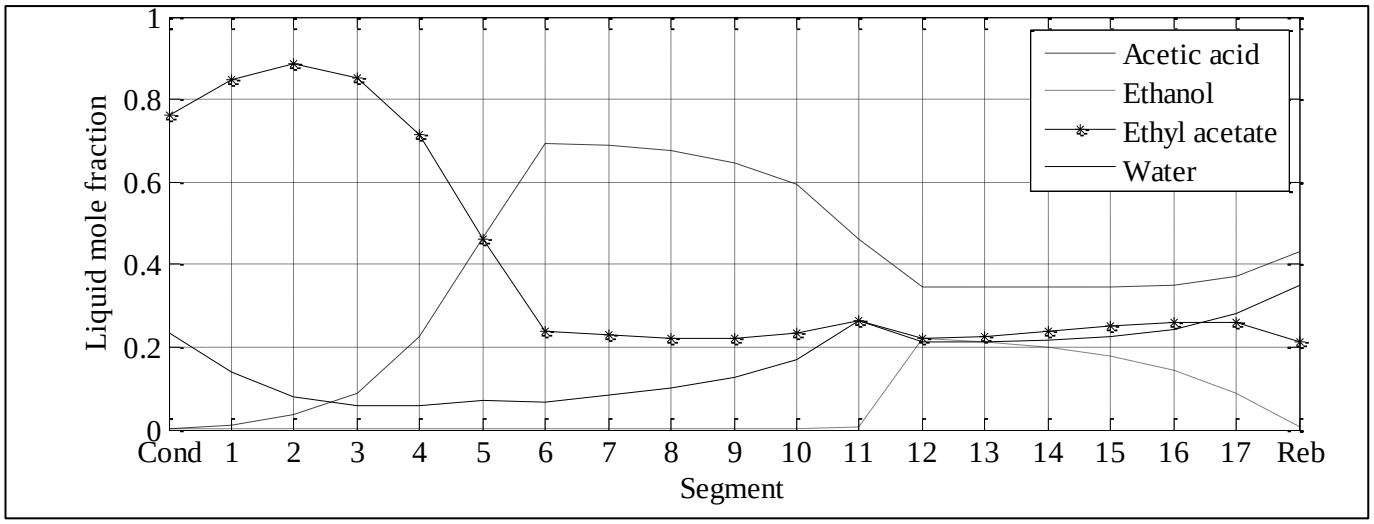

Figure 7 Aspen HYSYS reactive packed distillation column optimization composition profiles

The occurrence of the change in the temperature profile owing to the changes in the composition profiles of the components is an indication of the fact that the compositions of the components and the temperatures of the column segments are dependent on one another. In other words, column segment composition is a function of column segment temperature and vice versa.

Conclusions

The good relationship between the temperature estimated from the simulation using the developed Aspen HYSYS model for the reactive packed distillation process and the experimental ones measured from the pilot plant have revealed that Aspen HYSYS can be used to represent and simulate the process successfully. The three optimization algorithms investigated were found to produce relatively similar maximized mole fractions of ethyl acetate in the top segment of the column. When the optimum parameters of SQP were used to run an experiment for validation, a good agreement was found between the optimum top segment temperature and the experimental one.

Acknowledgement

Abdulwahab GIWA wishes to acknowledge the support received from The Scientific and Technological Research Council of Turkey (TÜBİTAK) for his PhD Programme. In addition, this research was supported by Ankara University Scientific Research Projects.

References

Aspen. (2003). *HYSYS 3.2 installation guide.* U.S.A: Aspen Technology.

Balasubramhanya, L. S. & Doyle III, F. J. (2000). Nonlinear model-based control of a batch reactive distillation column. *Journal of Process Control, 10,* 209-218.

Jana, A. K., & Adari, P. V. R. K. (2009). Nonlinear state estimation and control of a batch reactive distillation. *Chemical Engineering Journal, 150,* 516-526.

Khaledi, R., & Young, B. R. (2005). Modeling and model predictive control of composition and conversion in an ETBE reactive distillation column. *Industrial & Engineering Chemistry Research, 44,* 3134-3145.

Pérez-Correa, S., González, P., & Alvarez, J. (2008). On-line optimizing control for a class of batch reactive distillation columns. Proceedings of the 17th International Federation of Automatic Control (IFAC) World Congress, Seoul, Korea, 17, 3263-3268.

Sneesby, M. G., Tade, M. O., Datta, R., & Smith, T. N. (1997). ETBE synthesis via reactive distillation. 2. Dynamic simulation and control aspects. *Industrial & Engineering Chemistry Research, 36,* 1870-1881.

Völker, M., Sonntag, C., & Engell, S. (2007). Control of integrated processes: A case study on reactive distillation in a medium-scale pilot plant. *Control Engineering Practice, 15,* 863–881.

The Discovery of Enterprise Network Topology Created in a Virtual Environment with SNMPv3

Musa BALTA[1], İbrahim ÖZÇELİK[2]

[1,2] Computer Engineering Department, Faculty of Computer and Information Science
Sakarya Üniversitesi 54187 Serdivan / SAKARYA / TURKEY
[1]e-mail: mbalta@sakarya.edu.tr, [2]e-mail: ozcelik@sakarya.edu.tr

Abstract: To design network management systems in a best way, network topology have to be discovered with every features of network such as connectivity, device type, etc. Our goal is to discover an enterprise network which is created in a virtual environment (GNS3 and VMWARE Workstation) with SNMPv3. An algorithm which is used in previously academic researchs is redesigned according to features of virtual environments which are used in project.

Key words: Topology Discovery, Snmpv3, GNS3, VMWARE Workstation

Introduction

Nowadays enterprise networks have become more complex and wide because of huge number of users and a lot of applications that work in networks (Pandey, Choi, Won and Hong (2011), Siamwalla, Sharma and Keshav (1999), Breitbart, Garofalakis,Jai,Martin,Rastogi and Silberschatz (2004), Lowekamp, O'Hallaron and Gross (2001)). To benefit from this growing enterprise networks more effectively and efficiently, network management concept which means management and maintenance at the highest level has occured. Network management systems have some kind of basic concepts such as security, topology discovery, monitoring, controlling, coordination and schedule. To benefit from these concepts of network management more effectively, first of all, topology discovery and connection of between devices have to be detected in a best way. And then network management system can be designed according to these results.

There are several techniques in network topology discovery such as ping mechanism, trace-route, DNS (Domain Name System) and SNMP (Simple Network Management Protocol) (Pandey and et.al.(2011), Siamwalla and et.al.(1999), Breitbart and et. al. (2004), Lowekamp and et. al. (2001)). But only SNMP can provide better performance than others and also it pulls a lot of queries in completely and a secure way like as name of device, device type or connectivities between devices.

In this paper, an enterprise network topology that has been created in virtual environmet (GNS3 and VMWARE workstation) is going to be discover through an algorithm which uses SNMPv3 that is security version of SNMP. Due to work in virtual environment, the proposed algorithm is going to finish topology discovery more less time than a real environment.

Snmp

SNMP is a network management protocol for managing IP (Internet Protocol) networks. SNMP has a three structure; agent software which runs on managed devices, SNMP manager which communicates between NMS (Network Management System) and agent, and finally NMS which manages all network operations. SNMP'working mechanism is like as sending request and reply to request and to make these operations, UDP (User Datagram Protocol) is used (Harrington, Presuhn and Wijnen (1999a),Harrington and et. al. (1999b)). By means of SNMP, data can be pulled from device easily and configurations on device can be changed easily. For example, device can be restarted or a configuration file can be send to device. Hereby, we realize that SNMP is more important protocol in network management.

When SNMP pull data from the device, SNMP uses some kind of identifier to pull data. These identifiers are called as MIB (Management Information Base) values and these values are represented with numbers. For instance, 1.3.6.1.2.1.1.5.0 variable means device name (Harrington, Presuhn and Wijnen (1999b), Blumenthal and Wijnen

(1999)). The requested values in MIB are called also OID (Object Identifier) variables. Values of MIB and OID are existed in reference numbered (Levi, Meyer and Stewart (1998)) .

SNMP uses some criterias in for network security. Some more important criterias are given in below (Levi and et. al.(1998));

- Authentication: It provides data integrity and authenticate source of data.
- Community name: It is used for authetication parameter during message transmission between SNMP and managed devices.
- Encryption: It encodes SNMP packages.
- Privacy: It provides to keep content of SNMP packages in network in hidden.
- Security Level: This means an algorithm which is used on every SNMP packages. HMAC, MD5 or SHA are used.
- Data Integrity: It means not divided data situation of a message package.
- SNMP User: This is a user who manage the SNMP system. According to SNMP messages that comes from network management system, user can make any related changes about situation of network.
- Security Model: This is a security strategy that is used by SNMP agent. There are 3 version: SNMPv1, SNMPv2c, SNMPv3.

Unfortunalety, all of SNMP version can't support all these security criterias. There is a comprasion of SNMP version about security in table 1.

Table 1: SNMP Security Models and Levels (Levi and et. al. (1998))

	Model	Level	Authetication	Encryption
1	v1	noAuthNoPriv	Community name	No
2	v2c	noAuthNoPriv	Community name	No
3	v3	noAuthNoPriv	User name	No
4	v3	authNoPriv	MD5 or SHA	No
5	v3	authPriv	MD5 or SHA	DES, AES

As we see in above, SNMPv3 made SNMP queries are used in secure way with encryption algorithms during data communication because of supporting all security levels. So SNMP packages are encrypted during all communication and network security is ensured.

Application of Network Topology Discovery

Network topology discovery is very big and comprehensive area and there are also a lot of academic research about it (Pandey and et.al.(2011), Siamwalla and et.al.(1999), Breitbart and et. al. (2004), Lowekamp and et. al. (2001)). In addition, there are a lot of applications about network discovery in both academic and commercial environment (Lyon (1997) NMAP, Paessler AG (2003) PRTG). Most of these studies are made in real environment. In our study, we have referenced to Pandey's (2011) academic research which is made with using SNMPv2c. But in our study, both an enterprise network is created in virtual environment and the topology is discovered with SNMPv3 in securely.

With this goal, in the following sections, firstly information with related to modelling environment is going to be given and then information of algorithm in used will be given.

Modelling Environment

To modelling a network topology, we use a well-known program called as GNS3 (Graphical Network Simulator) that is a modelling program for network modelling simulator. Since GNS3 can model Cisco devices exactly, it has been used for this study (Grossmann, Marsili, Alt and Eromenko (2007), GNS3). To run the application codes, at first a virtual machine is created in VMWARE Workstation that is a well-known program in virtulization environment, and then this created virtual machine is attached to network topology that is created in GNS3 program with making related configurations (VMWARE (1995)).

An enterprise network means to connect all isolated departmental or workgroup networks into an intracompany network, with the potential for allowing all computer users in a company to access any data or computing resource. And also it would provide interoperability among autonomous and heterogeneous systems and have the eventual goal of reducing the number of communication protocols in use. In brief, it integrates all the systems within an organization.

Depending on the information given in above, for network topology discovery which is purpose of this study, an enterprise network structure which is created with GNS 3 and Vmware programs, is chosen as a sample model. In this model, part 1 is given a form as backbone of the network and for this part, Cisco 6509 switches are used. In part 2, cloud describes the virtual machine in VMWARE Workstation which we developed our application in. In part 3, 4, 5 and 6, different departments of the enterprise network are shown. One of the main backbones manages DMZ (Demilitarized Zone) which is shown in part 7. DMZ exposes an organization's external seriveces to a larger untrusted network (usually internet). The other one manages VPN (Virtual Private Network) servers which are shown in part 8. VPN provides remote offices or traveling users access to a central organizational network securely. On the other hand, the rest of topology consist of call managers and access points.

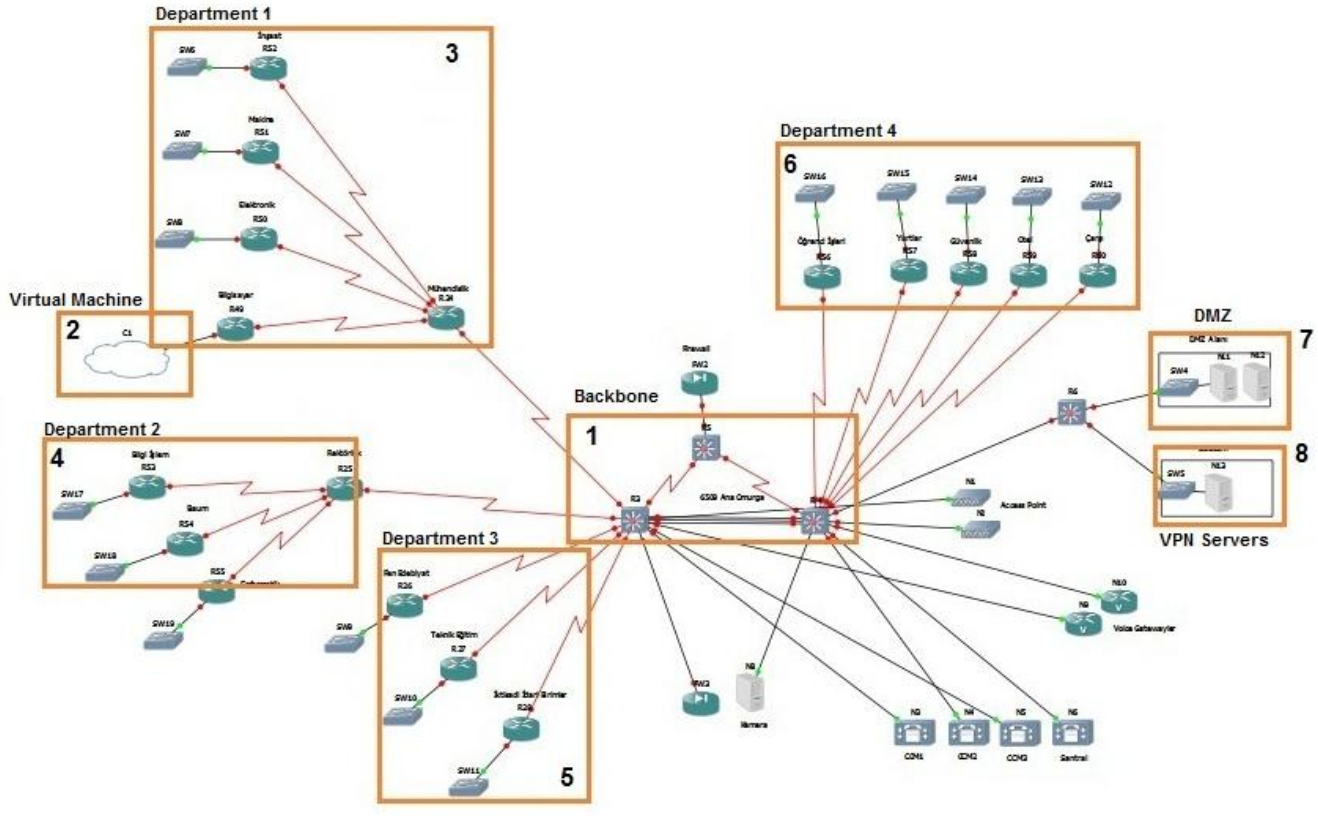

Figure 1: An Example of An Enterprise Network Topology

After finishing all required configurations (such as enabling SNMP, router configurations etc.) in GNS3 program, modelling of an enterprise network is completed. The part that application codes and algorithm run in, is created in VMWARE Workstation program and attached to topology as a cloud which is shown in part 2 of Figure 1.

Configuration

This proposed algorithm consists of a lot of subjects such as device type, connectivity of devices, routing table etc.

Before we start to run the algorithm, we have to check all configuration on devices are ok. To pull out datas from devices, we use SNMPv3 which is shown in row number 5 of Table 1. For enabling SNMP on each device, we have to observe these rules in below (Blumenthal and et. al.(1999), (Levi and et. al.(1998));

- Group is created: The security model and level that is given in row number 5 of Table 1 is selected. "grup1" is created for devices in same area in command line in below. This group is set to "read" feature and security level is selected as "v3". And then "grup1_oku" is created for "read" feature.

  snmp-server group grup1 v3 priv read grup1_oku

- User is created: According to security criterias, users are added to group. For user names, "kullanici" is used. To add security criterias, "md5" algorithm is used for authentication, "aes 256" algorithm is used for encryption. And this security criterias are set to "grup1".

  snmp-server user kullanici grup1 v3 encrypted auth md5 cisco priv aes 256

- Features is created: "read, write and notify" features can be set to group. Our study'aim is only about topology discovery, "read" feature ise enough for us. And "read" feature is related to "view" command. "izle" is created for "view" feature.

  snmp-server view izle system included

The Used Algorithm and Implementation

After all of the configurations have been completed, the algorithm is ready to start. As we told, SNMP mechanism is send request and reply to the request (Lowekamp (2001)). All values (such as system situation of device, routing table on device, mac address table of device, package that flows over device) are identified by MIB values. So when you want to pull out data from device, you have to add related MIB values to end of the SNMP query.

According to this SNMP MIB value responses from device, the algorithm is created and also in every step of algorithm, related MIB values are used.

The used algorithm for the project is shown in Figure 2. Since GNS3 doesn't support some features in swithes and logical topologies, this proposed algorithm is the renewed version of the algorithm that is given in academic research (Pandey and et. al. (2011)):

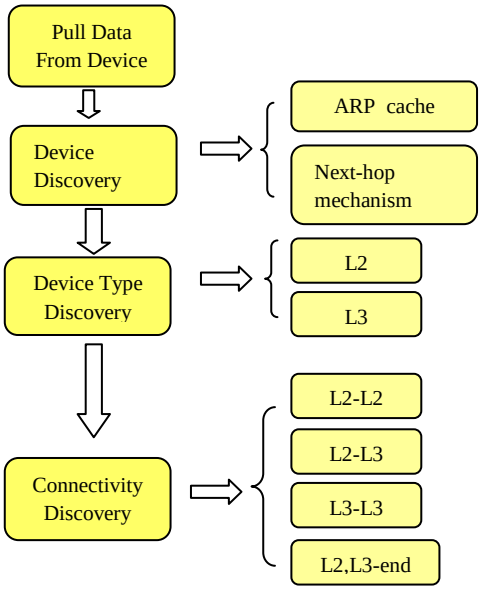

Figure 2*:* The Used Algorithm

Steps of the algorithm:

- **Pull data from device**: After creating network topology on virtual environment, we configure device and then we can pull datas from devices with SNMP queries. For pulling out data from device, we use "snmpwalk" query technique of "net-snmp" library which includes all SNMP PDU's (Protocol Data Units). For example, to get the name of device name, we have to add this query to our application:

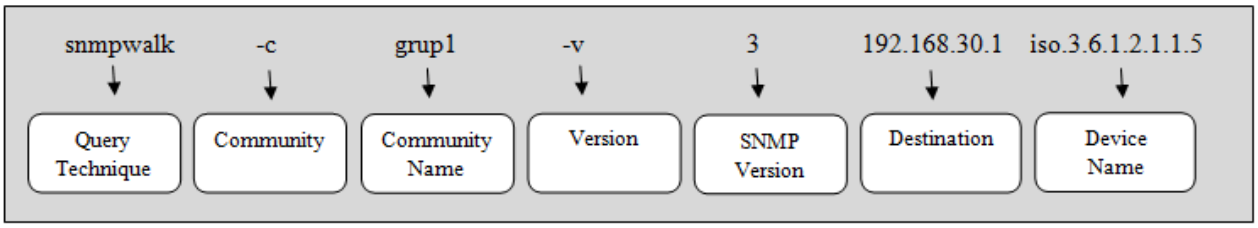

- **Device discovery**:"ipNetToMediaNetAddress" and "ipRouteNextHop" values are pulled out from devices with using ARP caching and Next-hop mechanism (Cisco 2005, Bierman and Jones (2000)). Firstly, we find out our subnet, then we start to ping all the subnet. After pinging all the subnet, we can find all alive devices. And then we send query of "sysServices" to all the alive devices. If the response that comes from device is equal to "78", we realize that device is a router and we look at the routing table of that device with query of "ipRouteNextHop". This tables includes all subnets of the network. Finally we ping again all of the subnets of the network. Hereby, we can find all alive devices. With ARP caching, we can find IPs of layer 2 devices with using query of "ipNetToMediaNetAddress".

- **Device type discovery**: According to "sysServices" value that is pulled from device, system decides that device is L2 or L3 device. After completing the device discovery part of the algorithm, system sends to query of "sysServices" to all of the alive devices. According to response comes from device, we can realize device is a what kind of device.

- **Connectivity discovery**: According to result of matching of ip and mac address that comes from device, we system decide that connectivity between devices is L2 or L3 connectivity. For finding L3-L3 connectivity, we use query of "ipRouteNextHop". According to the result of query, we can check out the routing table. In routing table, we can see only "direct" or "indirect". Direct means that ip is an interface of that router. Indirect means that ip is destination route of that router. For L2-L2 connectivity, we check out AFT (adres forwarding table) of L2 devices. If there is an match of this tables, we can realize these devices are connected to each others. For L2-L3 matching, we check out all the entries of mac tables of switches. If any entry is the same mac of any router's interface, we realize that router is connected to that switch.

Project is coded with C# programing language in Visual Studio. As a database, MySql is chosen for this study. For SNMP libraries, Web SNMP API.Net Edition 4 is used (Zoho, WebNMS). After running the program,we have a network view in Figure 3. In Figure 3, we have run the algorithm only on these parts of Figure 1.

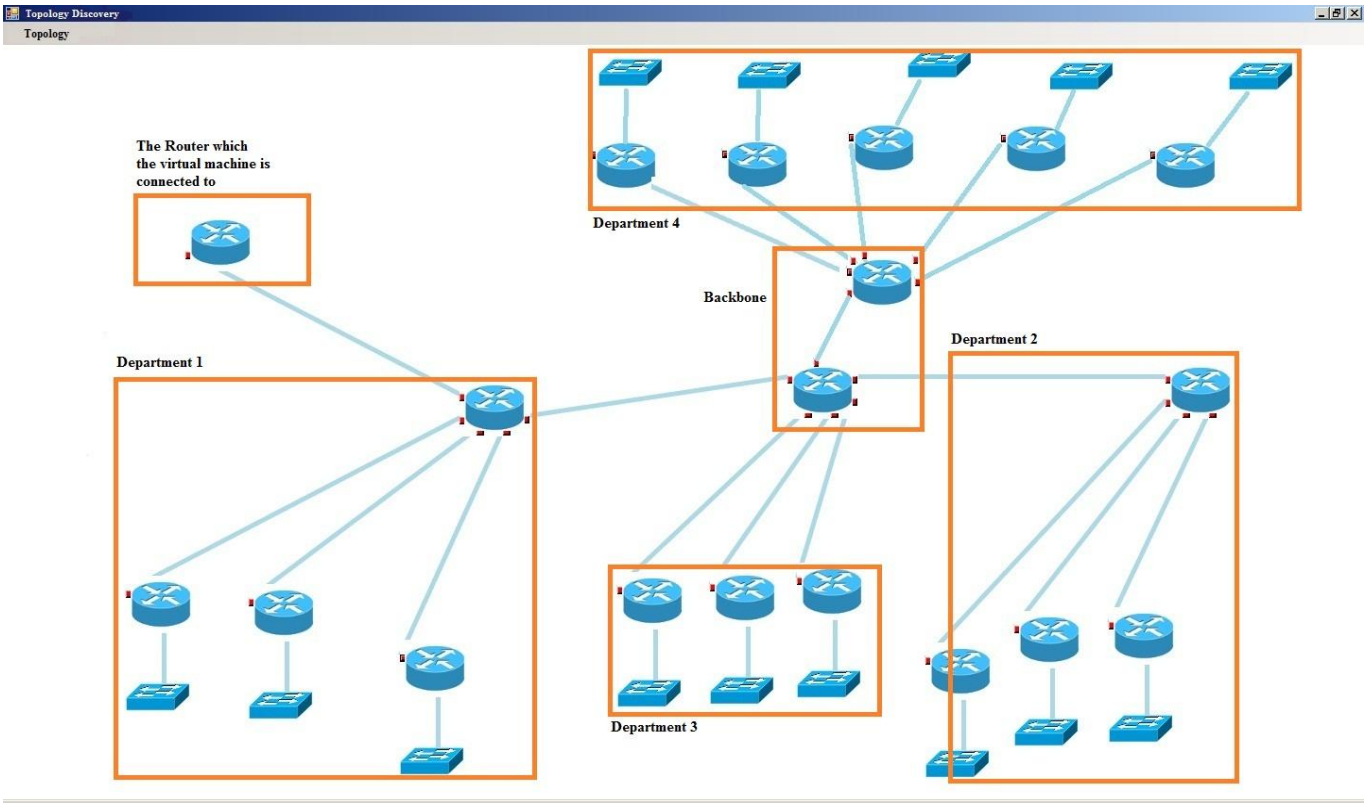

Figure 3: Graph View of Network

Conclusion

In this study, we have chosen a virtual environment instead of real environment in order to not come up some problems in real environment for network topology. For virtual environments, GNS3 and VMWARE programs are used, related configuration are made on this programs. Because of security features, we have chosen SNMPv3 for network discovery. Since network discovery is made in different virtual environments which communicate with each other, this study can be an example for futureworks.

Acknowledgement

This project is supported by SAU Committee of Academic Research Projects (Project number: 2011-50-01-072)

References

Bierman and Jones (2000). IETF web page, Physical topology MIB. <http://www.ietf.org/rfc/rfc2922.txt> (2011 June 27).

Blumenthal and Wijnen (1999). IETF web page, User-based Security Model (USM) for version 3 of the Simple Network Management Protocol (SNMPv3). < http://www.ietf.org/rfc/rfc2574.txt> (2011 July 24).

Breitbart, Garofalakis,Jai,Martin,Rastogi and Silberschatz (2004). Topology discovery in heterogeneous IP networks:the NetInventory system. *IEEE/ACM Transactions on Networking* 12(3) 401–414.

Cisco (2005). Cisco web page, SNMP community string indexing. <http://www.cisco.com/en/US/tech/tk648/tk362/technologies_tech_note09186a00801576ff.shtml> (2011 June 27)

Grossmann, Marsili, Alt and Eromenko (2007). GNS3 web page, Homepage. <http://www.gns3.net/documentation> (2011 June 25).

Harrington, Presuhn and Wijnen (1999a). IETF web page, A Simple Network Management Protocol (SNMP). <http://www.ietf.org/rfc/rfc1157.txt> (2011 July 22).

Harrington, Presuhn and Wijnen (1999b). IETF web page, An Architecture for Describing SNMP Management Frameworks. <http://www.ietf.org/rfc/rfc2571.txt> (2011 July 22).

Levi, Meyer and Stewart (1998). IETF web page, SNMPv3 Applications. <http://www.ietf.org/rfc/rfc2273.txt> (2011 July 24).

Lowekamp, O'Hallaron and Gross (2001). Topology discovery for large ethernet networks. *ACM SIGCOMM* August; 237–248.

Lyon (1997). NMAP web page, Homepage. <http://nmap.org/book/man.html> (2011 July 16).

Paessler AG (2003). Paessler web page, PRTG. <http://www.paessler.com/manuals/prtg8/quick_start_guide.htm> (2011 July 16).

Pandey, Choi, Won and Hong (2011). SNMP-based enterprise IP network topology discovery. *International Journal of Network Management* 21 (3) 169-184.

Siamwalla, Sharma and Keshav (1999). *Discovering internet topology*. (Report May). Cornell University.

VMWARE (1995). WMWARE web page, WMRARE Workstation. <http://www.vmware.com/support/pubs/> (2011 June 25).

Zoho. WebNMS web page, WebNMS SNMP API.NET EDITION 4. <http://www.webnms.com/netsnmp/datasheet.html> (2011 August 1).

TEACHER CANDIDATES' INFORMATION LITERACY SELF-EFFICACY

Ahmet Adalıer
Faculty of Education, Cyprus International University
Nicosia-North Cyprus
aadalier@ciu.edu.tr

Oğuz Serin
Faculty of Education, Cyprus International University
Nicosia-North Cyprus
oserin@ciu.edu.tr

ABSTRACT
The aim of this study is to reveal the relation between the teacher candidates' social demographic characteristics and their information literacy self-efficacy. The research was conducted among teacher candidates in North Cyprus. The sample consists of 142 [49.30% (n=70) female, and 50.70% (n=72) male] teacher candidates who were selected according to convenience sampling in Faculty of Education at Cyprus International University. In this study, the "Information Literacy Self-Efficacy" scale developed by Kurbanoğlu, Akkoyunlu and Umay (2006) with a Cronbach alpha reliability coefficient of .91 was used in data analysis. Considering the purposes of the study percentage documentation average, t-test, ANOVA, Scheffe test and Levene's test were figured out in data analysis. The statistical significance level was accepted as .05 in the study.

Keywords: Information Literacy, Self-Efficacy, Teacher Candidate, Teacher Education

INTRODUCTION
The phrase information literacy (IL) first appeared in print in a 1974 report by Paul G. Zurkowski written on behalf of the National Commission on Libraries and Information Science. Zurkowski (1974) used the phrase to describe the "techniques and skills" known by the information literate "for utilizing the wide range of information tools as well as primary sources in molding information solutions to their problems".

Subsequently a number of efforts were made to better define the concept and its relationship to other skills and forms of literacy. Although other educational goals, including traditional literacy, computer literacy, and critical thinking skills, were related to information literacy and important foundations for its development, information literacy itself was emerging as a distinct skill set and a necessary key to one's social and economic well-being in an increasingly complex information society (Kulthau, 1987).

A seminal event in the development of the concept of IL was the establishment of the American Library Association's Presidential Committee on IL, whose 1989 final report outlined the importance of the concept. The report defined information literacy as the ability "to recognize when information is needed and have the ability to locate, evaluate, and use effectively the needed information" and highlighted information literacy as a skill essential for lifelong learning and the production of an informed and prosperous

citizenry. The committee outlined six principal recommendations: to "reconsider the ways we have organized information institutionally, structured information access, and defined information's role in our lives at home in the community, and in the work place"; to promote "public awareness of the problems created by information literacy"; to develop a national research agenda related to information and its use; to ensure the existence of "a climate conducive to students' becoming information literate"; to include information literacy concerns in teacher education; and to promote public awareness of the relationship between information literacy and the more general goals of "literacy, productivity, and democracy." (ALA, 1989).

In 2003, the National Forum on IL, together with UNESCO and the National Commission on Libraries and Information Science, sponsored an international conference in Prague with representatives from some twenty-three countries to discuss the importance of information literacy within a global context. The resulting Prague Declaration proposed the following basic Information Literacy principles: (UNESCO, 2003).

- The creation of an Information Society is key to social, cultural and economic development of nations and communities, institutions and individuals in the 21st century and beyond.
- Information Literacy encompasses knowledge of one's information concerns and needs, and the ability to identify, locate, evaluate, organize and effectively create, use and communicate information to address issues or problems at hand; it is a prerequisite for participating effectively in the Information Society, and is part of the basic human right of lifelong learning.
- Information Literacy, in conjunction with access to essential information and effective use of information and communication technologies, plays a leading role in reducing the inequities within and among countries and peoples, and in promoting tolerance and mutual understanding through information use in multicultural and multilingual contexts.
- Information Literacy should be an integral part of Education for All, which can contribute critically to the achievement of the United Nations Millennium Development Goals, and respect for the Universal Declaration of Human Rights.

Self-efficacy is defined as people's beliefs about their capabilities to produce designated levels of performance that exercise influence over events that affect their lives. Self-efficacy beliefs determine how people feel, think, motivate themselves and behave. Such beliefs produce these diverse effects through four major processes. These include cognitive, motivational, affective and selection processes. A strong sense of efficacy enhances human accomplishment and personal well-being in many ways. People with high confidence in their capabilities approach difficult tasks as challenges to overcome rather than as threats to avoid. Such an efficacious outlook fosters intrinsic motivation and deep engagement in activities. They set themselves challenging goals and maintain strong commitment to them. They heighten and sustain their efforts in the face of failure. They quickly recover their sense of efficacy after failures or setbacks. They attribute failure to insufficient effort or deficient knowledge and skills which are to be developed. They approach threatening situations with confidence that they can exercise control over them. Such an efficacious outlook produces personal accomplishments, reduces stress and lowers vulnerability to depression (Bandura, 1994).

In contrast, people who doubt about their capabilities avoid difficult tasks which they view as personal threats. They have low aspirations and weak commitment to the goals they choose to pursue. When faced with difficult tasks, they dwell on their personal deficiencies, on the obstacles they will encounter, and all kinds of adverse outcomes rather than concentrate on how to perform successfully. They slacken their efforts and give up quickly in the face of difficulties. They are slow to recover their sense of efficacy following failure or setbacks. Because they view insufficient performance as deficient aptitude it does not require much failure for them to lose faith in their capabilities. They fall easy victims to stress and depression (Bandura, 1994).

With the information Age, the major principles of design for teaching and learning environments have changed dramatically. Therefore, possessing IL skills, as well as developing high self-efficacy, has become crucial skills in our day. Self-efficacy is a fundamental determinant in coping with and adapting to the system and it particularly affects what teachers do and what they manage, as stated by Bandura (2003). Self-efficacy has been a popular topic attracting the attention of many researchers from the education disciplines. Studies have been conducted in the context of teacher efficacy (Tschannen, 2001) and teachers' IL. These studies showed that teachers with higher self-efficacy are more likely to be effective in their classrooms by exhibiting enthusiasm for teaching, being open to students' ideas, using innovative instrumental methods that reflect their instruction and motivating students to learn.

Within the scope of relevant scientific studies, it is mentioned that information literacy is one of the significant parameter in education of teacher candidates' (Eisenberg & McGuire, 2004; Erdem, 2007; Akkoyunlu & Kurbanoğlu, 2003; Tschannen, 2001) and various scales were used to measure information literacy self-efficacy (Akkoyunlu & Kurbanoğlu, 2003; Kurbanoğlu, Akkoyunlu & Umay, 2006).

The aim of this study is to reveal the relation between the teacher candidates' social demographic characteristics and their information literacy self-efficacy (ILSE).

Problem Statements of the Study

The main problem statement of the study is stated as follows: "Is there a relation between the teacher candidates' social demographic characteristics and their information literacy self-efficacy?"

Sub Problems

The study aims to answer the following sub problem questions.

1. Is there any statistical difference teacher candidates' ILSE according to the gender?
2. Is there any statistical difference teacher candidates' ILSE according to the English proficiency level (self-perception)?
3. Is there any statistical difference teacher candidates' ILSE according to the experiences of computer usage?

RESEARCH METHODOLOGY

Research Design

The descriptive type of research was carried out via the descriptive type and is in accordance with the associational research model. This type of research aims to evaluate the degree and the variation between two or more variables (Karasar, 2009).

The Universe and Sample of the Study

The universe of the study consists of the teacher candidates at the universities in North Cyprus. The sample consists of 142 [49.30% (n=70) female, and 50.70% (n=72) male] teacher candidates' who were selected according to convenience sampling in Faculty of Education at Cyprus International University.

Research Instruments

Demographic Information Form

This 3-item form is prepared by the researcher to collect data about teacher candidates' gender, English proficiency level and their experiences of computer usage.

Information Literacy Self-Efficacy Scale

The scale for Information Literacy Self-Efficacy Scale was a 28-item and 7-point Likert scale developed by Kurbanoğlu, Akkoyunlu and Umay to define participants' self-efficacy level for IL. The participants were asked to rate each item on a scale ranging from 1 to 7. The minimum and maximum scores which could be received from the scale were 28 and 196 respectively. The Cronbach alpha reliability coefficient of the scale was calculated to be .91.

Data Analysis

In the statistical evaluation of the research all analyses are performed by using SPSS 15.0 for windows. When the number of individuals included within the scope of the research exceeds 50, it is recommended that Kolmogorov-Smirnov test be utilized for testing whether or not the data obtained from the attitude scales display a normal distribution (Coakes & Steed, 1997; Tabachnick & Fidell, 2000). In the Kolmogorov-Smirnov test, since the statistical null hypothesis states that "the distribution of the grades does not display a meaningful difference from the normal distribution", the fact that the calculated "p" value exceeds .05 has led to the evaluation that the grades do not display a significant difference from the normal distribution (Büyüköztürk, 2006). When the Kolmogorov-Smirnov test results are considered, t test and uni-directional variance analysis (ANOVA) tests were applied for the data with a normal distribution. The significance level was taken as .05 in this study.

FINDINGS

The data obtained from the research were studied and interpreted in accordance with the sub problems.

Comparing the scores obtained from the dependent variables ILSE, Kolmogorov-Smirnov test was used to check the convenience of the variables with respect to normal distribution. The results of the analysis are presented in Table 1.

Table 1: Analysis Result Regarding Normal Distribution Test of Dependent Variable

Dependent Variable	n	Mean	Std. Dev.	KS-Z	p
ILSE	142	124.978	11.353	1.233	.096

As can be seen in Table 1, the data regarding ILSE indicated a normal distribution therefore parametric tests were used to analysis data.

The following results were found according to the problem statement and the sub questions of the study.

Findings of the First sub-question of the Research

The first sub-question of the research was expressed as "Is there any statistical difference teacher candidates' ILSE according to the gender?"

Table 2: t- Test Results of the Teacher Candidates' ILSE According to the Gender

Gender		n	Mean	Std. Dev.	Df	t	p	Meaningful difference
ILSE	Female	70	124.571	11.201	140	.420	.675	p>.05
	Male	72	125.375	11.564				

Levene's Test for Equality of Variances: F=.120 p=.730

To determine whether or not there is a significant difference between teacher candidates' ILSE according to the gender t-test was applied. As it can be seen in Table 2, although male teacher candidates' average scores are better than female teacher candidates', there is no statistically meaningful difference according to gender.

Findings of the Second sub-question of the Research

The second sub-question of the research was expressed as "Is there any statistical difference teacher candidates' ILSE according to the English proficiency level?"

Table 3: ANOVA Results of the Teacher Candidates' ILSE According to English Proficiency Level

English proficiency level		n	Mean	Std. Dev.	Df	F	p	Meaningful difference
ILSE	Very Bad (a)	8	112.125	12.988	4	3.191	.015*	a-b**
	Bad (b)	52	126.653	10.108				a-c**
	Average(c)	55	125.054	10.973	137			a-d**
	Good (d)	18	124.222	12.730				a-e**
	Very Good (e)	9	127.777	11.042				
	Total	142	124.978	11.353	141			

Levene Statistic= .336; df1=4; df2=137; p=.853; *p<.05; ** Indicates that the difference is in favor of the group.

In order to determine whether there is a statistically significant difference between teacher candidates' ILSE according to the English proficiency level One-Way ANOVA test was applied. As it can be seen in Table 3, there is a statistically significant change, in other words there is a significant difference, teacher candidates' ILSE (F=3.191 p<.05) according to the English proficiency level

It was observed that the significant difference stemmed from the a-b**, a-c**, a-d**, a-e** groups by using Scheffe test. This difference is against to the teacher candidates' who perceives their English proficiency level as very bad.

Findings of the Third sub-question of the Research

The third sub-question of the research was expressed as "Is there any statistical difference teacher candidates' ILSE according to the experience of computer usage?"

Table 4: ANOVA Results of the Teacher Candidates' ILSE According to the Experiences of Computer Usage

Experiences of Computer Usage		n	Mean	Std. Dev.	Df	F	p	Meaningful difference
ILSE	None (a)	5	114.400	13.240				a-c**
	Limited (b)	10	116.700	14.552	4			a-d**
	Some (c)	68	124.882	10.488				b-c**
	Quite A Lot (d)	48	127.812	9.630	137	3.385	.011*	b-d**
	A Lot (e)	11	125.545	14.841	141			
	Total	142	124.978	11.353				

Levene Statistic=1.423; df1=4; df2=137; p=.230; *p<.05;** Indicates that the difference is in favor of the group.

To determine whether or not there is a significant difference between teachers candidates' ILSE according to the experiences of computer usage One-Way ANOVA analyze was applied. As it can be seen from Table 4, there is a statistically significant difference teacher candidates' ILSE (F=3.385 p<.05).

It was observed that the significant difference stemmed from the a-c**, a-d**, b-c**, b-d** groups by using Scheffe test. This difference is in favor to the teacher candidates' who perceives their experiences of computer usage as very bad.

DISCUSSION

The results and the discussion of the findings of the study presented below.

As it can be seen from table 1, the general mean score of teacher candidates' self-efficacy for IL is 124.98. This result indicates that teacher candidates' IL self-efficacy level is medium.

It is observed that there is no statistically significant change, in other words there is no significant difference, teacher candidates' ILSE according to the gender. The result is

also supported by the findings in the studies conducted by Korkut & Akkoyunlu (2008), Ata & Baran (2011) and Şendurur, Gülsoy, & Mutlu, (2011).

It is seen that there is a statistically significant difference teacher candidates' ILSE according to English proficiency level. The result is also supported by the findings in the studies conducted by Korkut & Akkoyunlu (2008) and Ata & Baran (2011).

It is observed that there is a statistically significant difference teacher candidates' ILSE according to experiences of computer usage. The result is also supported by the findings in the studies conducted by Nagira (2000) and Şendurur, Gülsoy, & Mutlu (2011).

CONCLUSIONS AND RECOMMENDATIONS

It is observed that there is a statistically significant difference teacher candidates' ILSE according to the English proficiency level, experiences of computer usage and whereas there is no statistically significant difference according to the gender.

The information literacy games can be used in teacher candidates' education. These games teach the teacher candidates' IL skills including creating citations, judging citation completeness, assessing author expertise, assessing source relevance and credibility, judging quality, and assessing accuracy.

Educational methods and practices, within our increasingly information-centric society, must facilitate and enhance a student's ability to harness the power of information. Key to harnessing the power of information is the ability to evaluate information, to ascertain among other things its relevance, authenticity and modernity. The information evaluation process is crucial life skill and a basis for lifelong learning. Therefore, lifelong activities related with information literacy have to be supported in teacher candidates' curriculum.

Also, education professionals should encourage students to examine "causes" of behaviors, actions and events. Such initiatives would aid educators help teacher candidates become more Information Literate.

REFERENCES

Akkoyunlu, B., & Kurbanoğlu, S. (2003). A study on teacher candidates' perceived information literacy self-efficacy and perceived computer self-efficacy. *H. U. Journal of Education* (24): 1-10.

American Library Association (ALA) Presidential Committee on Information Literacy (1989). Final report. Chicago, American Library Association, Retrieved 15/09/2011 from http://www.ala.org/ala/mgrps/divs/acrl/publications/whitepapers/presidential.cfm.

Ata, F., & Baran, B. (2011). Investigation of undergraduate students' information literacy self–efficacy according to foreign language level, gender, computer ownership and the internet connection duration. 5th International Computer & Instructional Technologies Symposium, 22-24 September 2011, Fırat University, Elazığ- TURKEY.

Bandura, A. (1994). Self-efficacy, In V.S. Ramachaudran (Ed.), *Encyclopedia of Human Behavior* (4): 71-81, New York: Academic Press.

Bandura, A. (2003). *Self-efficacy: The exercise of control*. New York: W. H. Freeman and Company.

Büyüköztürk, Ş. (2006). *Experimental designs pretest-posttest control group design and data analysis.* Ankara: Pegem Publishing.

Coakes, S. J., & Steed, L. G. (1997). *SPSS, analysis without anguish*. John Wiley & Sons Publication.

Eisenberg, M., & McGuire, C. (2004). *Information literacy: essential skills for the information age.* 2nd Edition. USA, Libraries Unlimited Publication.

Erdem, M. (2007). Self-efficacy levels of teachers in information and computer literacy. *World Applied Sciences Journal* 2(4): 399-405.

Karasar, N. (2009). *Bilimsel araştırma yöntemi.* Ankara: Nobel Yayın Dağıtım.

Korkut, E., & Akkoyunlu, B. (2008). Foreign language teacher candidates' information and computer literacy perceived self efficacy. *H. U. Journal of Education* (34): 178-188.

Kulthau Carol C. (1987). Information skills for an information society: A review of research, ERIC, Dec 1987, ED297740.

Kurbanoğlu, S., Akkoyunlu, B., & Umay, A. (2006). Developing the information literacy self-efficacy scale. *Journal of Documentation*, 62(6): 730-743.

Nagira, M. (2000). A study and an evaluation about information literacy education for computer beginners. *Japan Journal of Medical Informatics* 20(2): 1004

Şendurur, P., Gülsoy, V., Şendurur, E., & Mutlu, N., (2011). Pre-service teachers' information literacy self efficacy levels: factors in interaction. 2nd International Conference on New Trends in Education and Their Implications 27-29 April, 2011 Antalya-Turkey

Tabachnick, B. G., & Fidell, L. S. (2000). *Using multivariate statistics.* Boston: Allyn and Bacon.

Tschannen, M. (2001). Teacher efficacy: Capturing an elusive construct. *Teaching and Teacher Education* 17: 783-805

UNESCO (2003). The Prague Declaration–toward an information literate society, Retrieved 15/09/2011 from http://portal.unesco.org/ci/en/ev.phpURL_ID=19636 &URL_DO=DO_TOPIC&URL_SECTION=201.html.

Zurkowski, P. G. (1974). *The information service environment: Relationships and priorities.* Washington: National Commission on Libraries and Information Science.